ENGINEERING SERVICE CENTER
Port Hueneme, California 93043-4370

TECHNICAL MEMORANDUM
TM-2421-SHR

DYNAMIC RESPONSES OF MODULAR HYBRID PIER TO DOCKING AND DRIFTING SHIPS

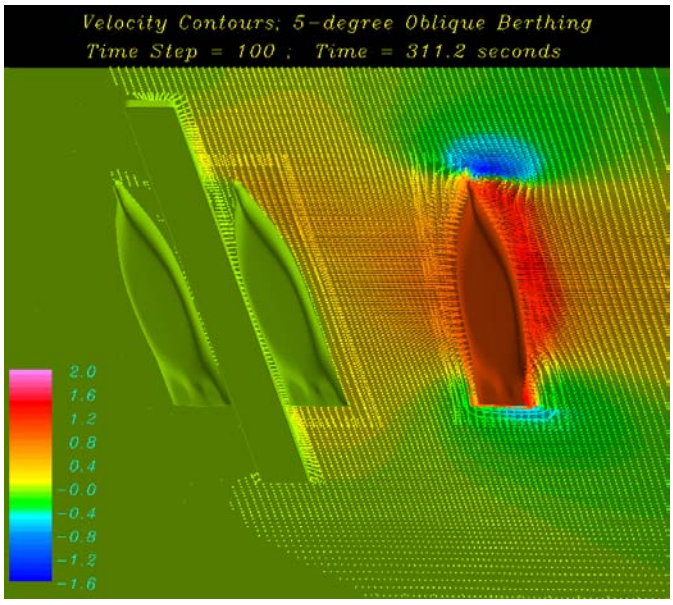

By:
Erick T. Huang, PhD, PE
Hamn-Ching Chen, PhD, PE
Texas A&M University, College Station, TX

October 2011

REPORT DOCUMENTATION PAGE (SF 298)

Form Approved
OMB No. 0704-0811

1. REPORT DATE *(DD-MM-YYYY)*	2. REPORT TYPE	3. DATES COVERED *(From – To)*
October 2011	Technical Memorandum	Oct 2002 – Sep 2004

4. TITLE AND SUBTITLE

DYNAMIC RESPONSES OF MODULAR HYBRID PIERS TO DOCKING AND DRIFTING SHIPS

5a. CONTRACT NUMBER

5b. GRANT NUMBER

5c. PROGRAM ELEMENT NUMBER

6. AUTHOR(S)

Erick T. Huang, NAVFAC ESC
Hamn-Ching Chen, Texas A&M University

5d. PROJECT NUMBER

5e. TASK NUMBER

5f. WORK UNIT NUMBER

7. PERFORMING ORGANIZATION NAME(S) AND ADDRESSES

NAVFAC ESC
1100 23rd Avenue
Port Hueneme CA 93043-4370

8. PERFORMING ORGANIZATION REPORT NUMBER

TM-2421-SHR

9. SPONSORING/MONITORING AGENCY NAME(S) AND ADDRESS(ES)

10. SPONSOR/MONITORS ACRONYM(S)

11. SPONSOR/MONITOR'S REPORT NUMBER(S)

12. DISTRIBUTION/AVAILABILITY STATEMENT

Approved for public release; distribution is unlimited.

13. SUPPLEMENTARY NOTES

14. ABSTRACT

This task measures the dynamic integrity of a conceptual Modular Hybrid Pier (MHP) in the design operational and survival environments with a proven simulation model in a manner closely resembling hydraulic model testing in a towing tank. The effort encompasses series of numerical tests to quantify the behaviors of impinging ships, in active control or disabled, and their impacts on the pier in typical inland waters with currents and winds. These exercises addressed all operational and environmental parameters pertinent to the ship-fluid and ship-pier couplings observed in the relevant events. The impinging ship behaviors and pier responses are clearly traceable to the driving fluid and ship activities. The results conclude that routine ship docking is unlikely to damage the pier or degrade its operational efficiency. A pier with two founding shafts is sufficient to withstand the impact by docking ships or a drift ship in currents less than 1.5 ft/sec. Four founding shafts are required to survive the impact by a drift ship in the design current of 2.3 ft/sec identified for the potential future pier sites. The pier displaces extensively once the interior fenders buckle and vibrates noticeably after the impact loads subside.

15. SUBJECT TERMS

16. SECURITY CLASSIFICATION OF:			17. LIMITATION OF ABSTRACT	18.NUMBER OF PAGES	19a. NAME OF RESPONSIBLE PERSON
a. REPORT	b. ABSTRACT	c. THIS PAGE			Erick Huang
U	U	U		114	19b. TELEPHONE NUMBER *(include area code)* 805-982-1256

EXECUTIVE SUMMARY

OBJECTIVE

This effort assesses the dynamic integrity of a conceptual Modular Hybrid Pier (MHP) in the design operational and survival environments. The pier integrity is gauged by its operational efficiency during ship docking routines and the survivability of its founding system against the worst operational and environmental threats. Both criteria were tested with the largest ship admissible to the facilities. Findings provide a measure to justify the position keeping concept and guide future fender designs.

CONCLUSIONS

The MHP permits finite lateral flexibility as a result of fender contractions and gaps in the founding pools intended to ease pier installation and to decouple the pier from seismic ground motions. This design complicates the path of load transfer and consequently the load distributions to the founding shafts. Simulations indicate that a bare MHP in deep water alone experiences the worst-case impact by impinging ships.

Ship speed dictates the docking loads. So does the location of ship impact along the pier but to a lesser degree. Water depth affects the fender loads through its influence on the approach speed of impinging ships. Exterior foam fenders in use effectively buffer the ship impacts and smoothly relay the impact loads via pier hull and interior fenders to the founding shafts. Ship inertia is responsible for the acute initial impact while the thrust empowered by trailing wakes sustains the impact loads at prolonged high intensities. Stiffer foam fenders transfer higher impact loads by ship inertia but make no difference to loads induced by trailing wakes. These two force components peak at different time separated by ample phase lag. The trailing wake accounts for 10 percent of the impact load in the case of docking ship, and 50 percent in the case of drifting ship in currents. Soft foam fenders tend to delay the maximum load induced by ship inertia and thus closer align with the maximum load induced by trailing wake. However, soft fenders also tend to transfer lower load induced by ship inertia.

Well-behaved docking ships are unlikely to damage the MHP or degrade its operational efficiency. The worst-case berthing loads imposed by the largest admissible client ship are well within the design capacity of the interior fenders around the founding shafts. The docking ship shakes the MHP slightly and hardly disturbs pier operations. The design of interior fenders to date seems decent in the operational environment. Two founding shafts are sufficient to withstand the impact by docking ships.

A 1,300-foot MHP held by four founding shafts guarded with single fenders survive impact by the largest admissible ship drifting in 2.3-foot per second (fps) currents. The same pier secured by two founding shafts will require double interior fenders to achieve comparable capacity, provided the founding shafts and their supporting dolphins hold. The pier displaces extensively once the interior fenders buckle and vibrates noticeably after the impact loads subside.

ACRONYMS AND ABBREVIATIONS

COSMA	Compound Ocean Structure Motion Analyzer
fps	foot per second
ft	feet
IPT	Integrate Project Team
kips	kilo pounds, 1,000 pounds
LHD	Landing Craft, Dock
m	meter
MHP	Modular Hybrid Pier
NAVFAC	Naval Facilities Engineering Command
NAVFAC ESC	Naval Facilities Engineering Service Center
NAVFAC LANT	Naval Facilities Engineering Command, Atlantic Division
NAVSTA	Naval Station
RANS	Reynolds-Averaged Navier-Stokes

TABLE OF CONTENTS

TABLE OF CONTENTS (continued)

LIST OF FIGURES

LIST OF FIGURES (continued)

Page

LIST OF FIGURES (continued)

LIST OF TABLES

1.0 INTRODUCTION

1.1 Objective

This effort assesses the dynamic integrity of a conceptual Modular Hybrid Pier (MHP) in the design operational and survival environments. The goal was achieved by gauging its operational efficiency during ship docking routine and the survivability of its founding system against the worst environmental threats and operational loadings. Both criteria were tested with the largest ship admissible to the MHP facilities. Findings provide a rational basis to justify the position keeping concept and guide future fender designs.

1.2 Background

Most of the United States Navy piers and wharves are at the late stage of their design life and require substantial maintenance and repairs. Shutdown during repair or replacement often results in high collateral cost to Navy operations. As such, the Navy is seeking an alternative relocatable pier with reduced life-cycle cost. The Naval Facilities Engineering Command Atlantic (NAVFAC LANT) is leading a consortium in the development, testing and evaluation of concepts and materials technology for a new generation of berthing piers. The Naval Facilities Engineering Service Center (NAVFAC ESC) is developing an innovative concept known as the MHP. In contrast to the conventional pile supported piers, the MHP is comprised of standardized pontoon floats on buoyancy support [Reference 1]. The MHP concept integrates functional versatility and construction flexibility in a robust structure that remains largely maintenance-free over a service life of 100 years. This new generation pier can rapidly adapt to the changing needs of a Navy base, allowing quick replacement of piers at capital cost comparable to functionally equivalent fixed piers.

A typical MHP assembled from four modules is illustrated in Figure 1(a). Each module measures 80 feet (ft) (27-meters (m)) width by 325 ft (99-m) length by 28 ft (9-m) height with a 13 ft (4.3-m) draft when fully loaded. Pier modules can be added/subtracted and disassembled/reassembled as needed. This floating pier is founded by two to four steel shafts extending from underwater pile dolphins (Figure 1(b)). The number of shafts and their design depends on local geology and environmental loads. This is the only portion of the MHP that is "site adapted." Buckling rubber fenders located in the founding well absorb energy and limit motion (Figure 1(c)). The founding design isolates the modules from seafloor ground motion; therefore, it can be sited in areas of high seismicity without excessive costs for strengthening.

The MHP is accessed from land via a ramp of nominally 30-m long depending on tidal variations (Figure 1(a)). These piers along with its client ships rides on tides concurrently and thus maintain a constant elevation differential from ship decks to the pier deck. This reduces labor spent in tending brows, mooring lines, and utility cables. Ships can be berthed at less standoff since there is no risk that flared hulls or ship appendages will contact the pier as the tide drops. MHP modules are double-decked for efficient ship support. Ship berthing, re-supply and intermediate maintenance are conducted on the top, "operations" deck. Utilities for ship "hotel" services are on the lower, "service" deck. This leaves the operations deck uncluttered for operation of mobile cranes. Utilities are readily accessible for maintenance and eventual change-out to meet new ship requirements.

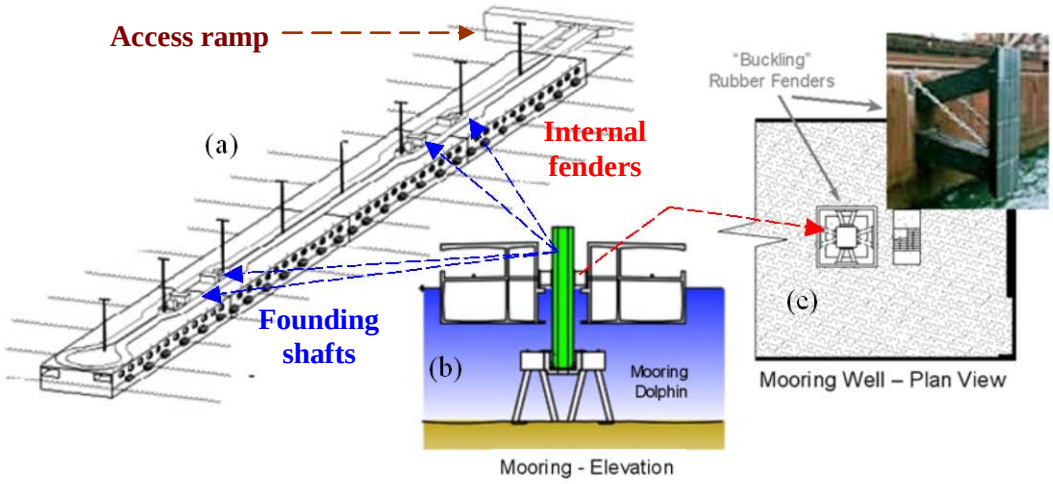

Figure 1. Modular Hybrid Pier, structural layouts, and founding (mooring) system

Despite the operational and constructional merits, MHP, like any other floating facility, is subject to the actions of client ships and ambient water through hydrodynamic and structural couplings. A variety of environmental and operational loadings concerning the pier performance and system survivability has been identified. For instance, sea level rise, land settlement, storm surge, tsunami, harbor seiche, ship collision, and severe metocean loading are risks for survivability whereas passing ships, docking ships, operational loads, and normal metocean loading are risk factors for pier performance. An Integrated Project Team (IPT) identified several high priority hydrodynamic issues relevant to the pier performance at site at the early stage of conceptual development. The list includes the worst-case design loads arise from ship berthing, ambient currents, hostile weathers, and seismic induced harbor oscillations as follows.

(a) Response of the MHP and client ships to docking ships
(b) Response of the MHP to impact from a large drifting ship
(c) Response of the MHP and client ships to harbor oscillation
(d) Response of the MHP to hurricane level current, wave, and wind forces
(e) Response of the MHP and client ships to nearby ship traffic

Item (a) quantifies the berthing loads imposed by a docking ship on MHP and the subsequent motion responses of MHP and its client ships alongside. Item (b) explores the consequence of accidental collision by a large drifting ship. This effort addresses the first two items. The results indicate the MHP will be suitable for operation of mobile cranes and the fenders are sufficient to absorb the impacts by docking ships and drifting ships in the realistic ambient currents. Item (c) was explored partially. Findings to date were documented in Reference 2. Item (d) was to be addressed under separate task. Item (e) explored the hydrodynamic influence of ship traffic in nearby navigation channels on the MHP system. The influence was demonstrated in a real waterfront environment at the NAVSTA Norfolk Virginia as summarized in Reference 3.

1.3 Scope

1.3.1 Analysis

The core effort of the study encompasses series of numerical simulations to quantify the docking ship behaviors, in active control or disabled, with or without the presence of ambient currents and winds, and their impacts on the MHP in typical inland waters.

Since the docking ship simulation to this accuracy was then the first of its kind, the simulation model was thoroughly inspected for its performance in shallow water from 2002 to 2003. An extensive pilot study was conducted to optimize the extent of simulation domain, boundary treatments, grid resolution, as well as the sizes of relaxation factors and time increments for the best simulation efficiency. Once the simulation code and the numerical model were settled in mid 2003, the simulations proceeded to explore the docking ship performance and its impact on the MHP with a variety of pier and client ship parameters. Parameters considered include pier and ship layouts, approach speed and angle of ship docking, location of impact, dynamics properties of coupling members, and current speeds. All simulations were conducted with model ships of LHD class, which represent the largest client ships admissible to the MHP. This sequence revealed the insights of ship-fluid and ship-pier interactions during ship docking in calm water. The coherence between fluid activities, docking ship behaviors, and MHP responses was clearly demonstrated and rationally justified.

The analysis revisited the ship docking cases in calm water in late 2003 and extended in 2004 to these cases of ship docking in the presence of currents and winds with a significantly enhanced simulation model capitalized on the lessons learned from previous stages. Major improvements made include the introduction of mechanical damping in the inner fenders and new techniques to suppress the shock loads induced by sudden changes in the water flows at the onset of releasing the docking ships to ambient currents. The new code provided a much more smooth, consistent, and realistic MHP responses with these upgrades. A final sequence was devoted to testify the design capacity of the inner fenders with MHP secured by two and four founding shafts. This sequence also identified the worst-case scenario environment the inner fenders as designed can withstand during ship docking process.

1.3.2 Documentation

This report describes the methodology, model setup, and simulation tool in use, as well as simulation results and findings. A brief description of the site condition and analysis procedure was also provided for reference. The results comprise a large database of flow fields over the entire fluid domain and the motion histories of the MHP and client ships. Raw data in terms of discrete velocity and pressure fields were electronically archived. This report consists of nine chapters. The first three chapters outline the objective, problems, and solution method. Chapter 4 describes the construction of the numerical towing tank in use. Chapter 5 addresses the hydrodynamic nature of the MHP with and without client ship alongside. Chapter 6 articulates the mechanism of pier-ship coupling in the process of tug assisted ship docking. Prevailing parameters pertinent to the event are fully inspected. Chapter 7 summarizes the docking ship impacts and the subsequent pier responses in the operational environment. Chapter 8 defines the worst-case scenario impact loads and testifies the holding capacity of the founding shafts and their fenders. Chapter 9 concludes the study and recaptures findings for design consideration.

2.0 METHODOLOGY

The interaction of a major floating pier to its client ships during docking process is relatively unexplored in the past. Like its traditional counterpart of fixed piers, a floating pier interfaces with its client ships through marine fenders at ship berths. These fenders provide cushion to stop a docking ship in order without incurring damage to the ship or berth. The present MHP design separates its pontoon-based pier modules from the position keeping founding shafts with a set of inner fenders attached around each founding shaft. This design isolates the modules from seismic ground motion and thus avoids extensive costs for strengthening the founding shafts to withstand excessive loads imposed by the oscillating pontoon modules. For the purpose of easing field installations, the founding pools are sized slightly larger than the dimensions of founding shafts with fenders, leaving small gaps between the fenders and the sidewalls of founding pools. These gaps along with the nonlinear behaviors of inner fenders and the free-body motion of the MHP modules introduce additional uncertainties in the load path from docking ships to the founding shafts far beyond the already troublesome issues of determining the berthing energy for fender design. Standard fender design practice to date uses a nominal berthing energy specified in terms of the displacement, approach speed, and attitude of a docking ship. Corrections due to ambient water, other ship characteristics, and site specific factors are included via decoupled coefficients. Fender characters are then selected to facilitate an optimal energy absorption or dissipation process and thus minimize fender reactions. This procedure can be found in any textbook or design manuals.

Unfortunately, a reliable correction factor for fluid influence, or the added mass coefficient, is hard to come by. Field measurements, if exist, are site specific and often disputable. This should not be a surprise as the present design method overly simplifies the complex, heavily site dependent, transient flow associated with ship berthing to a single correction factor. Engineering practice, as usual, protects the resulting uncertainties by escalating the berthing energy with a factor of safety. However, this approach may not be a sufficient safe guard against all risks relevant to fender design. An over estimated berthing energy could lead to fenders of improper size or adverse dynamic characteristics. An oversized fender, for instance, provides the highly desirable margin of energy absorbing capacity, nevertheless also increases the standoff distance after a ship is safely berthed. This imposes a stiff burden on cargo transfer operation and ship maintenance. Besides, the concept of added mass implies association with ship acceleration. Yet, this simulation demonstrated that the fluid contribution to fender forces may not be relevant to acceleration. This result partly explains the wide spreading of field measurements in the existing literature. There is indeed little support in favor of extending field measurements for use at other sites.

Fender design at a floating pier is further complicated by the presence of pier motion. As pier motion adds complexity to fender design, fender design also affects pier dynamics. Ship induced flow could influence fender design through ship, floating pier, and their couplings. Fender selection is therefore no longer separable form pier design. Added mass coefficient alone is unlikely capable of capturing sufficient insights of this crucial water flow in support of a proper engineering trade-off. A more accurate berthing energy assessment probably requires numerical simulation in time-domain. A feasible procedure as proposed by Chen and Chen [Reference 4] and Chen et al. [References 5-7] was further extended for time-domain simulation of ship

docking involving multiple vessels at a floating pier in shallow water basin as shown in Figure 2. Essential highlights of this method are briefly summarized in the next chapter.

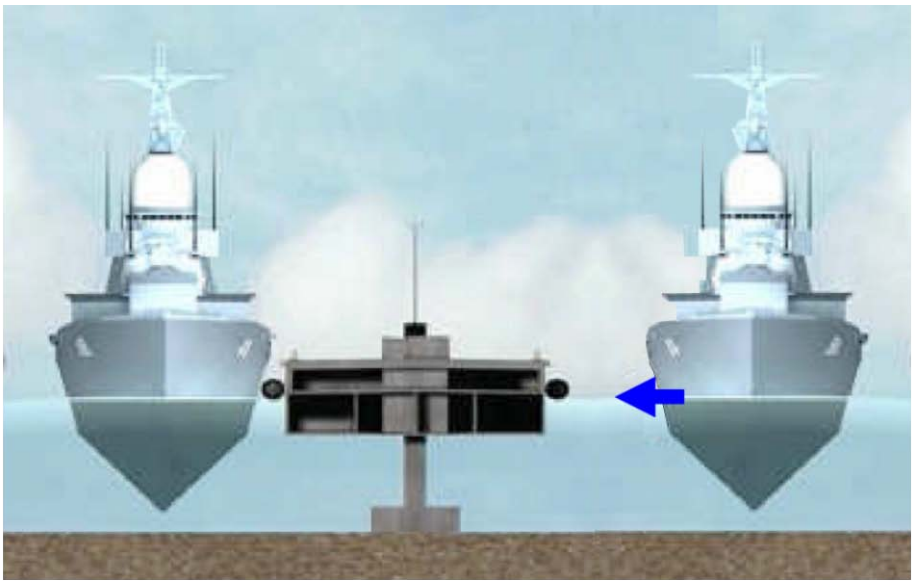

Figure 2. Modular Hybrid Pier, a floating pier concept

3.0 SIMULATION MODEL

3.1 Theoretical Considerations

A Chimera Reynolds-Averaged Navier-Stokes (RANS) method had been employed by of Chen, Chen and Davis [Reference 5] and Chen and Chen [Reference 4] for time-domain simulation of transient flow induced by a berthing ship. In their approach, the transport equations for both momentum and turbulence quantities are solved using the finite-analytic method of Chen, Patel, and Ju [Reference 8]. To solve for the pressure, the SIMPLER/PISO pressure-velocity coupling technique of Chen and Patel [Reference 9] and Chen and Korpus [Reference 10] is used. The governing equations and solution procedures is summarized in this section.

In order to provide accurate resolution of the transient turbulent flows induced by berthing ships, it is necessary to solve the Reynolds-Averaged Navier-Stokes equations for incompressible flow in curvilinear coordinates:

$$U^i_{,i} = 0 \tag{1}$$

$$\frac{\partial U^i}{\partial t} + U^j U^i_{,j} + \left(\overline{u^i u^j}\right)_{,j} + g^{ij} p_{,j} - \frac{1}{Re} g^{jk} U^i_{,jk} = 0 \tag{2}$$

where U^i and u^i represent the mean and fluctuating velocity components, and g^{ij} is conjugate metric tensor. t is time, p is pressure, and $Re = U_o L/\nu$ is the Reynolds number based on a characteristic length L, a reference velocity U_o, and the kinematic viscosity ν. Equation (1) represents the continuity equation and Equation (2) represents the mean momentum equation. The equations are written in tensor notation with the usual summation convention assumed. The

subscripts, $_{,j}$ and $_{,jk}$, represent the covariant derivatives. In the present study, the two-layer turbulence model of Chen and Patel [Reference 11] is employed to provide closure for the Reynolds stress tensor $\overline{u^i u^j}$.

In the Chimera RANS method, the solution domain is first decomposed into a number of computational blocks. The body-fitted numerical grids for ships, pier, and harbor fluid domain are generated separately with the ship and pier grid blocks completely embedded in the harbor grid. The ship and pier grids are allowed to move with respect to the harbor grid in arbitrary combinations of translational and rotational motions. The PEGSUS program [Reference 12] is employed every time step to determine the interpolation information for linking grids. It outputs a complete set of information corresponding to the interpolation performed. The most important information is included in a "blanking" array, the interpolation and boundary lists, the interpolation stencils, and the maps showing boundary and interpolation node locations. The blanking array and interpolation stencils are incorporated into the present Chimera RANS code to remove the hole points and update boundary conditions from the linking grids.

In order to predict the ship and fender coupling flows, the Chimera RANS method has been combined with a six-degree-of-freedom motion program developed by Huang [Reference 13] for Compound Ocean Structure Motion Analysis (COSMA) to facilitate the prediction of ship motions and fender loads. The COSMA program was developed originally for potential flow simulations with the structural responses represented by a lumped mass-spring model. In this model, the structure is divided into a finite number of rigid body elements. The size of elements is selected on the basis of the complexity of the structure and the level of analysis detail desired. Each element is further simplified to a point mass with proper inertia located at the 'node', which is usually the center of gravity of the element. Elements are then connected with massless elastic springs to form an idealized model of the physical structure. The motion is described at nodes in accordance with Newton's second law of motion. Motions at other locations on the structure can be calculated from the associated nodes by rigid body motion relations. The equation of motion implemented in the COSMA program can be written in the following general form:

$$[M+a]\{\ddot{X}(t)\}+[b]\{\dot{X}(t)\}+[K+C]\{X(t)\}=\{f(t)\} \tag{3}$$

in which

$[M]$ = generalized inertia matrix
$[a]$ = hydrodynamic mass matrix
$[b]$ = hydrodynamic damping matrix
$[K]$ = hydrodynamic restoring force matrix
$[C]$ = restoring forces due to coupling members
$\{X(t)\}$ = generalized displacement vector
$\{f(t)\}$ = generalized external excitation force vector

The COSMA program is capable of predicting the ship motions under wind, current, and waves. It handles multiple floating bodies with the presence of connectors, mooring lines, thrusters, and fenders. For the berthing operations considered here, ships and pier can be treated as rigid bodies and the coupling members to be included are fenders and mooring lines. Therefore, the

[C] matrix reduces to a diagonal matrix with the coefficients representing the fender stiffness for three translational modes. The floating pier and moored ship are rest in equilibrium and only the berthing ship is subjected to tug thrust. Moreover, wave forces are neglected as the scene is essentially in a fully sheltered harbor. As noted in Huang [Reference 13], the time dependent hydrodynamic force coefficients [a] and [b] were transformed from their frequency domain counterparts defined by potential theory with fluid viscosity being ignored. The present approach, however, directly computes the hydrodynamic forces acting on pier and ships in time without introducing added mass and damping coefficient matrices.

The present method solves the unsteady RANS equations at each grid node for the transient velocity and pressure fields induced by the berthing ships. Therefore, the hydrodynamic force vector $\{F_h(t)\}$ can be readily obtained by a direct integration of the surface pressure and shear stresses over the wetted hulls of the floating structures. Since the hydrodynamic forces $\{F_h\}$ includes both the added mass and damping forces, Equation (3) can be rearranged in a convenient form as follows:

$$[M]\{\ddot{X}(t)\}+[K+C]\{X(t)\}=\{F_h(t)\} \tag{4}$$

For ship induced flows, the Chimera RANS method was employed first to calculate the transient flow field and the associated hydrodynamic forces $\{F_h(t)\}$. The COSMA program was then used to solve the displacement vector $\{X(t)\}$ from Equation (4). Once the new ship position and the corresponding fender deflection are determined, the numerical grids can be updated by following the ship motion. The PEGSUS program of Suhs and Tramel [Reference 12] is then used to pass the updated information between coupled blocks as required for Chimera RANS simulations to proceed. In this coupled process, the COSMA code was considerably more sensitive to the size of time increments than the RANS program. Fender stiffness essentially limits the time increment for the motion code. In order to stabilize motion responses, the COSMA code advanced with a reduced time increment between steps of flow simulations. A ratio of 1/20 in general gave a good result in the present study. Yet, this shows little impact to the overall computation efficiency as the COSMA code requires only a negligible fraction of the CPU time used by the Chimera RANS simulations. The size of time increment for motion code is in fact determined by the stiffness of coupling members and the strength of fluid forces.

3.2 Essence of Chimera RANS Method

3.2.1 Unsteady Reynolds-Averaged Navier-Stokes equations

- Curvilinear, moving coordinate system
- Compressible and incompressible flows
- Finite-analytic method for transport equations
- Two-layer (near-wall) k-e eddy viscosity models
- Near-wall second-moment closure models
- Linear and nonlinear free-surface effects
- Specified motions or solving equations of motions for body dynamics

3.2.2 Chimera Domain Decomposition

- Embedding, overlapping, or matching boundary-fitted grids
- Select the most suitable grid structure for each computational block
- Local grid refinement to achieve maximum accuracy and efficiency
- Relative motions between different grid blocks
- Streamlined grid generation process
- Automated grid updates for minor changes in system design operating conditions

3.3 Validations

The performance of the present simulation model had been validated with a series of field and towing tank tests. This simulation model consistently reproduced field and laboratory measurements at great accuracy. Two important evidences acquired by NAVFAC ESC are recaptured here for references. One is a laboratory observation of wave-induced water particle velocity and vorticity fields around the corner of a partially submerged rectangular cylinder in regular wave trains as illustrated by Figure 3(a). Figure 3(b) compares the measured and simulated free surface elevations, velocity vectors, and phase-averaged vorticities at a selected instant. More details of this test were described in [Reference 14]. It is clearly seen that the computed free surface elevations are in close agreement with the corresponding measurements. Furthermore, the locations and sizes of the computed vortices were also accurately predicted. This feature is critical in the case that broadside currents prevail and significant flow separations present at sharp edges of the ship hull.

The other is a field measurement of berthing forces and flow patterns induced by a docking ship as shown in Figure 4(a). During the test a ship was docking against two instrumented fenders where the berthing forces were monitored. An array of eight current meters (see the top right insert of Figure 4(a)) was placed under the path of docking ship to record the ship-induced currents throughout the process. More details of this test were described in Reference 15. The test results indicated that the present simulation model is very effective in capturing the flow field induced by broadside ship motions. Figure 4(b) presents a snapshot of the pressure field as the docking ship approaches the ship berth. Figure 4(c) compares the water particle velocity predictions by the present model to the measurements at the eight current meters. It is also very reliable in the prediction of global force parameters as illustrated in Figure 4(d). This figure compares the predicted fender reactions to the corresponding measurements from the test. The results are exceptionally convincing. Chen et al. [Reference 16] and Huang et al. [Reference 3] further demonstrated the credibility of the present simulation model for cruising ships or motions along the ship length.

Overall, experimental evidences unanimously substantiate the performance of the present simulation model over a wide range of applications. Its credibility for use with the present passing ship effect assessment at NAVSTA Norfolk waterfront is robustly validated.

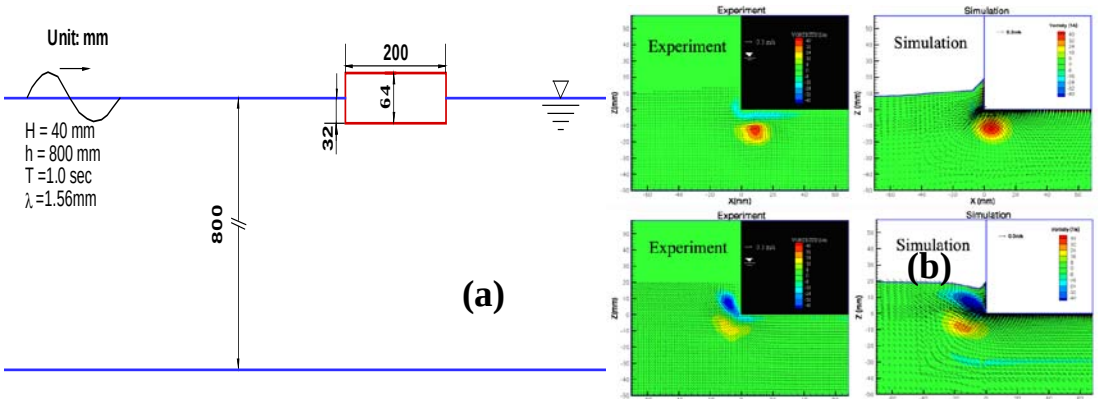

Figure 3. (a) Test setup and (b) velocity and vorticity fields.

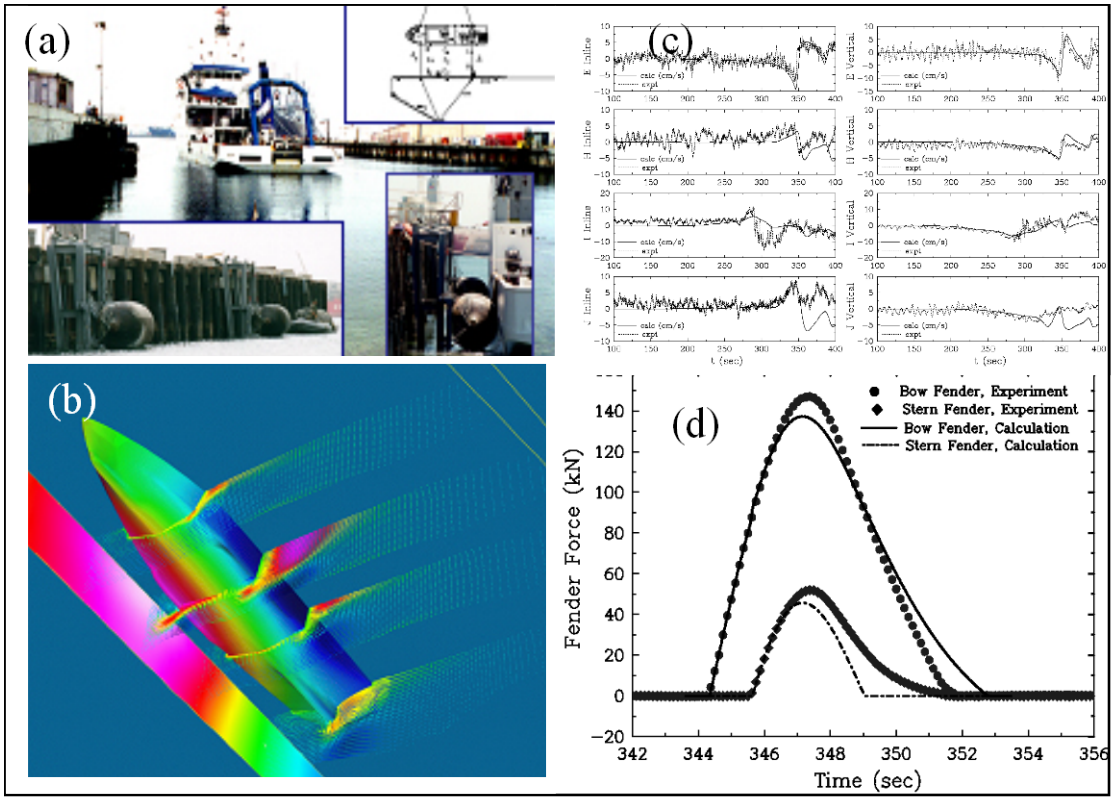

Figure 4. (a) Test setup, (b) pressure field, (c) current velocities, and (d) fender loads.

4.0 SIMULATION SCENARIO

4.1 General Layouts

Figure 5 illustrates a typical MHP layout for the consideration of the present simulations. In this case, the floating pier is extending from a vertical quay (in orange color), with a gap of 100 ft

(32.3 m), into an otherwise open harbor basin. Note that the founding shafts and fenders shown are not to scale. Vicinity piers and vessels in a realistic harbor are normally beyond the range of docking ship induced flows and are not expected to noticeably influence the simulation results. The outboard end of the pier will be considered as the bow in this article. A global reference is set at where the center plane of the pier intersects the quay wall at the elevation of free water surface. The x-axis extends along the pier length into the basin, while y-axis points to the port side and z-axis directs upward to complete a right hand coordinate system. The floating pier is secured with two dolphin shafts through moon pools at roughly the quarter points along the pier. These founding shafts are surrounded by fenders within the moon pools. These fenders will be referred as inner fenders in the text follows. A most probable largest client ship of LHD class as illustrated in Figure 6 is chosen as the model for this simulation. This vessel features a bulbous bow and a transom stern. Its streamlined hull presents clear flaring cross sections at the bow, which gradually transitions to a fuller hull in the stern half as illustrated by the sectional profiles in Figure 7. Ship keel remains flat from the bow until the last quarter of the ship length and then rises to pierce the water surface at the transom stern. The influence of these geometry features to the flow pattern across the ship length is significant as will be shown later in the chapters of simulation results. For the purpose of exploring the general features of berthing loads and subsequent motion responses of MHP and its client ships, one model ship is moored to the port side with six symbolic mooring lines to represent important features of a typical ship mooring. Four foam fenders are hung on both sides of the pier at the water surface to facilitate coupling with vessels. Designations of these coupling structures are assigned in Figure 5. Fender 5 is attached near the stern of docking ship to prevent hard contact when the ship approaches obliquely to the pier. A docking ship initially at roughly 106 m from the pier (center to center) will berth to pier under tug assistance. The tug applies a constant thrust of 22 tons on the way after going through a linear startup ramp in the initial 100 seconds. The docking ship eventually reaches a speed of 16 cm/s by the time fluid resistance offset tug thrust. The docking ship was released by the tug at a distance about 9 m from touching the fenders and since drifted on its own into the berth.

In fact, the flow pattern induced by the MHP and ships may extend far beyond the area described in Figure 5, which will be referred as the inner basin. The approximated open boundary, as is, tend to bounce the supposedly outgoing flow activities back into the simulation domain and subsequently contaminate the quality of near field solutions. This adverse boundary effect may be suppressed by installing an energy absorber along the open boundary or mitigated by extending the simulation domain. The present study adopts the later by embedding the inner basin in a broader outer basin five times as wide and three times as long as the inner basin as depicted in Figure 8. The inner basin was populated with fine grids to preserve the details of flow activities while the outer basin uses coarse grids to minimize the computation burden. The extra space of the outer basin ensures the residual water activities to radiate out of the area. Most significant flow activities are likely to occur in the near field within the inner basin.

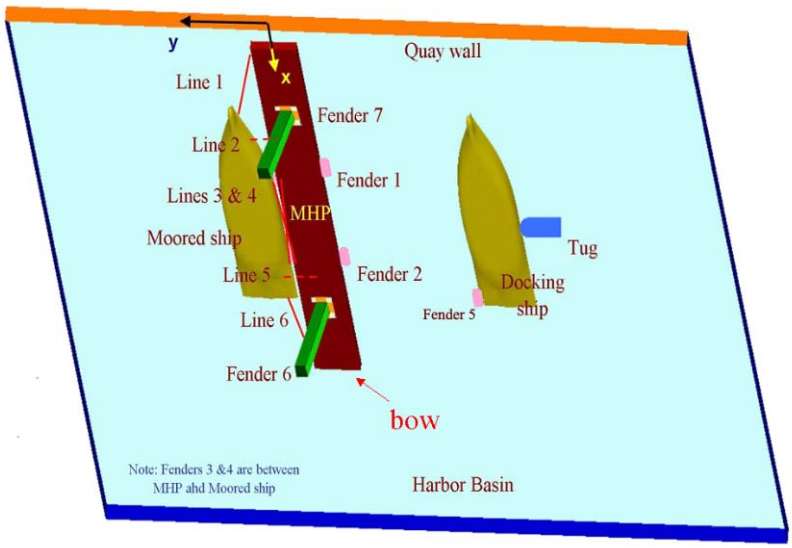

Figure 5. Sketch of the simulation scenario

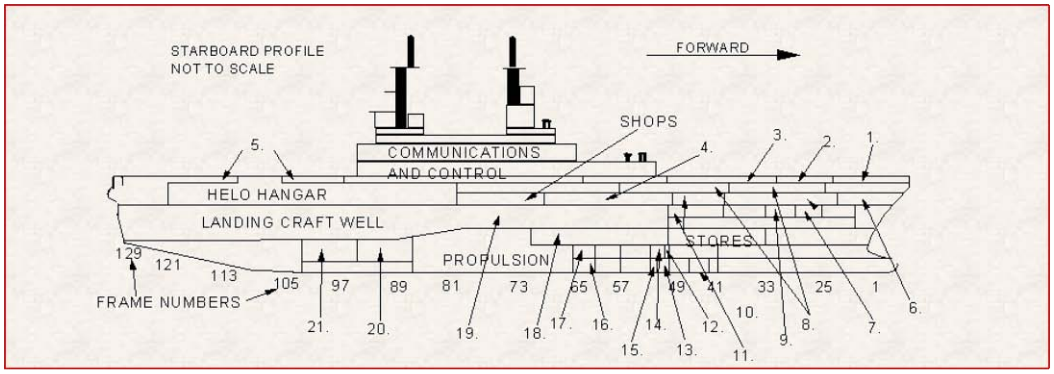

Figure 6. LHD ship form

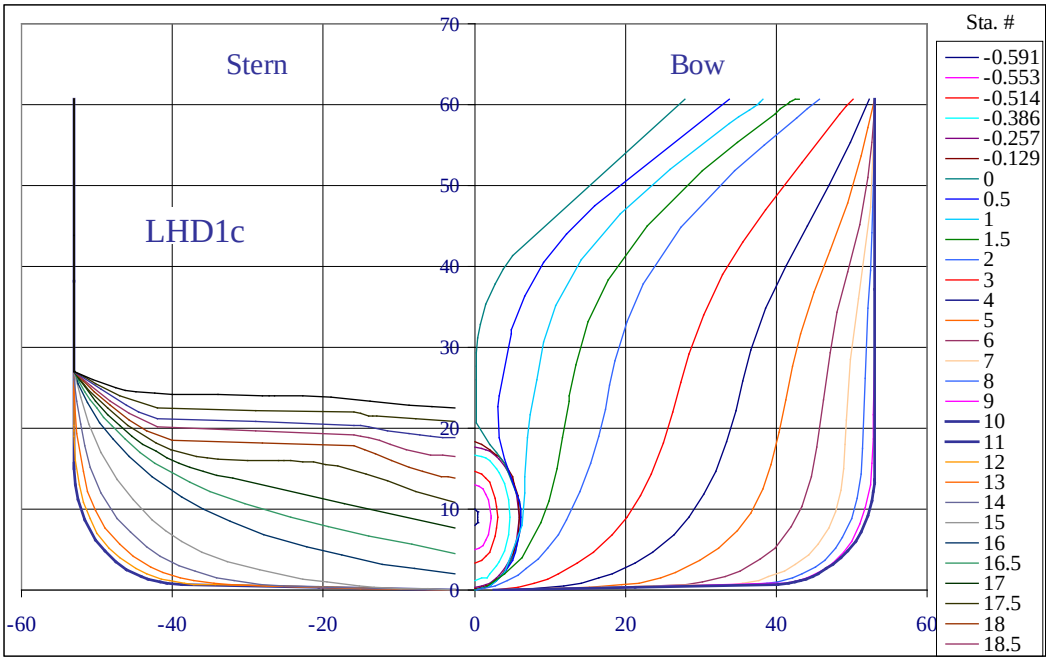

Figure 7. Sectional profiles of LHD5

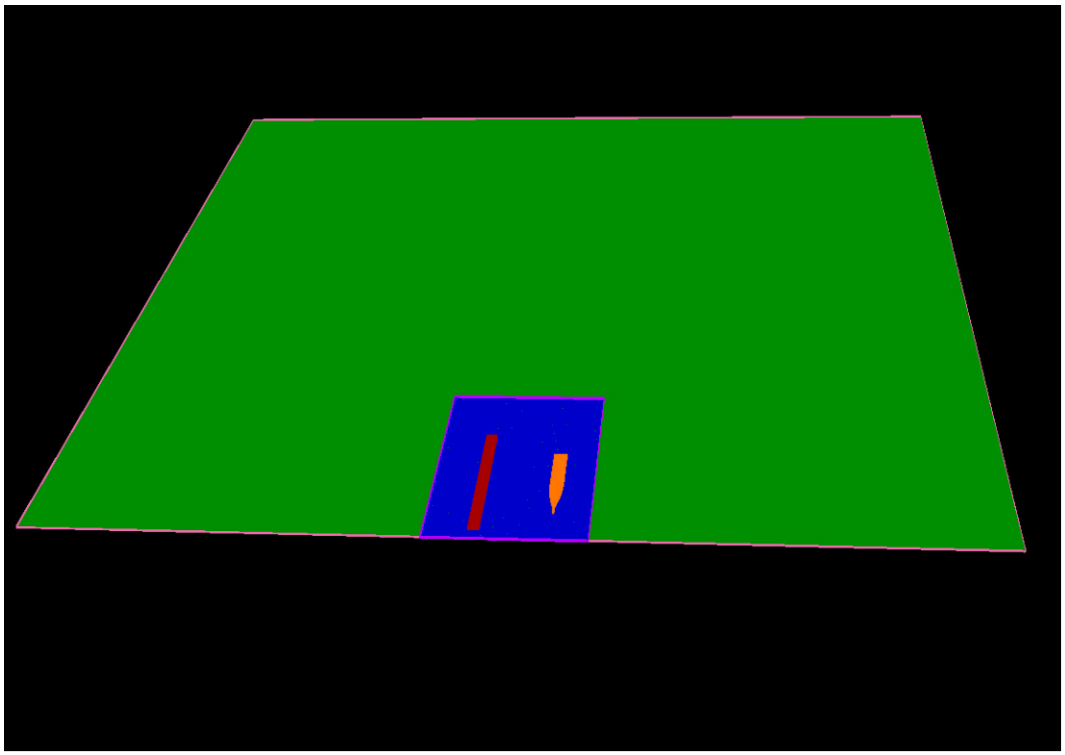

Figure 8. Layout of the fluid domain

4.2 Ship and Pier Particulars

This MHP is a 1,300- by 88-foot (396.25- by 26.82-meter) double deck floating pier constructed from identical 325-foot-long (106.68 meter) modules. The pier is secured by two founding shafts with vertical shafts going through moon pools at roughly the quarter points of the hull. This unique mooring system along with internal fenders isolates the pier from earthquake effects and will hence reduce the premium for facilities built in earthquake areas. For the purpose of identifying the maximum design loads imparted by docking ships, a worst-case scenario is selected as the test bed for the present simulation. Important particulars of the floating pier and vessels used in the simulation are summarized in Table 1.

Table 1. Particulars of the floating pier and vessels

Characteristics	Pier	Ship
Displacement (tons)	42,550	41,150
Overall length (m)	396.25/1300	237.14/778
Beam (m/ft)	26.82/88	32.31/106
Draft (m/ft)	4.36/14.3	8.23/27
Xcg from bow (m/ft)	198.12/650	113.08/371
Ycg from centerline (m/ft)	0/0	0/0
Zcg from waterline (m/ft)	0/0	0/0

4.3 Dynamic Characteristics of Ship Coupling Members

Figure 9 is a numerical representation of the structural layouts of the MHP with one client ship along side. MHP is modeled with a rectangular pontoon of 1,300 ft long and 88 ft wide with a mean draft of 14.3 ft. This floating pier is secured by four steel founding shafts (magenta) supported by underwater pile dolphins. These founding shafts are treated as rigid members and do not deform subject of external forces. They interface with the MHP hull through a set of four buckling rubber fenders as illustrated in Figure 1(c). These rubber fenders absorb all relative movements between the MHP hull and mooring shafts. They are represented by one-dimensional elastic members as shown in Figure 10. One client ship (the LHD in this case) was secured to the MHP by four to six theoretical mooring lines (green) with two foam fenders (white) in-between. These mooring lines and fenders are treated as linear elastic members in the present study; even the simulation model in use is capable of addressing all relevant nonlinear features. The client ship may be relocated to any position along the pier and more client ships may be added to explore the ship docking to more congested pier environments.

The characteristics of coupling members including fenders and mooring lines are listed in Table 2. For the purpose of identifying the fluid influence, all coupling members are simplified to linear springs.

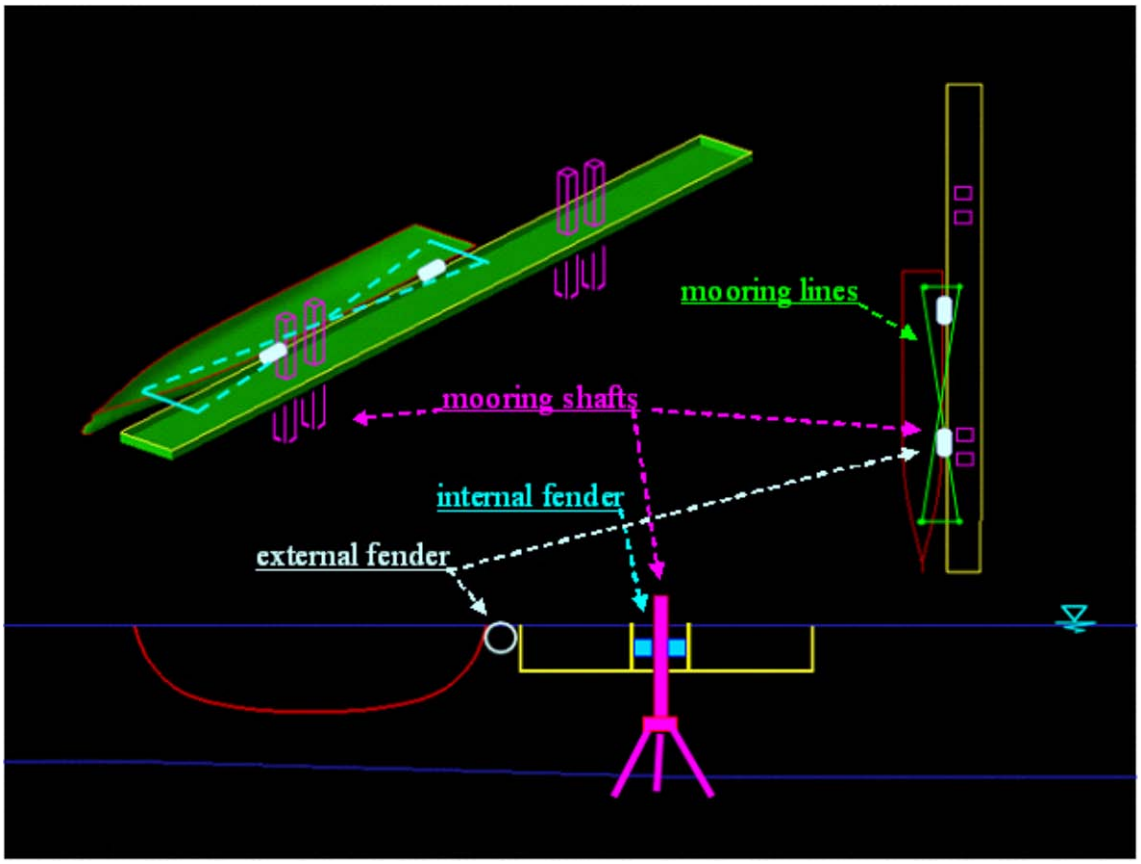

Figure 9. Structure layouts, coupling members, and nomenclatures

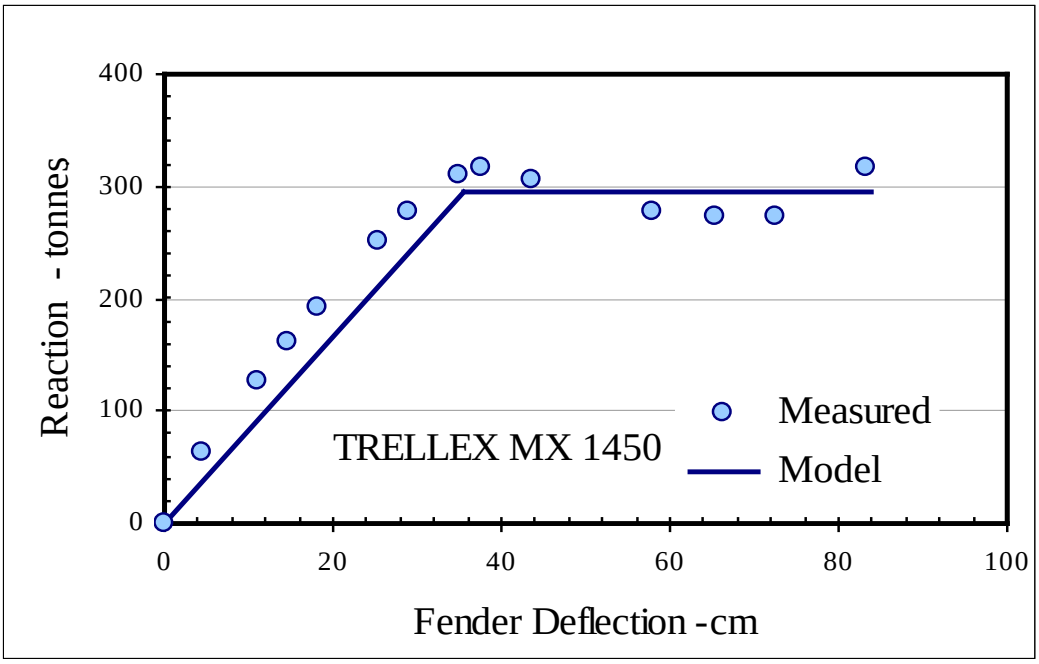

Figure 10. Load deflection curve of the internal fender.

Table 2. Dynamic characteristics of coupling members

Item	Characteristics
Foam fender (outer)	Diameter: 8 ft OD (2.44 m) Stiffness: 96 tons per meter
Trellex fender (inner)	Model: Trellex MX 1450 Stiffness = 806 tons per meter Maximum reaction: 318 tons
Mooring lines	Diameter: 3 inches (7.6 cm) Maximum tension: 13 tons

4.4 Numerical Grid System

Figure 11 illustrates the details of chimera decomposition of the inner basin. A generic harbor basin of constant depth (in green color) was selected for the initial exercise. This simulation domain includes a rectangle of 396 meter wide and 616 meter long surrounded by a solid, vertical quay wall on the lower left edge near the inboard end of the floating pier and three open boundaries (Figure 11(a)). The MHP assumed a positive heading away from the solid quay wall. One LHD is moored to the port side of the pier and a docking ship also represented by LHD is initially positioned at roughly 184 m (600 ft) away on the starboard side of the pier (Figure 11(b)). A shallow water depth of 8.53 m was intentionally chosen to confine the under keel clearance of the docking and moored ships to roughly 30 centimeters, or 3.7 percents of the ship draft. Both ships are of identical hull of 41,150 tons. This combination of a deep draft with a small under keel clearance gives a worst-case berthing force for fender design consideration. At the late stage of the berthing process, these two ships along with the floating pier confine a narrow passage, within which the flow activities are of special significance to behaviors of pier and two vessels.

In the chimera domain decomposition approach, the ships, pier, and harbor grids can be generated independently with arbitrary grid overlaps between different computational blocks. The entire fluid domain of the present model was digitized into a chimera grid system as shown in Figure 2. For better computation efficiency, the harbor basin was further divided in two grid blocks as shown in Figure 11(a). Figure 11(b) illustrates the footprints of floating pier and vessels in the basin as well as the block structure at the beginning of simulation. Grids for the pier, Figure 11(c), docking ship, Figure 11(d), and moored ship, Figure 11(e), were generated separately and then embedded in the harbor basin grids accordingly. Grids for the moored ship are identical to those of the docking ship with one block next to the floating pier omitted to enhance computation efficiency. Different numerical scheme was used to pass information across block boundary in each case. This difference exemplifies tradeoffs in grid structure between flexibility and accuracy. In this case, the docking ship uses an extra block of fine grids to ensure communication accuracy with harbor grids on her way toward the pier. The grids for moored ship only move within a limited range and are therefore able to maintain contact with pier grids at all time without the extra block. The chimera grid-embedding technique described in

Reference 4, the pier grids and ship grids are allowed to move with respect to the harbor grids in arbitrary combinations of translational and rotational motions. This enables us to accommodate the relative motions among the pier, ships, and the harbor without adaptive generations of body-fitted numerical grids at each time step. Essentials for coupling grid blocks for information exchange by interpolations were described in Reference 7. This model uses a total of slightly over one million grids.

This basin was used in the initial stage to evaluate the efficiency of the grid system. Although the code performed reasonable well with this numerical grid, moderate reflections from the open boundary were nonetheless visible. This boundary effect continued to grow and eventually deteriorated the quality of near field solutions in the main area of interest. It was decided to expand the simulation domain by adding a large outer basin around the core basin as shown in Figure 12 to allow proper propagation of the outbound flow activities out of the main area of interest. Figure 13 illustrates another configuration with two client ships straddling the MHP. The grid system for the additional client ship on the starboard side of the pier was copied from its counterpart on the port side. The outer block around this additional LHD grid (in yellow color) is a mirror image of its counterpart. While the ship blocks were fully embedded in the inner basin, the later was connected to the outer basin via finite layers of overlapping grids along the interfacing edges in the pilot study for grid efficiency tests. The overlapping technique is normally used between stationary blocks, while embedding technique is used between blocks presenting relative motion. Along with the grid embedding technique, phantom blocks were used to preserve the quality of grid systems in extremely shallow water, where the well-structured ship grids tend to cut below the sea floor. Phantom blocks instruct the code to blank out any grid node of chosen grid blocks extending into the spaces they embrace. Figures 14 (a) and (b) illustrate the ship grids before and after blanking. Note the thin water layers below the LHD hulls in Figure 14(b). Normally, the grids of lower resolutions and grids extending outside the physical boundaries get blanked out.

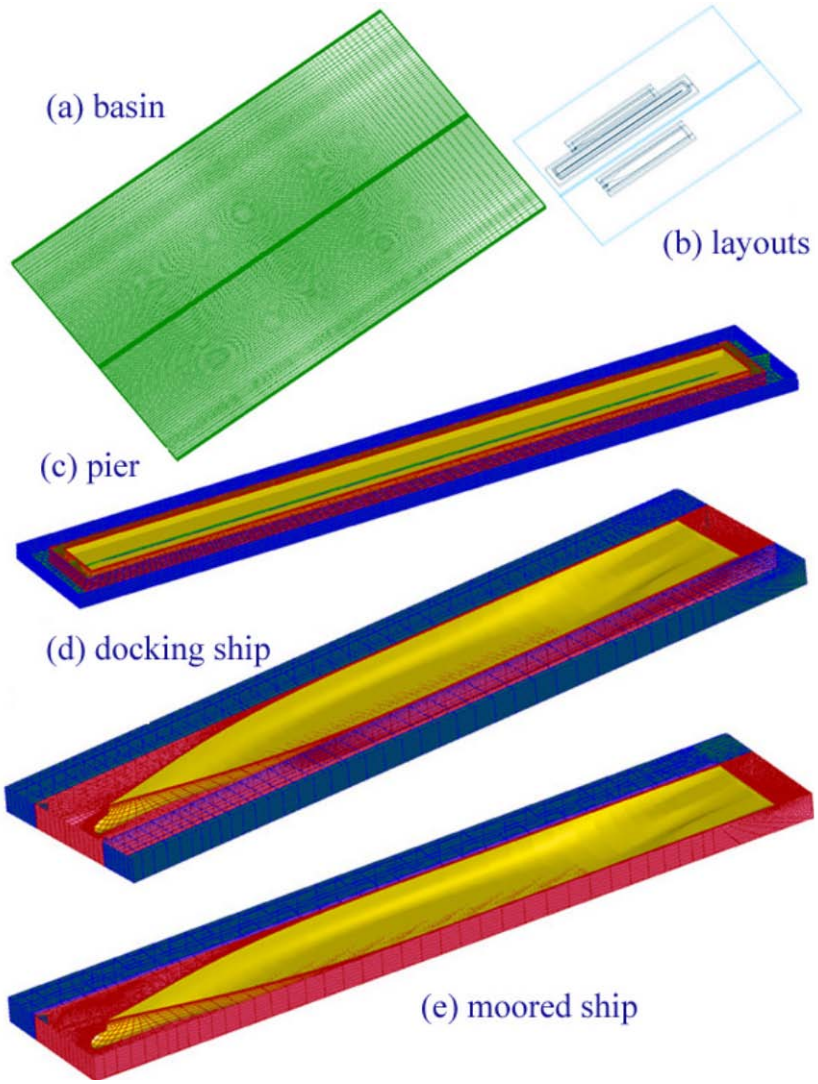

Figure 11. Chimera grid systems

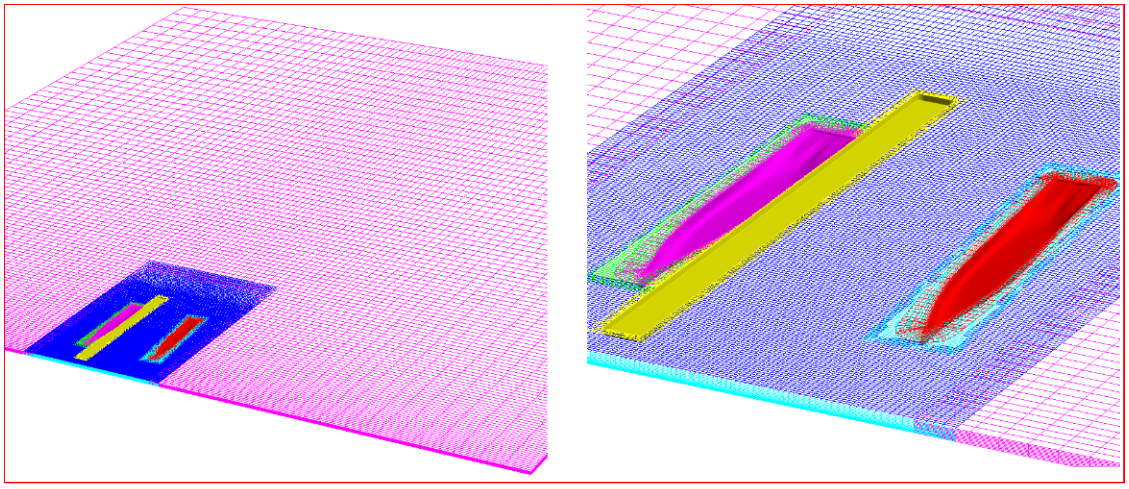

Figure 12. Expanded fluid domain

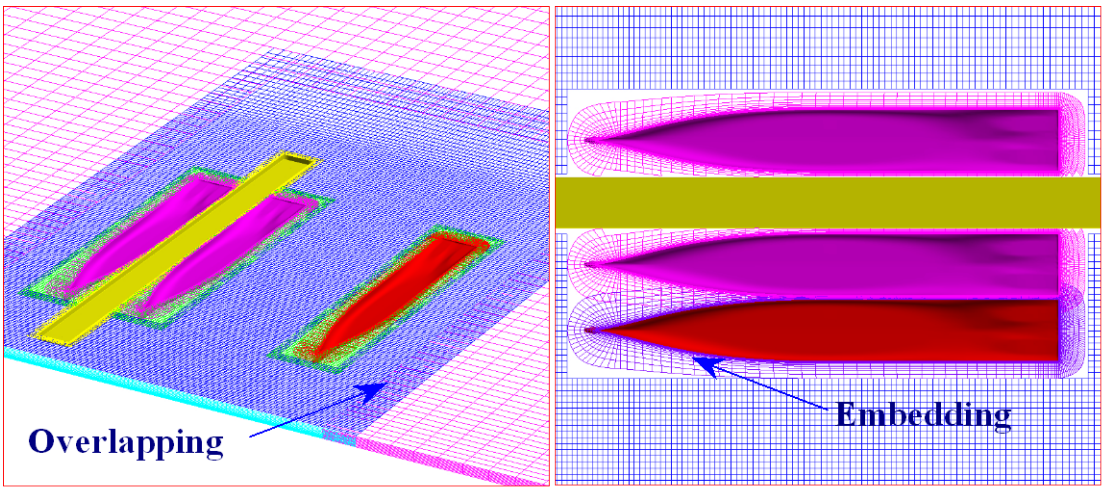

Figure 13. Grid overlapping and embedding.

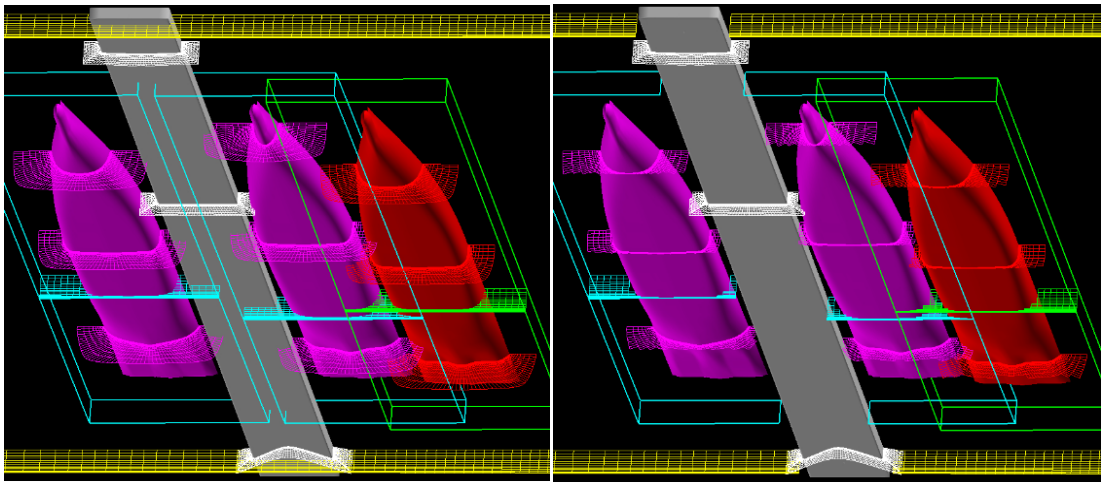

(a) Before Blanking **(b) After Blanking**

Figure 14. Grid system with phantom block techniques.

4.5 Simulation Procedure

These Chimera grid systems were used in a parametric study to explore docking ship impacts on the MHP performance in calm water. Parameters considered include approach speed and angle, characteristics of coupling members, and position of the docking ship relative to the floating pier. The floating pier and moored ship were assumed in their static equilibrium positions when the docking ship started to approach from 200 to 500 ft away under tug assistance. Figure 15 illustrates a typical docking procedure. In this example, the tug gradually applied a constant thrust through an initial linear startup ramp (Figure 15(a)), and steadily accelerated the docking ship to a terminal speed of 16 cm/s as the fluid resistance offset tug thrust as shown in Figure 15(b). It is assumed that the tug boat was in full control and is able to maintain the docking ship parallel to the pier before being released at a short distance from touching the fenders, Figure

15(c). The blue solid line in the same figure illustrates the excursion history of the docking ship through the process. The red line is a close up view to emphasize the ship position while interacts with fenders. As matter of fact, the docking ship had never reached a constant terminal speed on its way to the berth due to the influence of a complicated pressure system that bounced back and forth between two ships. The docking ship velocity oscillated slightly from early out and started to decelerate around the 480-second mark as shown in Figure 15(c), even though the tug maintained the same thrust. Upon released by the tug, docking ship was free to motions in water plane, namely surge, sway, and yaw, and continued to drift at a decreasing speed toward the pier under her own inertia until making contact with fenders at a speed of 10 cm/s as shown in Figure 15(c). It is surprising to note that the docking ship decelerated the most rapidly, although very briefly, at the on set of fender compression when the fender reaction is low, Figures 15(a) and 15(b). This implies a time lag of the trailing water behind ship deceleration. The docking ship acted on the fenders alone with little force enhancement by the trailing water. The ship inertia is the primary attribute responsible for the fender reactions during this duration. The trailing water caught up in a few seconds and overtook ship inertia as the primary contributor to the fender reactions. The time lag between the contributions of ship inertia and trailing water is likely relevant to the stiffness of foam fenders. This process will be further elaborated later in the section of fender reactions.

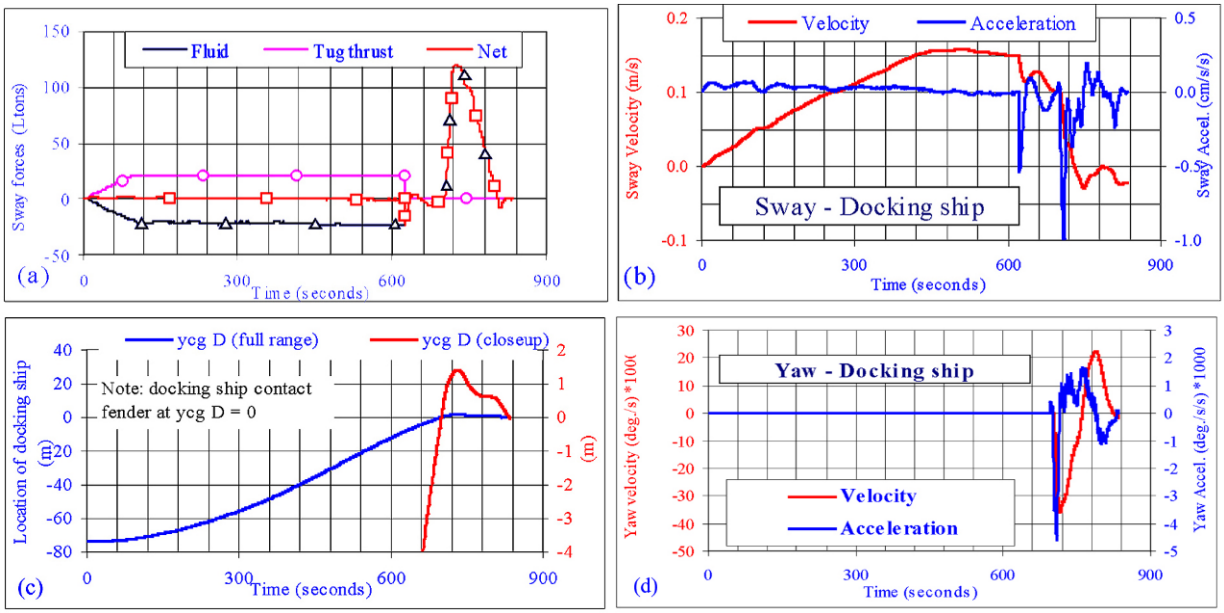

Figure 15. Typical ship docking process

5.0 HYDRODYNAMIC NATURE OF MHP

A floating pier under the restraint of its mooring system resembles a typical spring-mass oscillator in the air. However, with the presence of free water surface, the effective mass inertia and damping of the system are motion dependent and not known ahead of time. Fluid damping is particularly pronounced for floating structures of blunt hull shape in shallow water. The mechanism of fluid damping involves the process of flow separation behind sharp edges and fluid viscosity. Traditionally, these fluid influences can only be determined experimentally through a free decay test in the towing tank. This test observes the motion of the structure after

being released from an initial offset in a specific principal direction without further disturbance. The resulting motion histories are then processed to determine the fluid damping and the nature frequency of the structure. The present RANS code accounts for the effects of fluid viscosity and free surface internally without the need of these empirical parameters. A sequence of free decay tests was conducted to validate these internal functions and quantify the hydrodynamic nature of the MHP with the presence of client ships. Findings from this series will be used as a measure for quality control of the simulation results.

5.1 Free Decay of MHP

In this sequence, the pier was displaced slightly from its equilibrium position in surge, sway, or yaw and then released to free oscillations. Figure 16 illustrates a sample case which compares the sway motions of a standalone pier engaging the founding shafts with fenders of different stiffness. It can be seen the period of oscillation increases from 8 seconds to 16 seconds when the stiffness of fender decreases from 1,612 Ltons/m to 403 Lton/m. The tests were further conducted to check the sensitivity of pier performance with the docking ship at various locations on its course. Figure 17 shows two extreme cases in the process. The docking ship was retreated to a separation distance of 600 ft (center to center) from the floating pier in Case A. This distance should be far enough to isolate the MHP from the docking ship. A second configuration with the docking ship at 127 ft away from the pier representing the influence of the vicinity vessel is designated as Case B. Other conditions remain unchanged. No foam fender or mooring line is in action. In these tests, the floating pier started from its equilibrium position with an initial velocity of 0.5 foot per second (fps) in surge and sway, and 0.05 degrees per second in yaw. The corresponding accelerations are all set to zero. The pier continues to oscillate under its own inertia once released with its amplitudes decrease in time. As anticipated, surge motions are only slightly damped while sway and yaw motions decay substantially. The pier behaved nearly identical regardless the ship position as shown in Figure 18. The nearby ship does not seem to bother pier behaviors at all. This is most likely due to the shallow drafts of the pontoon modules.

The corresponding natural frequencies, ω_d and damping coefficient, η could be extracted from these time histories. In case of small damping, the decay coefficient can be determined by the relation follows.

$$\eta = \frac{1}{\pi} \log_e \left(\frac{x_{oJ}}{x_{o(J+1)}}\right), \tag{5}$$

where x_{oJ} and $x_{o(J+1)}$ are the J^{th} and $(J+1)^{th}$ extremities of the displacement histories.

For a linear oscillator, the damping is expected to slow down the oscillation by a factor as indicated by the follows.

$$\omega_d = \omega_* \sqrt{(1-\eta^2)}, \tag{6}$$

where ω_d and ω_* are the damped and undamped natural frequencies, respectively.

$$\omega_* = \sqrt{\left(\frac{c}{a}\right)}, \tag{7}$$

where a is the mass inertia and c is the spring stiffness of the oscillation system.

The results are summarized in Table 3 and Figure 19. The influence of fluid is much more pronounced then the presence of nearby ships.

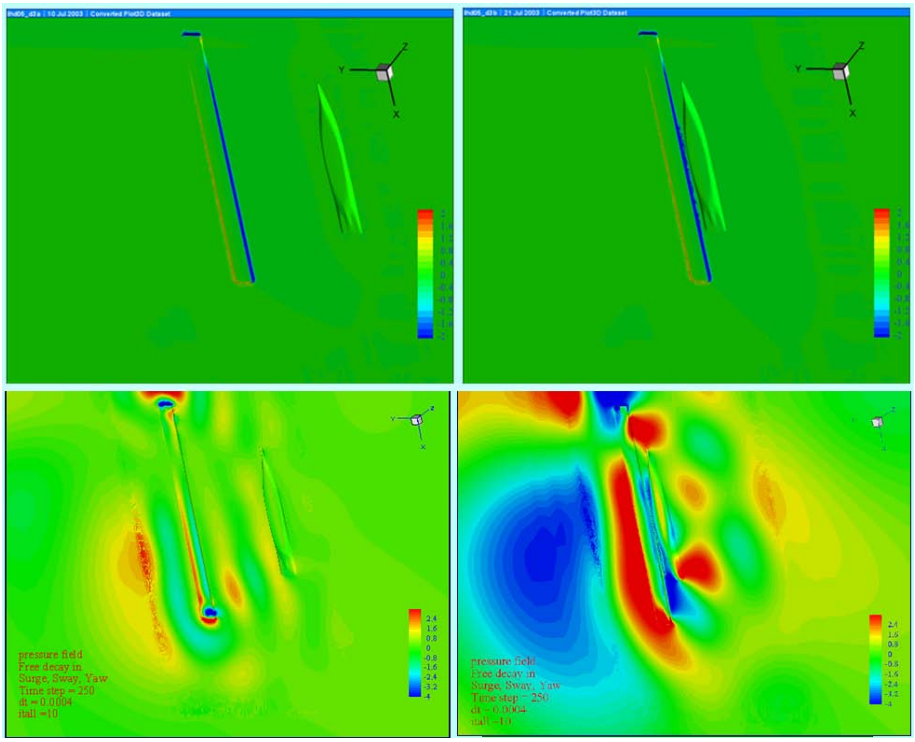

Figure 16. Pressure fields during free decay tests

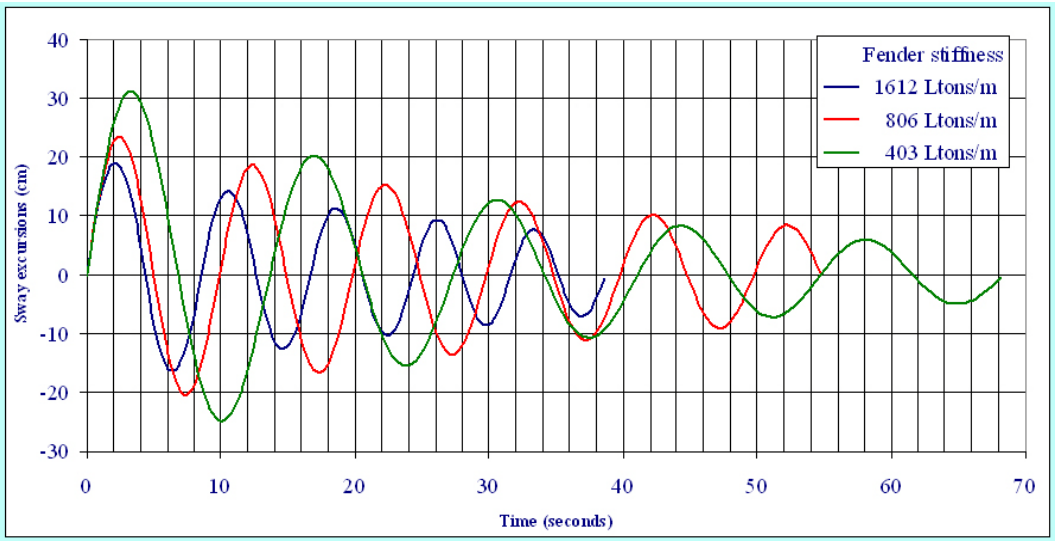

Figure 17. Sway motions of the MHP with various fender stiffness

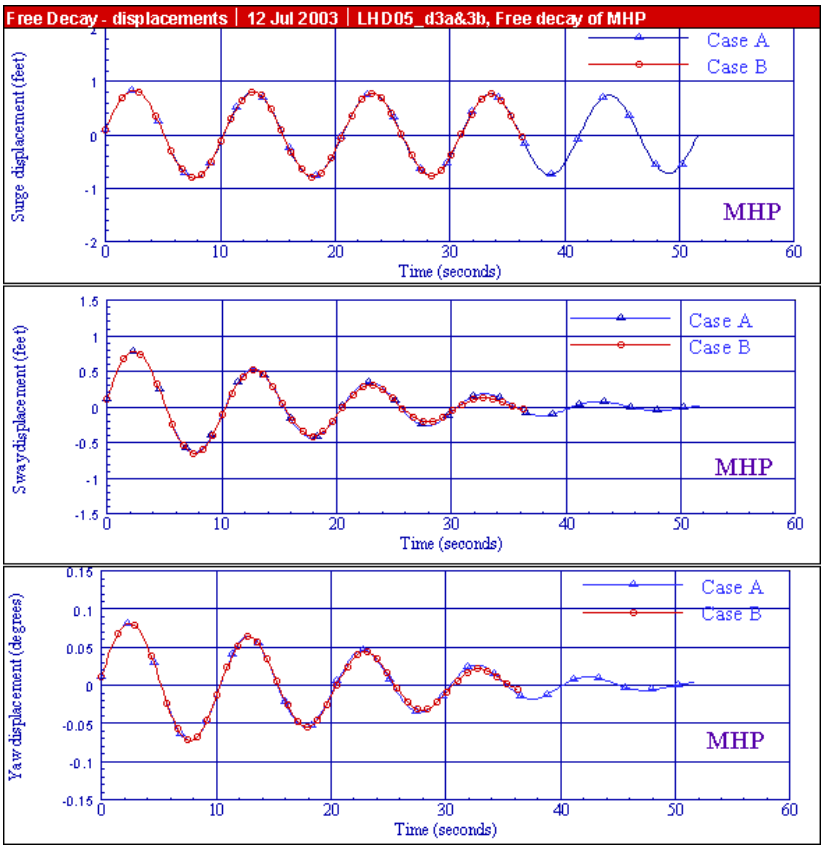

Figure 18. Free decay of MHP

Table 3. Natural frequencies of MHP in the air and in the water

Case ID	ω_* (in the air) Undamped frequency (Equation 7)			$\omega_{d'} = \omega_* * \sqrt{(1-\eta^2}$ Theory (Equation 6)			ω_d Simulated frequency			η Damping coefficient (Equation 5)		
	Surge	Sway	Yaw	Surge	Sway	Yaw	Surge	Sway	Yaw	Surge	Sway	Yaw
Case A	0.609	0.609	0.618	.609	.607	.617	.603	.607	.610	.0004	.0730	.0562
Case B	0.609	0.609	0.618	.609	.607	.617	.602	.604	.606	.0004	.0786	.0529

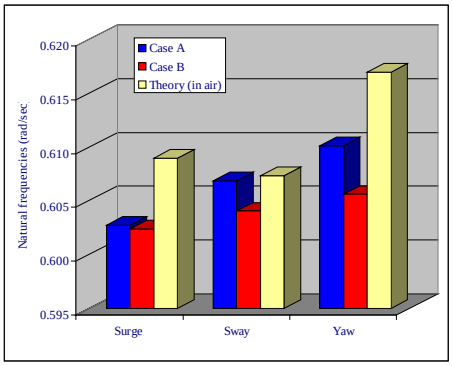

Figure 19. Influences of fluid reactions on the natural frequency

More important to note is the mechanism of fluid forces on the pier. Theoretically, an accelerating object in unbound calm water expects fluid resistance proportional to the acceleration and the velocity squared of the motion. Figure 20 traces the fluid force (red) experienced the pier during a free decay test in sway versus the associated velocity (green) and acceleration (blue) of the pier. The trend depicted in Figures 21(a) and (b) in general agrees with the theoretical expectations. Keep in mind that the forces comprise both components. The offsets from the respective diagonal in each figure account for the other component. In fact, Figure 21(a) indicates the fluid force is better correlated to pier velocity (red line) than velocity squared (blue circle). This suggests that the pier bears more radiation damping than viscous damping. The observations from the LHD, depicted in Figure 21(c) and (d) are quite different. This much deeper hull moving at faster speeds experiences fluid forces closely correlate to the square of the speed of the ship (Figure 21 (c)) and is essentially irrelevant to the acceleration of the ship (Figure 21(d)). In other words, these reactive forces are dominated by form drags resulting from the flow separations around the sharp edges of the ship hulls. A proper assessment of this force component requires precise information of the flow field at the instant and fluid viscosity. A potential theory based simulation model is unlikely to capture this reactive force. Without this term, the simulation model tends to over predict the dynamic responses of a moored ship and its couplings with the pier. The role of this form drag component to the ultimate impact loads on the fenders will be discussed in the subsequent chapters.

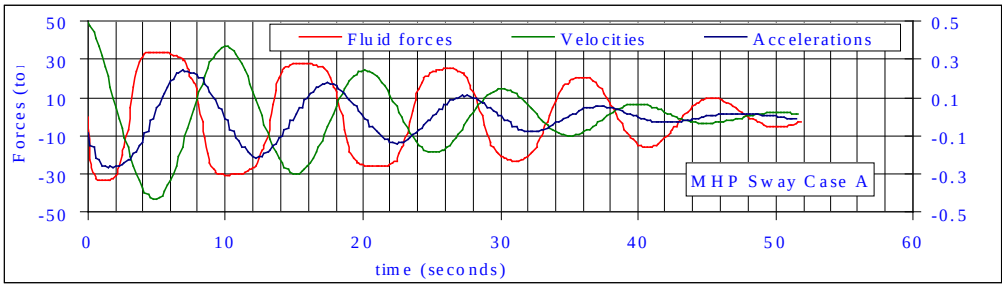

Figure 20. Fluid resistance is 180 out of phase with ship velocity.

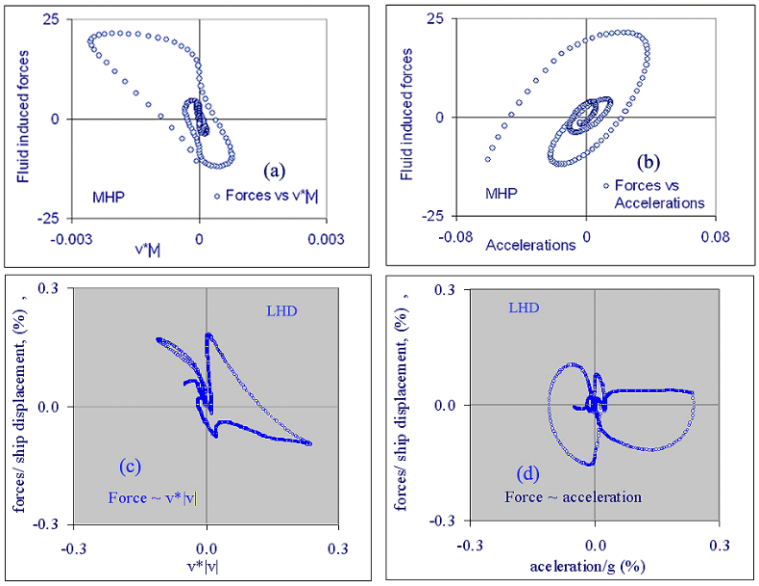

Figure 21. Fluid reaction forces versus ship motion.

5.2 Free Decay of MHP Secured by Four Founding Shafts

The free decay test was reiterated for an MHP of four founding shafts surrounded by single Trellex fenders. Figure 22 summarizes the motion histories of the MHP (red curves) in response to an initial offset in surge, sway, and yaw, respectively. The blue curves represent the MHP performance in the air without the influence of fluid damping. Note that the surge motion decays much slower than do the sway and yaw motions. The surge and sway periods in the air are identical at the theoretical anticipation of 7.3 seconds because of the identical fender layouts in the longitudinal and transverse directions. The yaw period is however substantially longer than the theoretical value at 12.4 seconds. The nature periods in the water are only slightly longer in all modes. However, the profile of yaw excursion even without fluid damping (blue curve) are noticeably distorted. A closer inspection of the internal fender reactions reveals that these fenders buckle and become softer during more than half of the oscillation cycle in this test. An additional test run was executed with one tenth of the previous initial yaw offset. The resulting yaw oscillation (yellow curve) resumes the simple harmonic nature with the anticipated resonance period of 8.4 seconds. This example clearly demonstrates the significance of coupling members to the dynamic performance of a floating structure.

Figure 23 further confirms the accuracy of these resonance periods. The MHP responses to a simple sinusoidal excitation near the resonance period (red) are substantially stronger than the same excitation at slightly different period (blue). Again, the large excitation excursion of the MHP near resonant period buckles the internal fenders and subsequently induces motion components of longer periods. The induced components combined with the active excitations to create a clear harmony effect as shown by the red curves. Note that this effect is highly exaggerated with the MHP in the air. In reality, the fluid damping will greatly mitigate the MHP responses. However, the idea is the same. Similar effects are anticipated with the mooring lines through coupling with client ships.

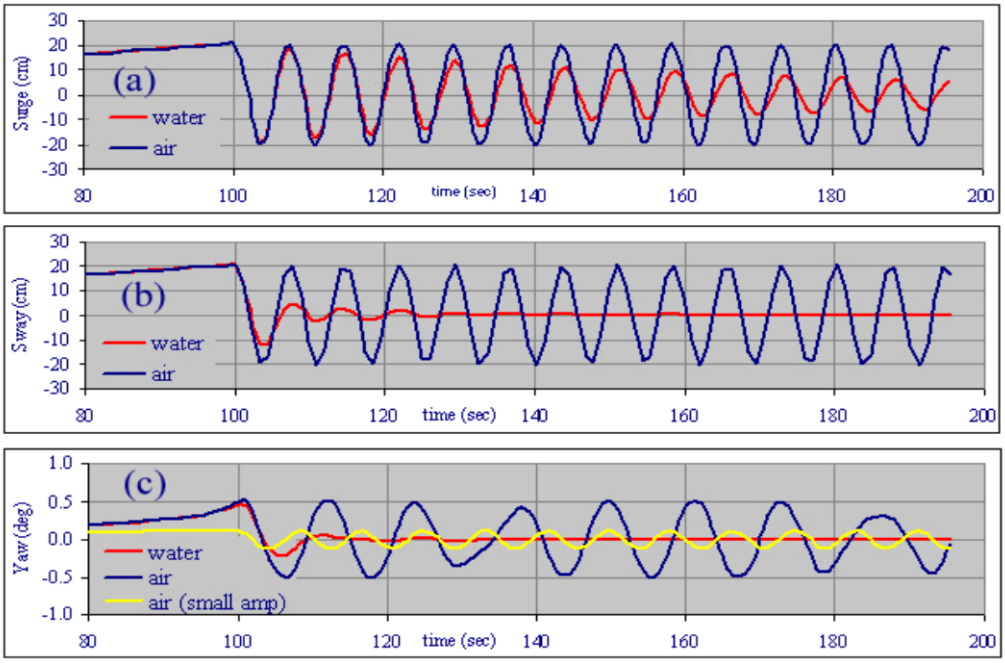

Figure 22. Free decays of the MHP with four founding shafts

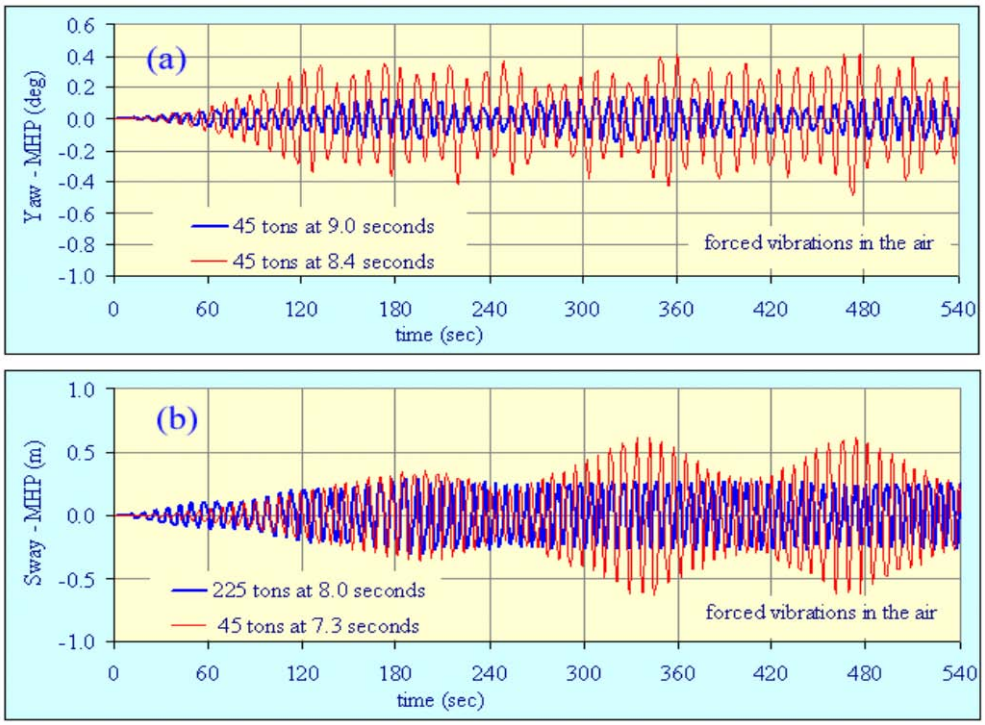

Figure 23. Forced vibrations of the MHP near resonance periods

6.0 PROCESS OF SHIP DOCKING AND PIER RESPONSES

Ship-pier couplings at a congested waterfront are rather complicate. It is not clear how the ships moored along the pier influence the load transferring from docking ship to pier. A sequence of

simulations is therefore devoted to explore how these ships diffract the water flow induced by the docking ship and identifies the worst-case pier configuration, which allows the most severe docking ship impact to the MHP. Results of two major cases with one and two client ships moored at the pier were summarized as follows.

6.1 MHP with One Moored Ship

One model ship is moored to the port side with six symbolic mooring lines to represent important features of a typical ship mooring. Four foam fenders are hung on both sides of the pier at the water surface to facilitate coupling with vessels. Designations of these coupling structures are assigned in Figure 24. Fender 5 is attached near the stern of docking ship to prevent hard contact when the ship approaches obliquely to the pier. A docking ship initially at 152.4 m (500 ft) from the pier (center to center) will berth to pier at either 0 degree (parallel berthing) or 5 degree oblique angles under tug assistance. The tug applies a constant thrust of 21.85 tons on the way after going through a linear startup ramp in the initial 100 seconds. The docking ship eventually reaches a nearly constant speed by the time fluid resistance offset the tug thrust. The docking ship was released by the tug at a short distance from touching the fenders and since drifted on her own into the berth.

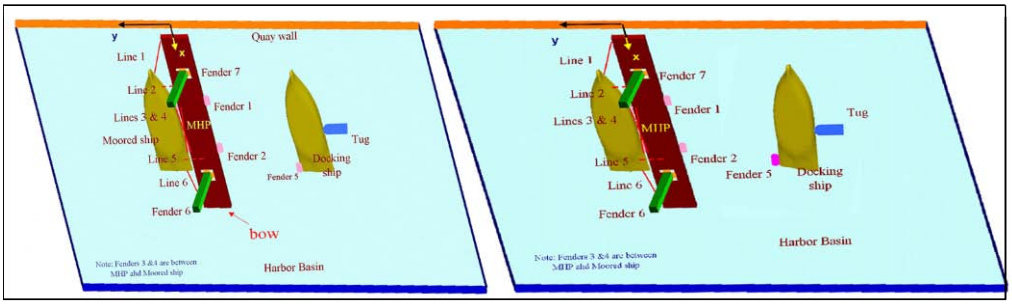

Figure 24. Tug assisted docking to MHP with one client ship on the starboard side.

6.1.1 Numerical grid system

A generic harbor basin of constant depth was selected for this simulation. A shallow water depth of 8.53 m was intentionally chosen to confine the under keel clearance of the docking and moored ships to roughly 0.3 m, or 3.7 percent of the ship draft. Both ships are of identical hull of 41,150 tons. This combination of a deep draft with a small under keel clearance gives a worst-case berthing force for fender design consideration. At the late stage of the berthing process, these two ships along with the floating pier confine a narrow passage. Flow activities within this passage are critical to the structural couplings.

In the Chimera domain decomposition approach, the ships, pier, and harbor grids can be generated independently with arbitrary grid overlaps. Figure 25(a) shows the overall structure of a 10-block numerical grid used in this series. The pier and ship grids are embedded in the harbor basin grid (Figure 25(b)) and are free to move with respect to the harbor grids in arbitrary combinations of translational and rotational motions. This enables us to accommodate the relative motions among the pier, ships, and the harbor without adaptive generations of body-

fitted numerical grids at each time step. It should be noted that the domain size, grid topology, and blanking technique employed in the present study is significantly different from those used earlier in Huang and Chen (2003) for a parallel berthing case. The ship grids used in Huang and Chen (2003) provided a perfect fit to the hull surfaces and the basin floor to minimize interpolation errors between relevant blocks. Elements were highly distorted due to the extremely narrow under keel clearance, and thus somewhat impaired the convergence and accuracy. This drawback is erased by improved grid scheme. The grid system shown in Figure 25(c) allows the ship grids to extend below the basin floor for better grid quality. A phantom grid was then used to remove the grid points outside the harbor basin as shown in Figure 25(d). This new scheme remarkably improved the accuracy of simulation while the total number of grid points was reduced by 10 percent.

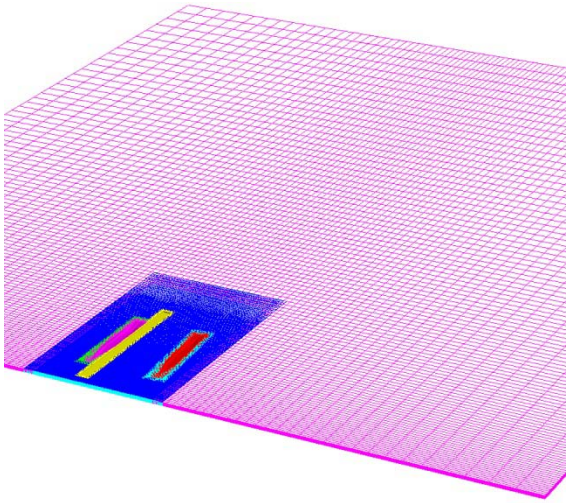

(a) Solution domain

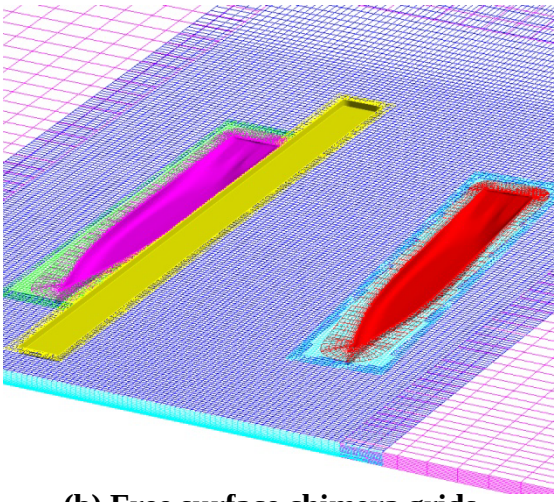

(b) Free surface chimera grids

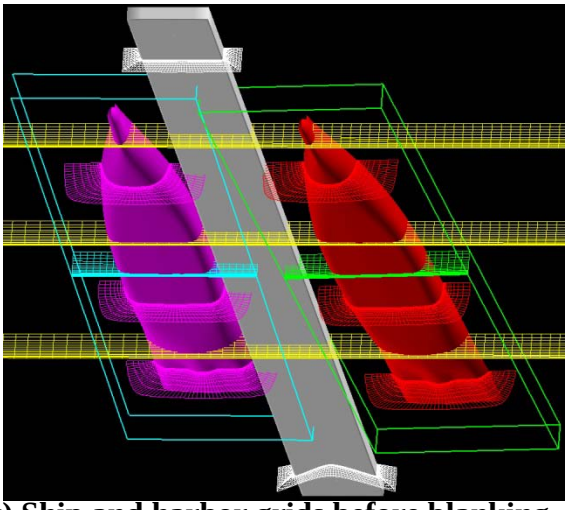

(c) Ship and harbor grids before blanking

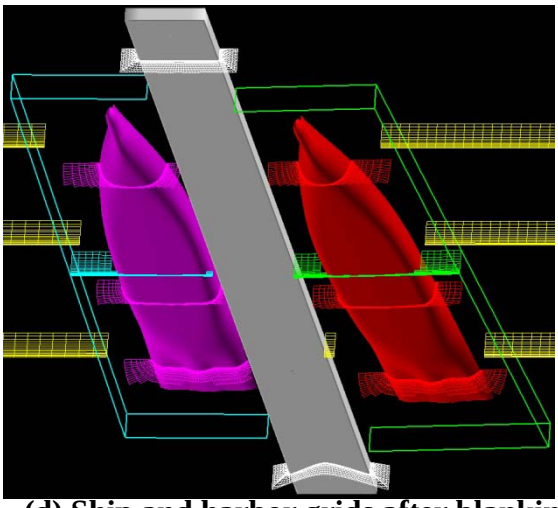

(d) Ship and harbor grids after blanking

Figure 25. Solution Domain and Numerical Grids

6.1.2 Results

This Chimera grid system as shown in Figure 25(b) was used to explore the impacts of ship

berthing on pier dynamics. Simulations were performed with the docking ship approaches the pier at either 0 degree (parallel berthing) or 5 degree oblique angle. For the sake of brevity, we shall present detailed results for the 5 degree oblique angle case only. Figures 26 and 27 show the computed pressure contours and velocity vectors at selected instants to illustrate the transient flow field induced by the docking ship and the interaction among the docking ship, moored ship, and the floating pier. Complete force and motion histories of the ships, floating pier, and coupling members were shown in Figures 28 through 31 to facilitate a detailed discussion on the dynamic characteristics of the integrated pier system.

Docking Ship The docking ship started out with zero speed under tug assistance. The tug eventually applied a constant thrust of 21.85 tons after going through an initial linear startup ramp of 100 seconds as shown in Figure 28(a). The docking ship continued to accelerate and gradually approaches a nearly constant speed of 0.20 m/s as seen in Figure 31(a) when the fluid resistance offset the tug thrust. It is further assumed that the tug was in full control and is able to maintain the docking ship at a 5 degree oblique angle to the pier before the tug thrust was shut off at t = 709.5 sec. It is seen from Figure 26 that the docking ship induced a strong pressure field in front and behind the ship path. The high-pressure in front of the ship path propagates rather quickly toward the floating pier, subsequently bounces off the pier and the moored ship, and returns to impact the docking ship. The pressure system continued to bounce back and forth between the two ships. Consequently, the sway force acting on the docking ship as shown in Figure 31(a) oscillated slightly even though the tug maintained the same thrust.

Upon released by the tug at a distance of about 9 m away from the pier, the docking ship was free to motions in water plane, namely surge, sway, and yaw, and continued to drift at a decreasing speed toward the pier under her own inertia until making contact with fenders at t = 776.8 sec. It is seen from Figure 29(a) that Fender 5 touched the stern first because of the oblique approach of the docking ship towards the floating pier. After the initial contact with pier, the ship begins to yaw clockwise as seen in the motion histories shown in Figure 30(a). It is surprising to note in Figure 31(a) that the docking ship decelerated the most rapidly, although very briefly, at the onset of fender compression when the fender reaction is low. This is mainly caused by the slight delay of the trailing water in response to ship deceleration. The docking ship acted on the fenders alone without the "help" from the trailing water. This is the only period of time ship inertia being the primary contributor to the fender reactions. The trailing water caught up in a few seconds and quickly surpassed ship inertia as the primary contributor to the fender reactions. A high pressure region was developed on the port side of the docking ship (behind the ship path) as seen in Figure 26(h) due to the impingement of the trailing water on the ship hull as the ship decelerated and eventually rebounded completely from the pier at t = 791.7 sec. After the first rebound, the Fender 5 make a second contact between t = 824.4 sec and t = 837.4 sec since the trailing water continued to push the ship towards the pier.

After the second rebound, the docking ship continued to yaw clockwise towards the pier as seen in Figures 26(i) – 26(l) and Figure 30(a). Due to the combined actions of the trailing water and ship yaw motion, the docking ship touched the Fender 2 at t = 886.0 sec and made a very brief (t = 886.9 ~ 893.5 sec) third contact with Fender 5 moments later as shown in Figure 29(a). Shortly before rebounding completely from Fender 2 at t = 914.9 sec, the ship made the primary contact with Fender 1 between t = 911.2 sec and t = 992.4 sec. It is seen from Figure 29(a) that a large share of the berthing energy of the docking ship was absorbed during this stage with Fender

1 took most of the impact loads. It is further noted from Figure 28 that a large yaw moment was developed at this stage with a rapid decrease of yaw velocity (Figure 31(a)) and a sudden slow down of the yaw motion as seen in Figure 30(a). Finally, it is also noted that the docking ship made a second contact with Fender 1 at t = 1040.0 sec, but the fender compression is significant lower than that experienced during the primary fender impact.

The complete interaction among the docking ship, floating pier, moored ship, and fender systems produced a complex pressure system as shown in Figure 26. It is quite obvious that the transient flow induced by the vessel and pier motions (see Figures 26 and 27) plays a dominant role in determining the fender compression and maximum berthing loads. As noted earlier, the ship inertia is not the primary contributor to the fender reactions except for a very brief period during initial fender compression. As soon as the trailing water caught up and fluid pressure developed, the pressure force overwhelmed ship inertia for the rest of berthing cycle. This pressure force is indeed hard to track to the ship acceleration at all. Ship inertia force is relatively small most of the berthing cycle.

Moored ship The moored ship and the floating pier began to experience pressure forces produced by the accelerating docking ship shortly after the latter took off as demonstrated by Figure 23. Mooring lines clearly witnessed these forces from early on as seen in Figure 29(c). Tensions in mooring lines increased as the docking ship approached, and relaxed rapidly when docking ship hit the Fenders 2 and 1. When the docking ship approaches the pier, it induces a high pressure region on the starboard side which pushed the moored ship away from the pier as shown in Figures 26(c) – 26(g). It is noted from Figure 29(c) that Lines 2 and 5 picked up most of the loads since they were used primarily to restrict the sway motion of the docking ship away from the pier.

After the docking ship hit Fender 1 at t = 911.2 sec, a strong pressure depression was developed in the narrow passage between the two ships as shown in Figures 26(m) – 26(r). The moored ship was pulled back to the pier by the mooring line tensions and the suction pressure forces between the two ships. As noted in Figure 29(a), the returning moored ship hit Fender 4 first at t = 968.1 sec before hitting Fender 3 at t = 982.1 sec. The tensions on Lines 2 and 5 relaxed while Fenders 3 and 4 picked up loads when the returning moored ship hit the pier. After the fender impacts, the moored ship experience significant yaw as seen in Figures 30(b) and 31(b). The mooring Lines 3 and 4 picked up substantial tension due to the surge motion of the moored ship (see Figure 29(c)) since they were used to restrict the ship drifting along the pier.

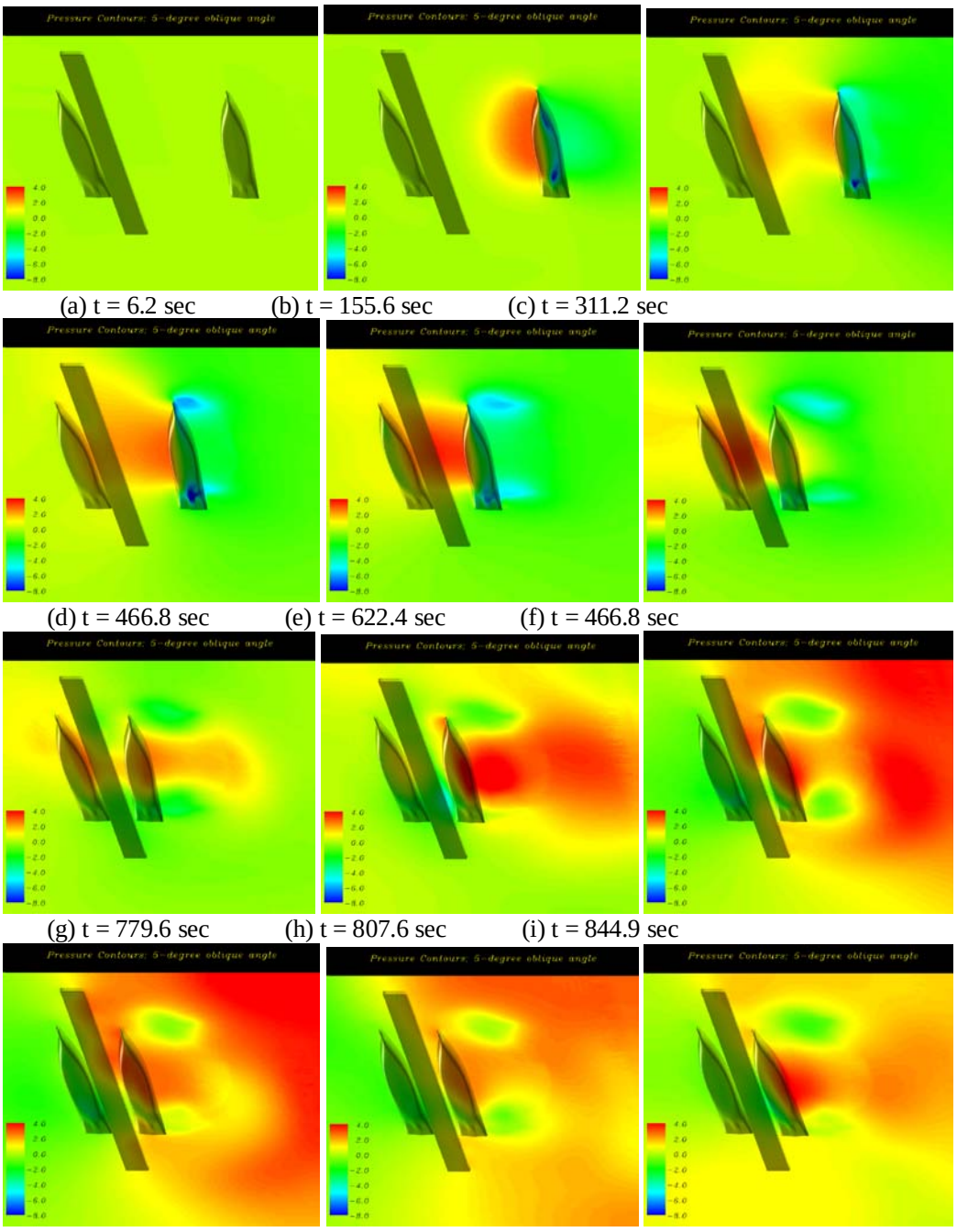

(a) t = 6.2 sec (b) t = 155.6 sec (c) t = 311.2 sec

(d) t = 466.8 sec (e) t = 622.4 sec (f) t = 466.8 sec

(g) t = 779.6 sec (h) t = 807.6 sec (i) t = 844.9 sec

(j) t = 863.6 sec (k) t = 900.9 sec (l) t = 938.3 sec

Figure 26. Pressure contours during oblique docking.

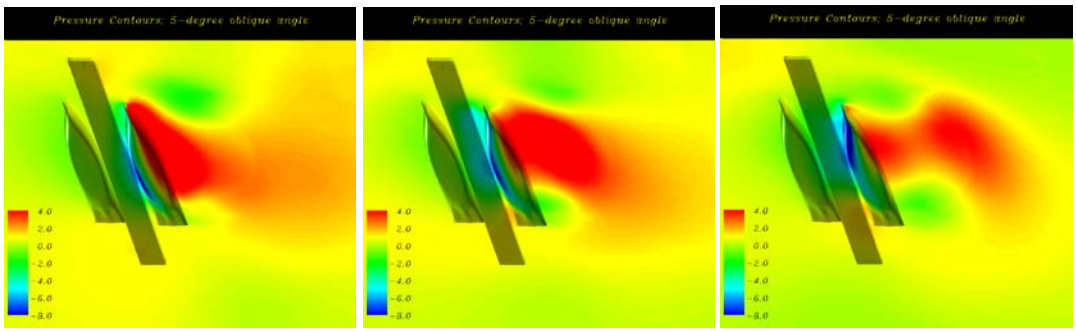

(m) t = 956.9 sec (n) t = 975.6 sec (o) t = 994.3 sec

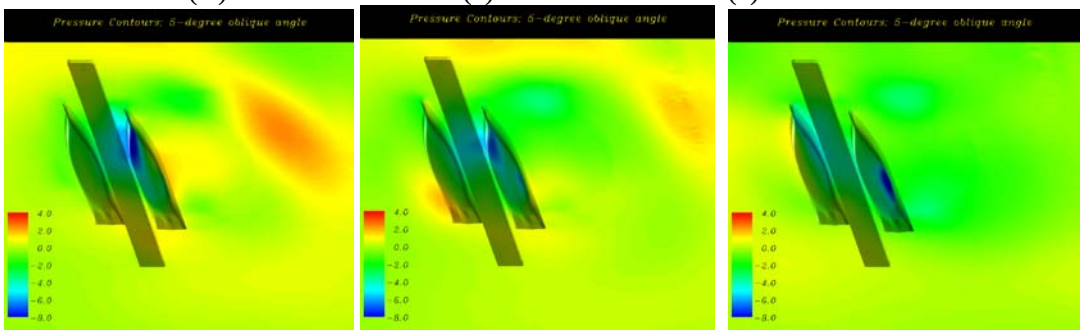

(p) t = 1013.0 sec (q) t = 1031.6 sec (r) t = 1087.6 sec

Figure 26. Pressure contours during oblique docking. (continued)

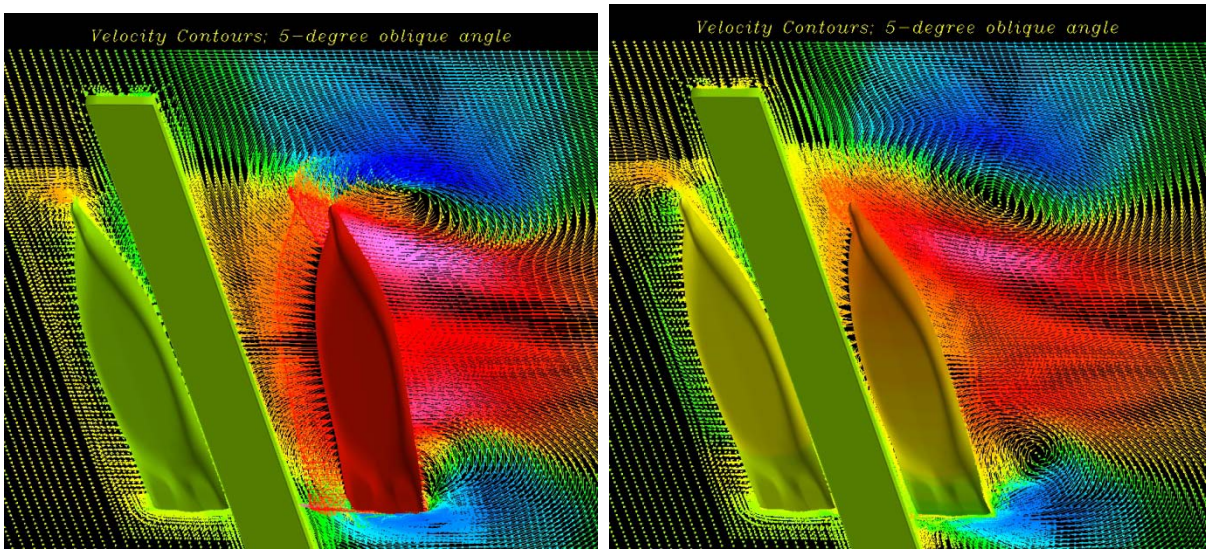

(a) t = 622.4 sec (b) t = 900.9 sec

Figure 27. Free surface velocity vectors.

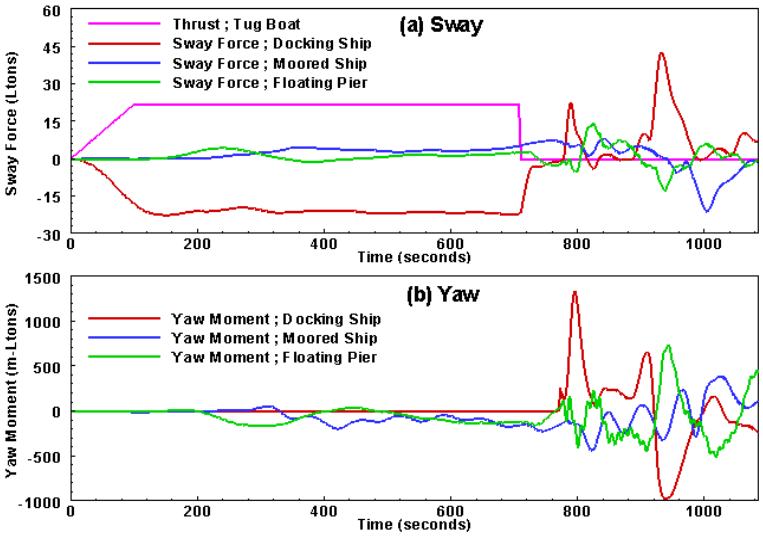

Figure 28. Sway forces and yaw moments acting on the ships and pier.

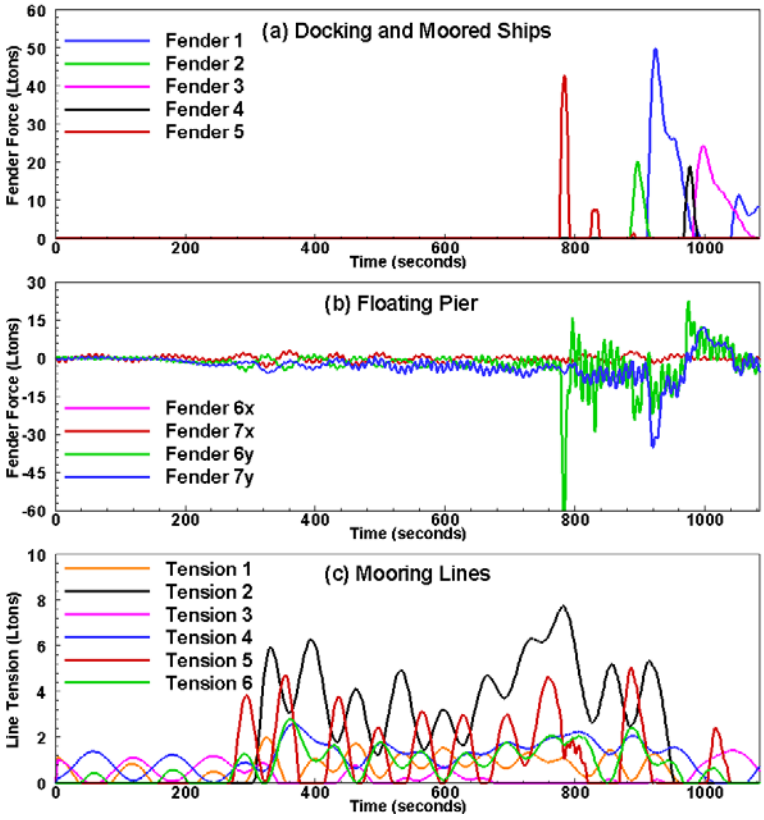

Figure 29. Fender forces and mooring line tensions

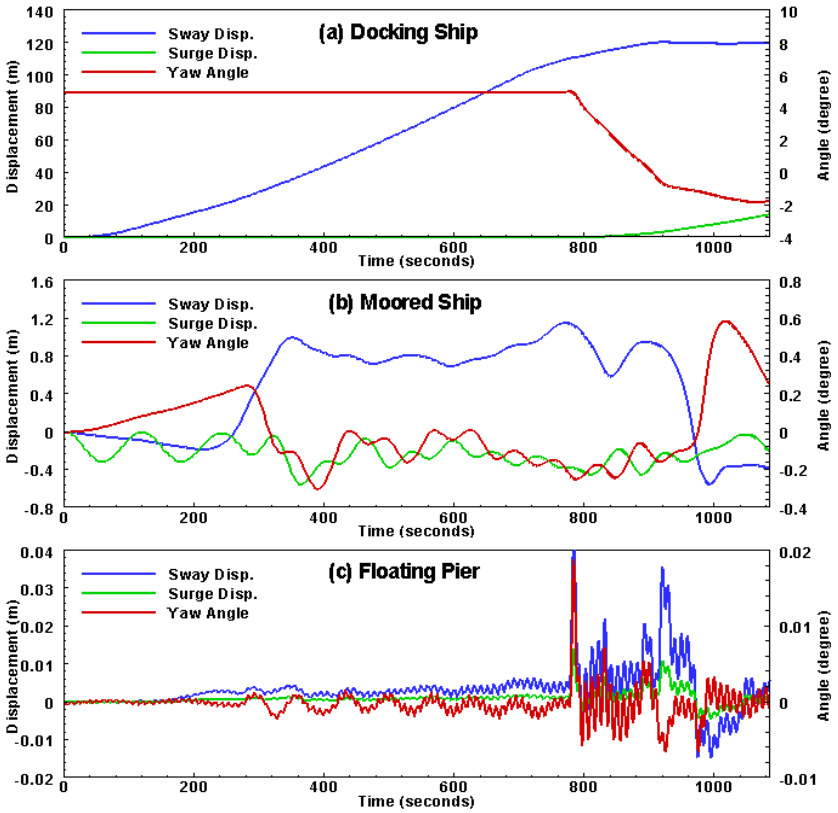

Figure 30. Motion histories of the ships and pier

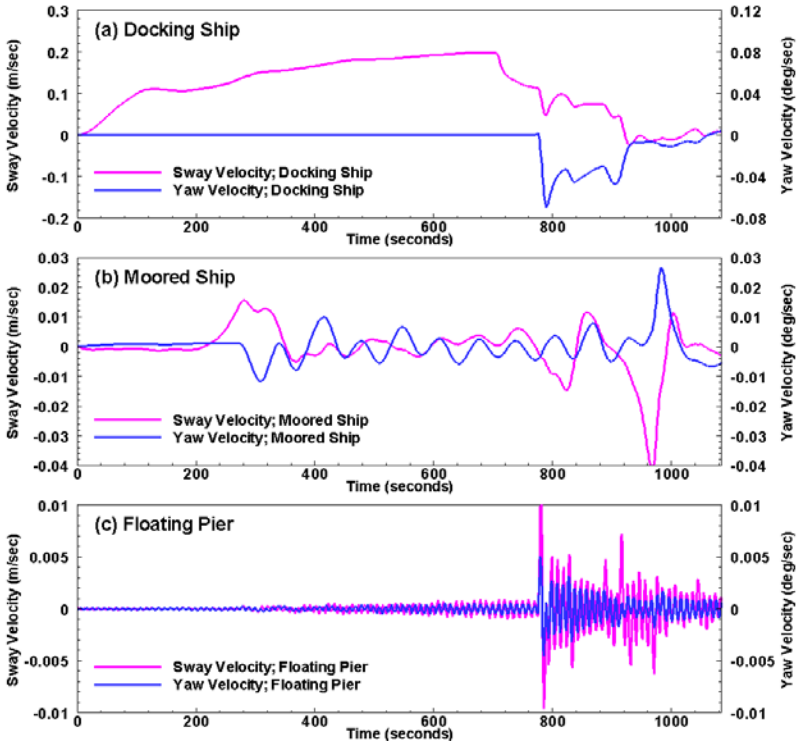

Figure 31. Sway and yaw velocities of the ships and pier

Floating pier The floating pier is held by two stiff mooring dolphins and is free to heave otherwise. These dolphins are the ultimate anchors for the entire system. In addition to holding the floating pier from drifting, they also resist berthing loads transferring through outer fenders and secure ships at berth through mooring lines. Figures 30(c) and 31(c) summarize pier motion responses during berthing process. These dolphins are very effective in restricting the pier movement. The pier moved by no more than 0.10 m and rotated by less than 0.04 degrees in the berthing operation considered here. It reacted primarily to berthing force and moment shown in Figure 28. Direct fluid force is too small to make meaningful impact. The pier surged at its nature frequency and was further modulated by the motion of the moored ship as seen in Figures 30(b) and (c). The high frequency oscillation in sway mode was reduced by the large displacements imposed by the docking ship. The pier deflected according to which of the two ships dominated. The dynamic pressure throughout the berthing process was insignificant in comparison with the buoyancy force. The pier is expected to float at its mean draft all the time. Its minor sway motion did not seem to affect the outer fenders either.

It can be seen from Figures 29(a) and (b) that the fender forces on the pier are more or less in balance. The net force could be applied to drive pier motion is relatively small. This implies a static process from the pier's point of view. In other words, the transient flow induced by the docking ship changed at a much slower pace than the pier can react. The pier vibrates insignificantly in comparison with the deflection produced by the berthing forces.

Effects of approach angle This series examined parallel and oblique berthing scenarios, respectively, for pier layouts involving only one moored ship on the port side of the pier. These studies indicate that the flow field in the narrow conduit enclosed by the ships, the pier, and the sea floor critically affects the ship behaviors, especially as the docking ship draws near the close vicinity of the pier. The water mass driven by the docking ship primarily goes under the pier and around the moored ship due to the extremely small clearance under keel. This flow pattern continues due to the established fluid momentum despite the water supply being cut off as the docking ship stops at the fenders. This leads to an intense pressure deficit in the conduit, which continues to suck both vessels into the pier for an extensive duration. Figure 32 compares the pier responses to docking ships approaching at 0 and 5 degrees. The oblique ship appears to hit the pier slightly harder and shake the pier a little more.

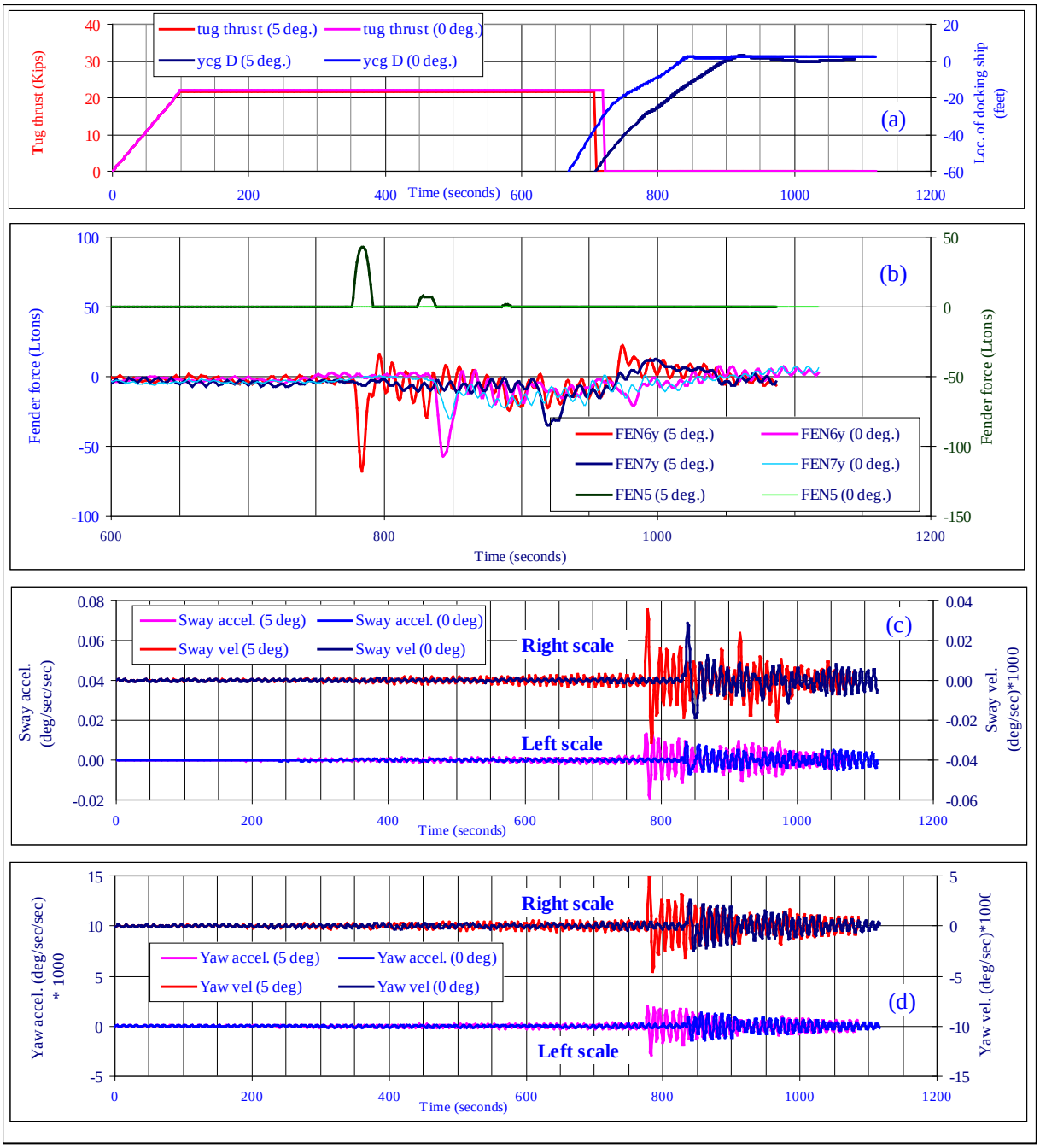

Figure 32. Compare MHP responses induced by parallel and oblique docking

6.2 MHP with Multiple Moored Ships

A second moored ship was added between the pier and docking ship in the wake of the previous cases with one client ship at the MHP to investigate the flow pattern at a congested MHP and its impacts on MHP performance as well as the interactions among vessels. One model ship is moored to the port side and a second ship was moored to the starboard side as shown in Figure 33. Each moored ship was restrained by six symbolic mooring lines, which represent important

features of a typical ship mooring. Four foam fenders are hung on both sides of the pier at the water surface to facilitate coupling with vessels. Fender 5 is attached near the stern, on the starboard side, of the docking ship to prevent hard contact when the ship approaches obliquely to the pier. In addition, Fenders 6 and 7 are hung on the port side of the second moored ship to facilitate coupling with the docking ship. Designations of these coupling structures are assigned in Figure 33. A docking ship initially at 182.88 m (600 ft) from the pier (center to center) will berth at either 0 degree (parallel berthing) or 5 degree oblique angles to pier under tug assistance. The tug applies a constant thrust of 21.85 tons on the way after going through a linear startup ramp in the initial 100 seconds. The docking ship was released by the tug at a short distance from touching the fenders and since drifted on her own into the berth.

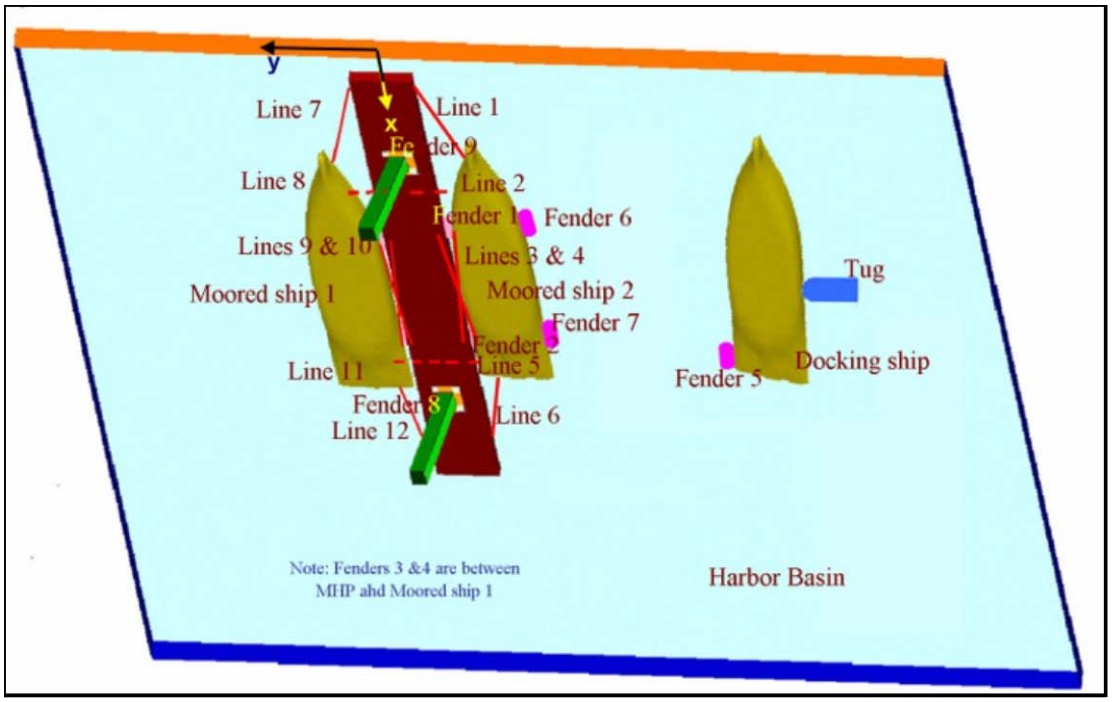

Figure 33. Tug assisted, oblique docking to MPH with two moored ships.

6.2.1 Numerical grid system

A generic harbor basin of constant depth was selected for this simulation. A shallow water depth of 8.53 m was intentionally chosen to confine the under keel clearance of the docking and moored ships to roughly 0.3 m, or 3.7 percent of the ship draft. All three ships are of identical hull of 41,150 tons. This combination of a deep draft with a small under keel clearance gives a worse case berthing force for fender design consideration. In the chimera domain decomposition approach, the ships, pier, and harbor grids can be generated independently with arbitrary grid overlaps. Figures 34 (a) and (b) show the 13-block numerical grid used in the present study. A fine grid, inner block (blue) is embedded in a coarse grid, outer block to balance the local details and computation efficiency. The pier and ship grids are embedded in the harbor basin grid and are free to move with respect to the harbor grids in arbitrary combinations of translational and rotational motions. Furthermore, the ship grids were allowed to extend below the basin floor as shown in Figure 34(c) such that the grid distortions can be minimized in the narrow under keel region. A phantom grid was then used to remove the grid points outside the harbor basin as

shown in Figure 34(d). This chimera grid system enables us to accommodate the relative motions among the pier, ships, and the harbor without adaptive generations of body-fitted numerical grids at each time step. This model uses a total of slightly over 1.1 million grid points.

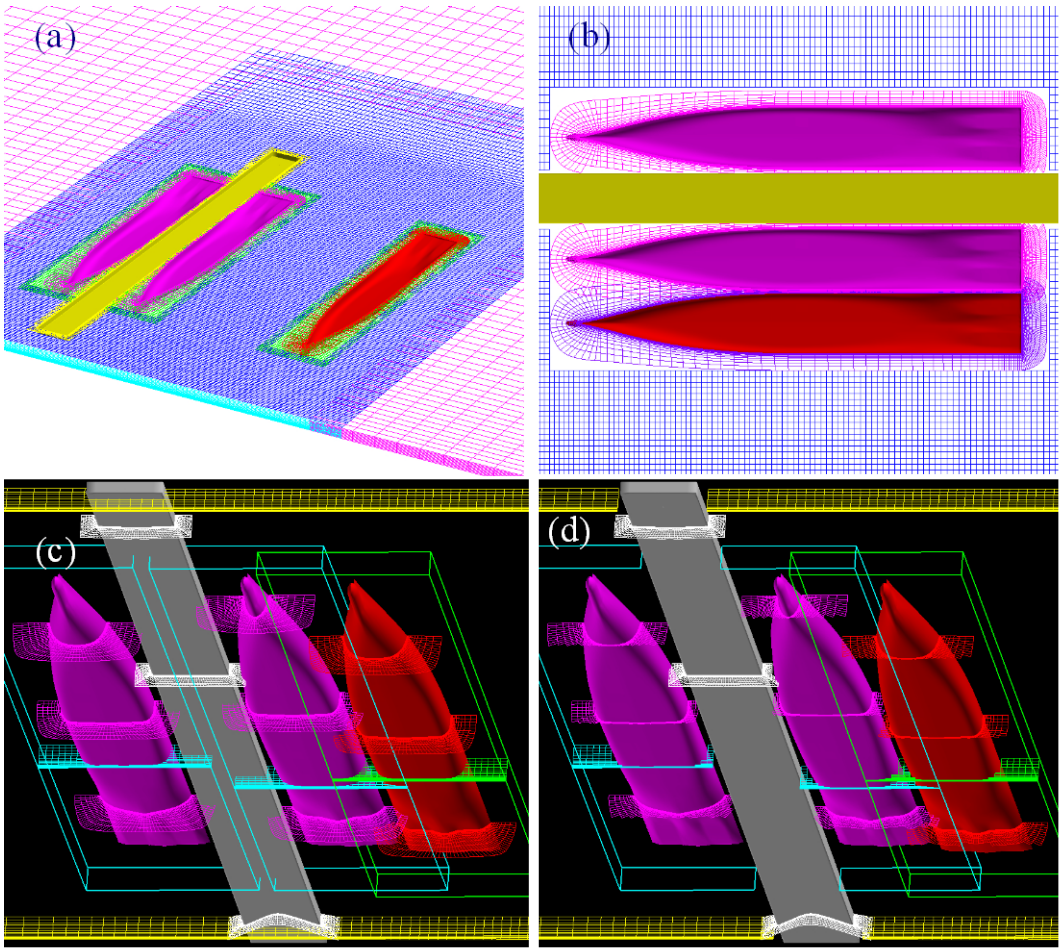

Figure 34. Solution domain and numerical grids

6.2.2 Results

Simulations were performed with the docking ship approaching the pier parallel to or at an oblique angle of five degrees. The results are similar and only the case of oblique berthing is presented in details. Figures 35 and 36 show the computed pressure contours and velocity vectors at selected instants to illustrate the transient flow field induced by the docking ship and the interaction among the docking ship, moored ships, and the floating pier. For completeness, the force and motion histories of the docking ship, moored ships 1 and 2, floating pier, and coupling members (i.e., fenders and mooring lines) were also shown in Figures 37 through 42 to facilitate a detailed analysis on the dynamic characteristics of the integrated pier system.

Docking Ship The docking ship started out with zero speed under tug assistance. The tug eventually applied a constant thrust of 21.85 long tons (Ltons) after going through an initial linear startup ramp of 100 seconds as shown in Figures 37(a) and 38(a). The docking ship

continued to accelerate and gradually approaches a nearly constant speed of 0.19 m/s as seen in Figure 39(a) when the fluid resistance offset the tug thrust. It is further assumed that the tug was in full control and was able to maintain the docking ship at a 5 degree oblique angle to the pier before the tug thrust was shut off at t = 680 sec. It is seen from Figure 35 that the docking ship induced a strong pressure field in front and behind the ship path. The high-pressure ahead of the ship path propagates rather quickly toward the floating pier, subsequently bounces off the second moored ship, and returns to impact the docking ship. This has led to a pressure buildup between the docking ship and the second moored ship (Figures 35(d) through (i)), and a notable increase of fluid resistance on the docking ship (Figure 37(a)) prior to fender impact. Consequently, the docking ship oscillated slightly from early on and started to decelerate noticeably around 582 second time mark as seen in Figure 39(a), even though the tug still maintained the same thrust.

Upon released by the tug at a short distance away from the second moored ship, the docking ship was free to motions in water plane, namely surge, sway, and yaw, and continued to drift at a decreasing speed (Figure 39(a)) toward the pier under her own inertia until making fender contact with the second moored ship at t = 715 sec. It is seen from Figure 38(a) that the yaw angle of the docking ship increased to a maximum of 5.55 degree shortly after being released. The additional yaw in the counterclockwise direction can be attributed to the larger fluid resistance around the bow. As noted in Figure 36, the deep and narrow bow section produced much stronger flow recirculation and much higher resistance in comparison with the relatively flat and shallow stern section. This recirculation pattern persisted long after the docking ship stopped at the berth.

It is seen from Figure 40(a) that Fender 5 touched the second moored ship first because of the oblique approach of the docking ship towards the floating pier. The maximum fender compression force is about 44.5 Ltons during the initial impact. After the initial contact with pier, the docking ship begins to yaw clockwise as seen in the motion histories shown in Figure 38(a). It is interesting to note in Figure 40(a) that the docking ship decelerated the most rapidly, although very briefly, at the onset of fender compression when the fender reaction is low. This is mainly caused by the slight delay of the trailing water in response to ship deceleration. The trailing water caught up in a few seconds and quickly surpassed ship inertia as the primary contributor to the fender reactions. A high pressure region was developed on the port side of the docking ship (behind the ship path) as seen in Figure 35(i) through (k) due to the impingement of the trailing water on the ship hull as the ship decelerated and eventually rebounded completely from the pier at t = 725 sec. Shortly after the first rebound, Fender 5 made a second contact with even higher fender compression force of 59.0 Ltons between t = 732 sec and t = 741 sec (see Figure 40(a)) since the trailing water continued to push the ship towards the pier. The fender reactions for the three-ship interaction case considered here is significantly more complicated than those observed in case with one client ship at the MHP with the docking ship contacting the pier directly.

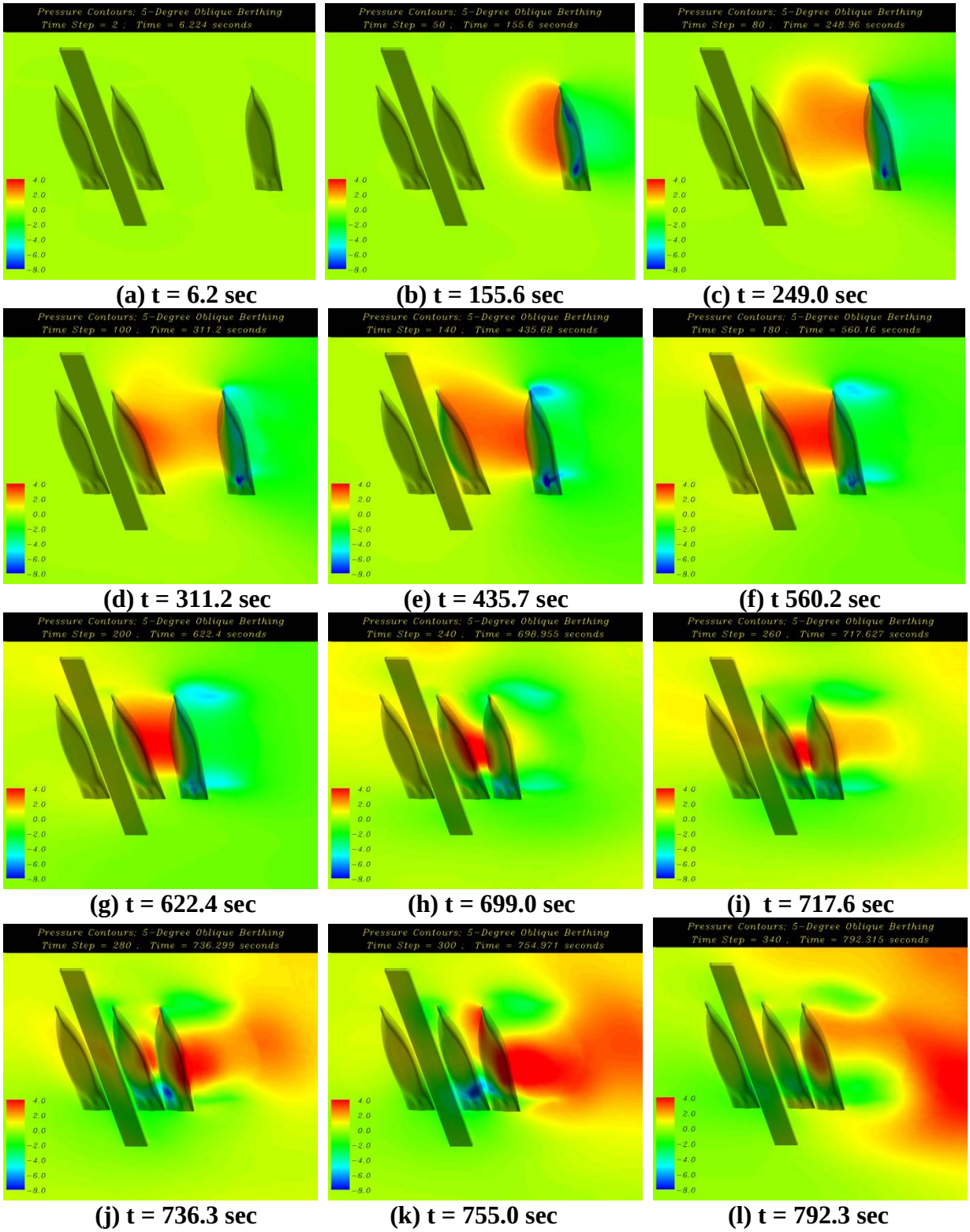

(a) t = 6.2 sec **(b) t = 155.6 sec** **(c) t = 249.0 sec**

(d) t = 311.2 sec **(e) t = 435.7 sec** **(f) t 560.2 sec**

(g) t = 622.4 sec **(h) t = 699.0 sec** **(i) t = 717.6 sec**

(j) t = 736.3 sec **(k) t = 755.0 sec** **(l) t = 792.3 sec**

Figure 35. Pressure contours around ships and pier.

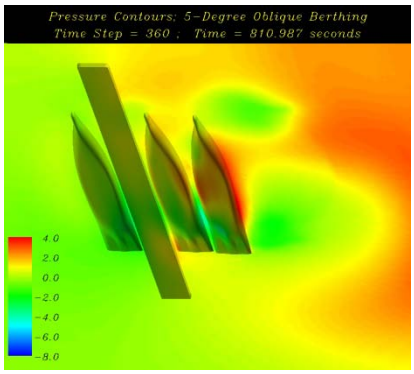

(m) t = 811.0 sec

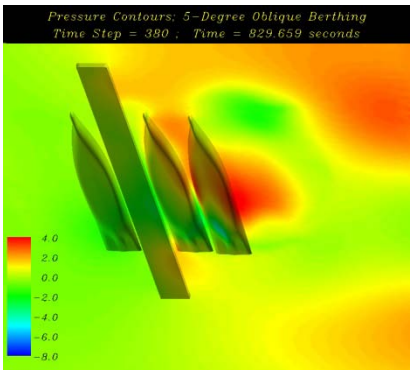

(n) t = 829.7 sec

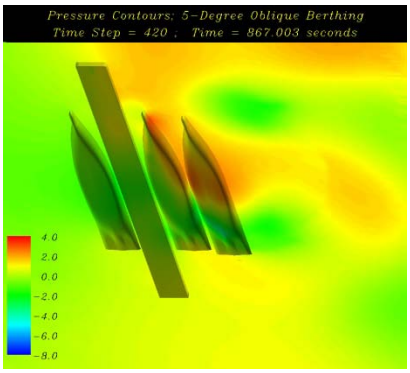

(o) t = 867.0 sec

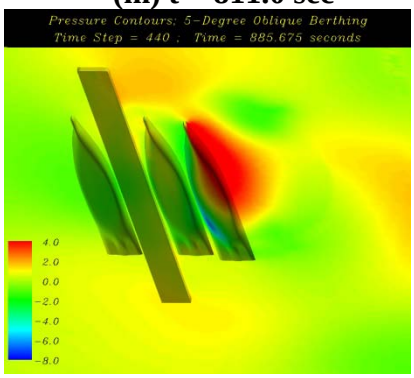

(p) t = 885.7 sec

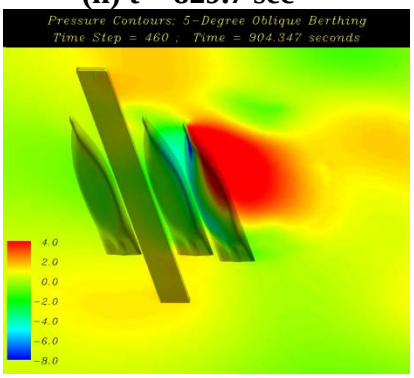

(q) t = 904.3 sec

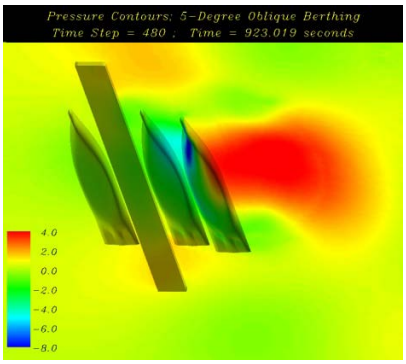

(r) = t = 923.0 sec

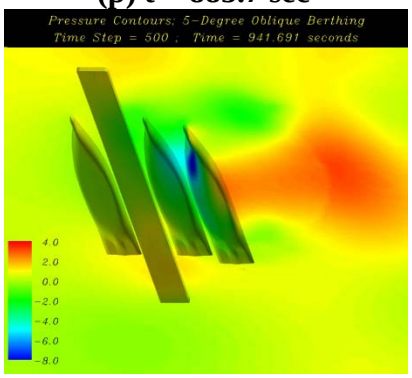

(s) t = 941.7 sec

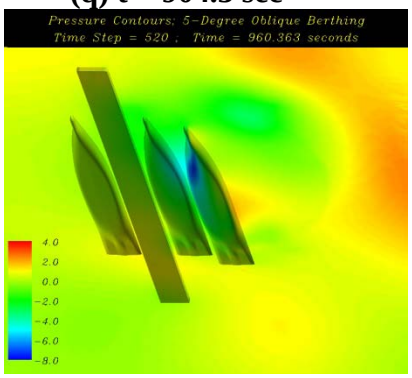

(t) t = 960.4 sec

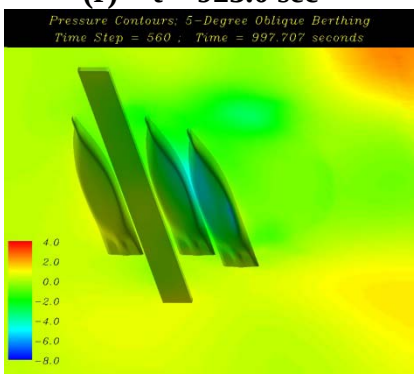

(u) t = 997.7 sec

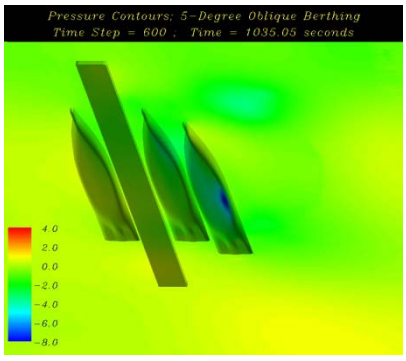

(v) t = 1,035.1 sec

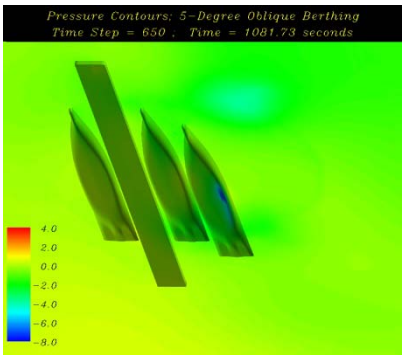

(w) t = 1,081.73 sec

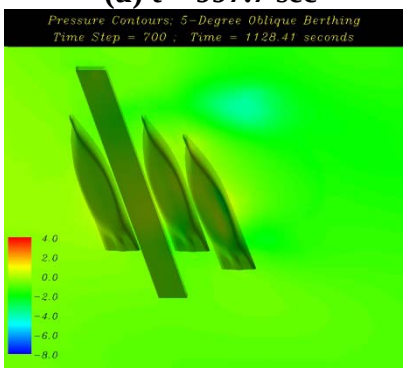

(x) t = 1,128.41 sec

Figure 35. Pressure contours around ships and pier. (continued)

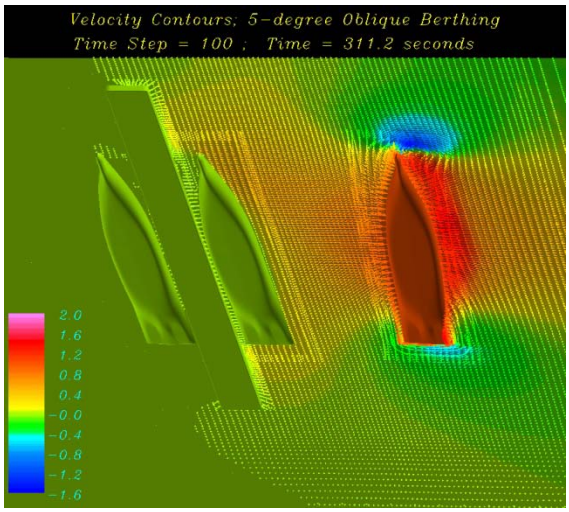

(a) t = 311.2 sec

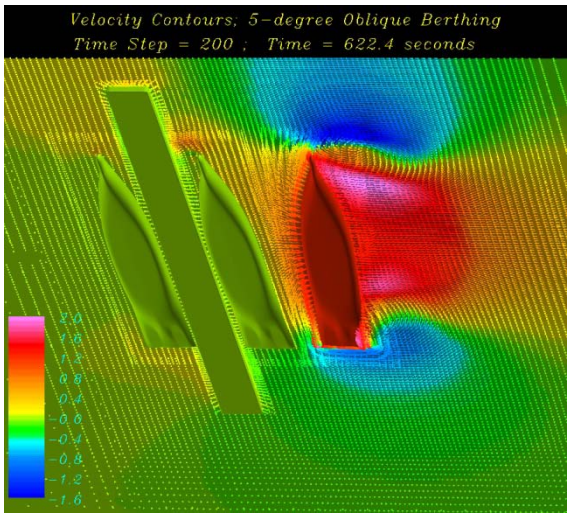

(b) t = 622.4 sec

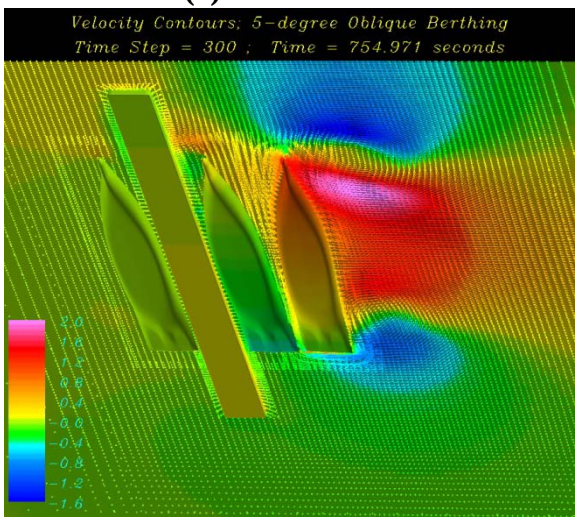

(c) t = 755.0 sec

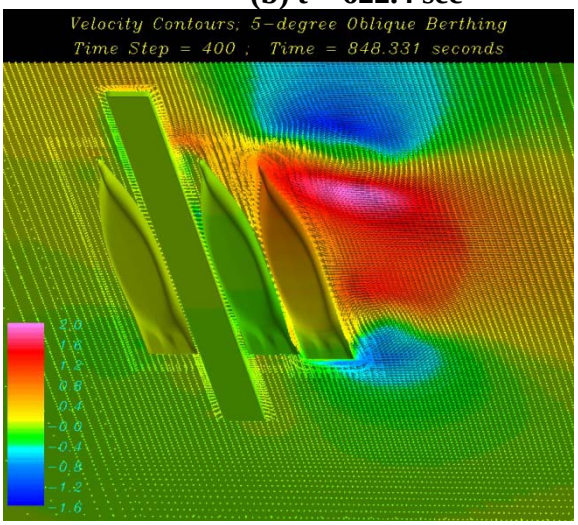

(d) t = 848.3 sec

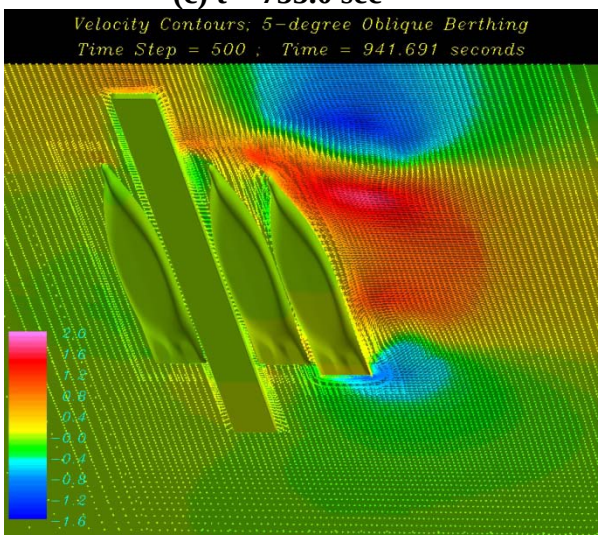

(e) t = 941.7 sec

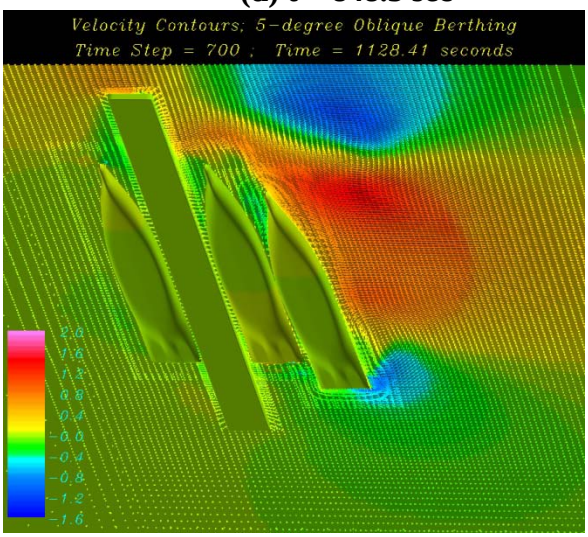

(f) t = 1,128.4 sec

Figure 36. Velocity vector plots.

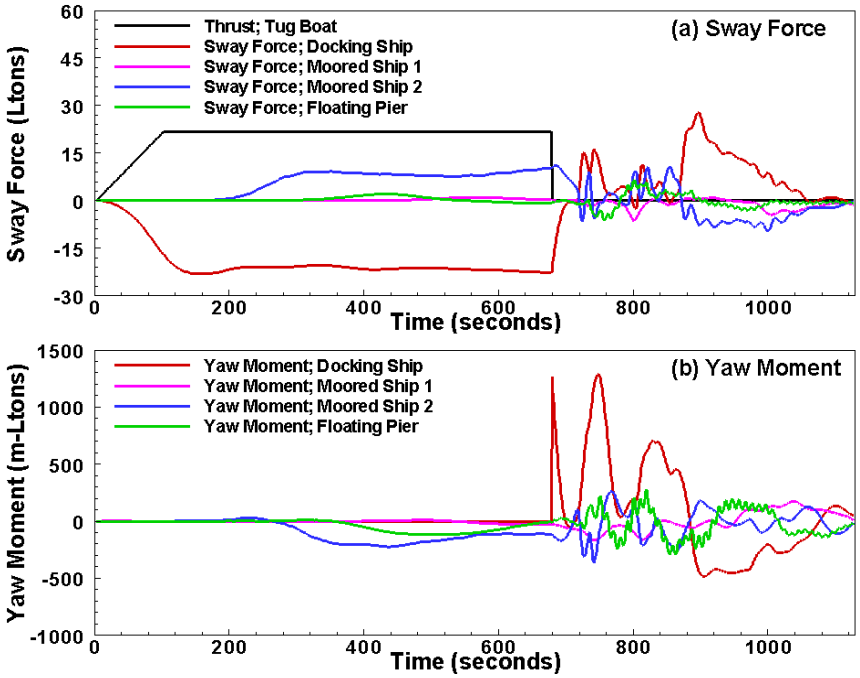

Figure 37. Sway forces and yaw moments acting on the ships and pier.

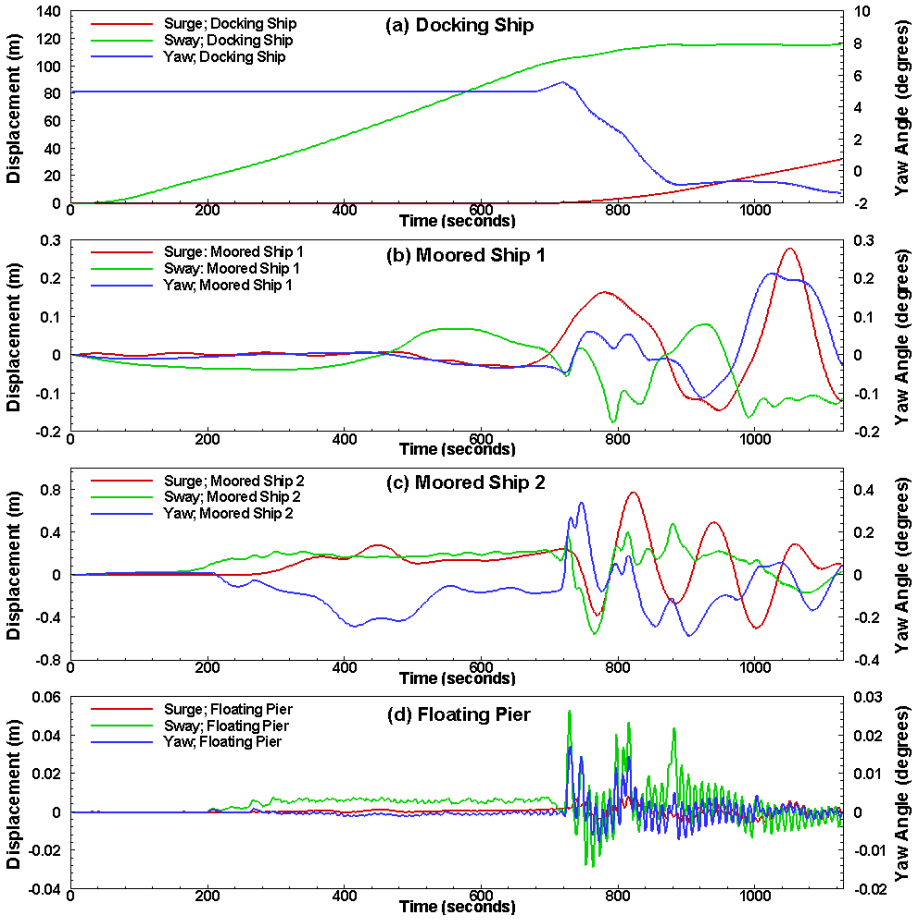

Figure 38. Motion histories of the ships and pier.

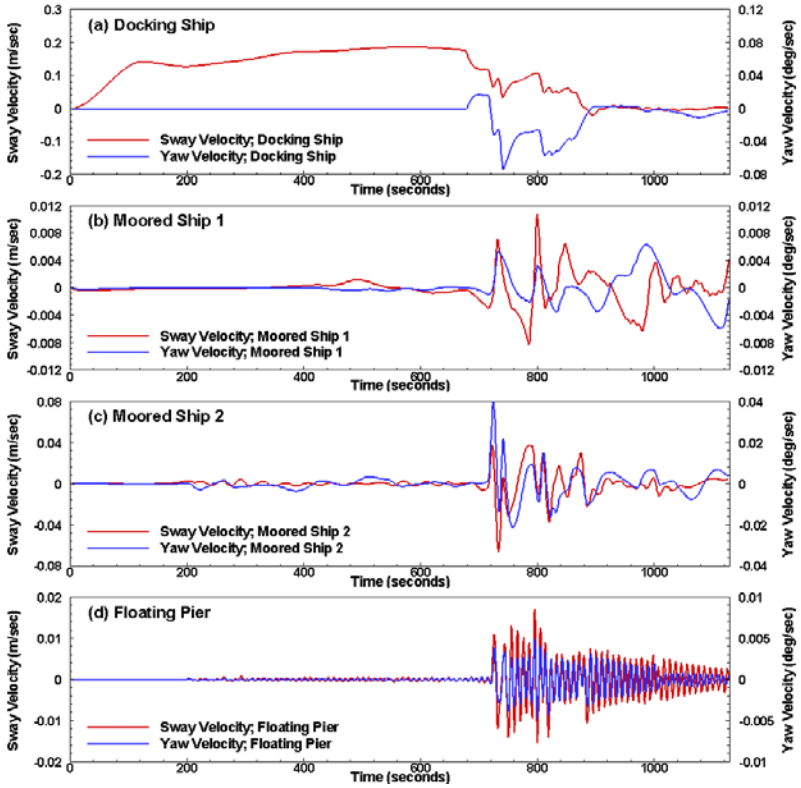

Figure 39. Sway and yaw velocities of the ships and pier.

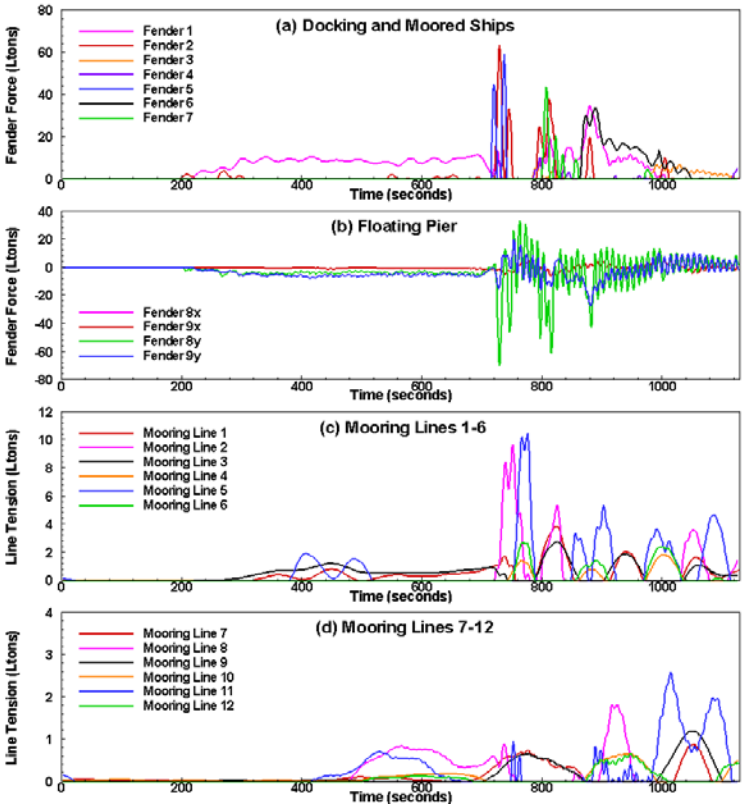

Figure 40. Fender forces and mooring line tensions.

After the second rebound, the docking ship continued to yaw clockwise towards the pier as seen in Figures 35(j) through 35(n) and Figure 39(a). Due to the impact of the docking ship, the second moored ship was pushed towards the floating pier and made the primary impact with Fender 2 at t = 720 sec with a maximum fender force of 62.3 Ltons. The second moored ship rebounded from Fender 2 at t = 736 sec, but made another contact between t = 740 sec and 750 sec with a maximum loading of 33.1 Ltons. It is seen from Figure 40(a) that a large share of the berthing energy of the docking ship was absorbed during this stage with Fenders 5 and 2 took most of the impact loads. A detailed examination of Figure 40(a) indicates that the berthing energy was imparted first on Fender 5, and then transferred through the second moored ship to Fender 2 with several seconds of time delay. It is further noted from Figure 32 that a large yaw moment was developed around the docking ship at this stage with a rapid decrease of yaw velocity (Figure 39(a)) and a sudden slow down of the yaw motion as seen in Figure 38(a).

Due to the combined actions of the trailing water and the yaw motion, the docking ship made the primary impact with Fender 7 during t = 799 through 812 sec, followed by three additional impacts with smaller magnitude between t = 818 sec and t = 860 sec as seen in Figure 39(a). Shortly after rebounding completely from Fender 7, the docking ship made the primary contact with Fender 6 between t = 864 sec and t = 1,049 sec. A large part of the berthing loads acting on Fender 3 was subsequently transferred through the second moored ship to Fender 1. It is seen from Figure 35(a) that stern Fenders 2, 5 and 7 took most of the initial impact loads. However, the majority of the berthing energy was actually absorbed by the bow Fenders 6 and 1 since they were in contact with the moored ship and floating pier for a much longer period of time.

The complete interaction among the docking ship, floating pier, moored ship, and fender systems produced a complex pressure system as shown in Figure 35. It is quite obvious that the transient flow induced by the vessel and pier motions (see Figures 35 and 36) plays a dominant role in determining the fender compression and maximum berthing loads. As noted in the previous cases, the ship inertia is not the primary contributor to the fender reactions except for a very brief period during initial fender compression. As soon as the trailing water caught up and fluid pressure developed, the pressure force overwhelmed ship inertia for the rest of berthing cycle. This pressure force is indeed hard to track to the ship acceleration at all. Ship inertia force is relatively small most of the berthing cycle.

Moored ships The moored ships and the floating pier began to experience pressure forces produced by the accelerating docking ship shortly after the latter took off as shown in Figures 37. Mooring lines clearly witnessed these forces from early on as seen in Figure 40. Tensions in mooring Lines 7 through 12, which were used to restrain the motion of the first moored ship, increased as the docking ship approached the pier and relaxed rapidly after the docking ship hit the fenders. It is noted from Figure 40(d) that Lines 8 and 11 picked up most of the loads since they were used primarily to restrict the sway motion of the first moored ship away from the pier. It is worthwhile to note that the tensions on Lines 7 through 12 are much smaller than those observed in the case with one client ship at the pier. This can be attributed to the sheltering effects of the second client ship, which absorbed most of the berthing energy during fender impacts. Indeed, the sway and yaw motions of the second moored ship are two to three times of those encountered by the first moored ship as shown in Figure 33. Consequently, the maximum tensions on mooring Lines 1 through 6 are also significantly higher than those experienced by

Lines 7 through 12 as shown in Figure 40. It is also noted that the tensions on Lines 2 and 5 are higher than the other mooring lines since they were used primarily to restrict the sway motion of the second moored ship.

After the docking ship hit the second moored ship at t = 715 sec, a strong pressure depression was developed in the narrow gap between the docking and moored ships as shown in Figures 35(j) through 35(k). As seen in Figure 38(c), the second moored ship was pulled towards the docking ship by the suction pressure forces after the initial fender impact. The tensions on Lines 2 and 5 increased sharply while the second moored ship was pulled away from the pier. It should be noted that the total forces acting on the second moored ship including fender forces from Fenders 1, 2, 5, 6, and 7 tensions from mooring Lines 1 through 6, and hydrodynamic forces. The sway and yaw motions shown in Figure 38(c) were driven by the net forces and moments acting on the second moored ship. It is, therefore, essential to treat the floating pier, moored ships, docking ship, and coupling members (fenders and mooring lines) as an integral system in the analysis of the berthing loads.

Floating pier The floating pier is held by two stiff mooring dolphins and is free to heave otherwise. These dolphins are the ultimate anchors for the entire system. In addition to holding the floating pier from drifting, they also resist berthing loads transferring through outer fenders and secure ships at berth through mooring lines. Figures 39(d) and 40(d) summarize pier motion responses during berthing process. These dolphins are very effective in restricting the pier movement. The pier moved by no more than 0.10 m and rotated by less than 0.05 degrees in the berthing operation considered here. It reacted primarily to berthing forces and moments shown in Figure 37. Direct fluid force is too small to make meaningful impact. The pier surged at its nature frequency and was further modulated by the motion of the moored ships as seen in Figures 39. The pier deflected according to which of the two moored ships dominated. Since the motion of the second moored ship is significantly larger than that experienced by the first moored ship, the high frequency oscillation in sway mode of the floating pier was observed to be nearly in phase with the large displacements imposed by the second moored ships. The dynamic pressure throughout the berthing process was insignificant in comparison with the buoyancy force. Therefore, the pier is expected to float at its mean draft all the time. Its minor sway motion did not seem to affect the outer fenders either.

6.3 Effect of Ship Configurations

The moored ships at the MHP substantially complicate the near field flow patterns around the pier as demonstrated by the two cases presented in this chapter. Although the overall patterns are similar, local disparities are clearly noticeable. These disparities drive pier and vessels to act differently. However, the effects are case dependent and are believed secondary to the primary factors, such as docking ship inertia and the water mass it draws during docking process. The details are more of academic interests and will not substantially benefit the conceptual design. Instead, the influence of moored ships will be assessed as perceived by the MHP. Realistic ship configurations at the MHP facility are innumerable. Two basic parameters concern the holding capacity of the founding shafts are the approach angle of the docking ship and the configuration of moored ships alongside the pier. These two parameters will be screened to pick the most representative scenario for the search of the most probable docking load.

6.3.1 Effect of approach angle

Traditional wisdom recommends docking a large ship at a small oblique angle. This process eases the transfer of tremendous kinetic energy of a large docking ship to pier via multiple fender contacts. The previous exercises tested this convention by docking the same ship at approach angles of 0 and 5 degrees to MHP with one and two moored ships, respectively. Other conditions remain identical. Figures 36 and 37 compare the results of ship docking to MHP with two moored ships. Figure 41(a) summarizes the force histories imposed on the docking ship. Figures 41(b) through (d) trace the load path of load transfer. For the case of oblique docking, Fender 5 made initial contact and passed the load through Fender 2 and then Fender 8 to the outboard founding shaft. The docking ship rotated counterclockwise subsequently and touched Fender 7 and Fender 6 consecutively. Likewise, proper foam fenders response and transferred the load to the inboard founding shaft as Fender 6 took major part of the docking load. The same worked for the case of parallel docking. The oblique docking ship loaded Fender 5 more than the parallel docking ship did to Fender 7 on the initial impact. The oblique docking ship landed softer than the parallel docking ship on the second impact at Fender 6 in this case. Regardless the differences in load paths, Fenders 8 and 9 experienced similar loads as shown by Figure 41(d). Figure 42 indicates the resulting motions of MHP due to parallel and oblique dockings are also comparable. However, Figure 42(a) derived from the case with one moored ship at the MHP painted a slightly different picture. In this case, the load path still aligned properly and the interior fenders experienced comparable loads for parallel and oblique dockings. However, the second impact on Fender 1 was much heavier in the case of oblique docking (blue) than in the case of parallel docking (red) as shown in Figure 43 (b). This difference can be traced back to the histories of trailing water induced fluid load on the docking ship (Figure 43(a)). Note that the parallel docking ship was held against Fender 1 since the second impact while the oblique docking ship hit Fender 1 and transferred loads due to ship inertia and trailing water simultaneously. The benefit of oblique docking is not as obvious as in the previous case with two moored ships. But the small difference of 5 degrees in the approach angle does not seem to be critical to the ultimate loading experienced by the interior fenders around the founding shafts.

6.3.2 Effects of client ship configuration

Figure 44 summarizes the effects of client ship configuration on the berthing forces experienced by the interior fenders. This figure compares berthing loads on the interior fenders experienced during the two previous exercises to those observed with the same ship docking to the bare MHP alone. Figure 44(a) depicts the time histories of the fluid induced forces imposed on the docking ship in three respective scenarios with zero, one, and two moored ships alongside the pier. The ship docking to the bare MHP experienced markedly higher fluid forces loads than the others, and subsequently pushed the founding shafts much harder as shown in Figure 44 (b) and (c). Besides, the fluid forces in the case of bare MHP occur briefly while the others endure much longer. This agrees with the observations of a persistent pressure deficit in the conduit confined by the pier and ships discussed in Section 6.2. Note that the fluid induced forces in the case of bare MHP are closer inline with the docking ship deceleration upon fender contact. At this point, fenders bear the inertia force from the docking ship and thrust from the ambient fluid simultaneously as seen from the sharp spike in the force history of inner fender at the outboard

end. As the docking ship normally stops rather quickly taking ship inertia out of the action, fluid forces remain solely responsible for the fender forces throughout the rest of the docking cycle. The result is a milder but broader peak in the fender force histories. The fluid forces rise to the peak long after the docking ship stops. are can be further demonstrated by comparing to the case with ship docking to bare MHP as shown in Figure 44.

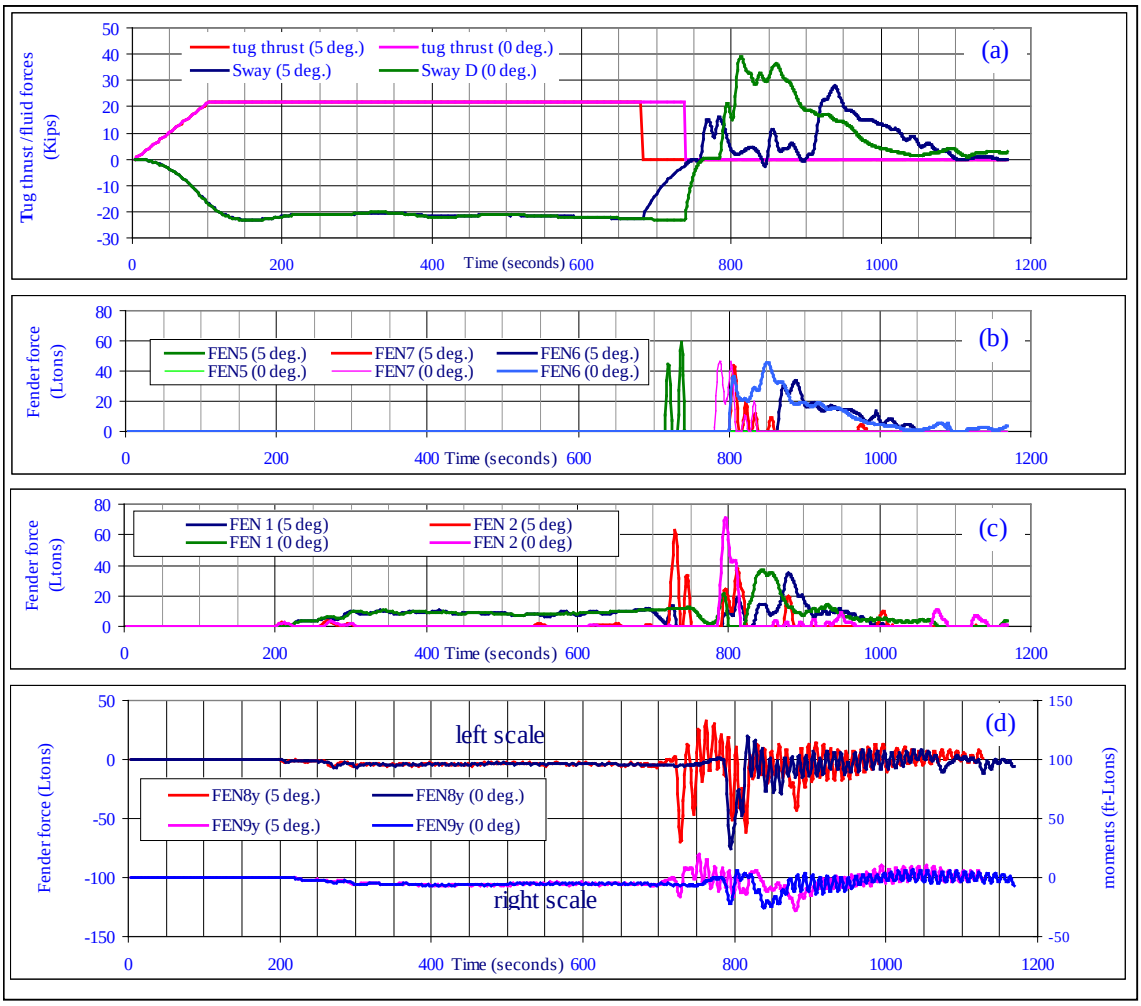

Figure 41. Effect of approach angles on founding shafts

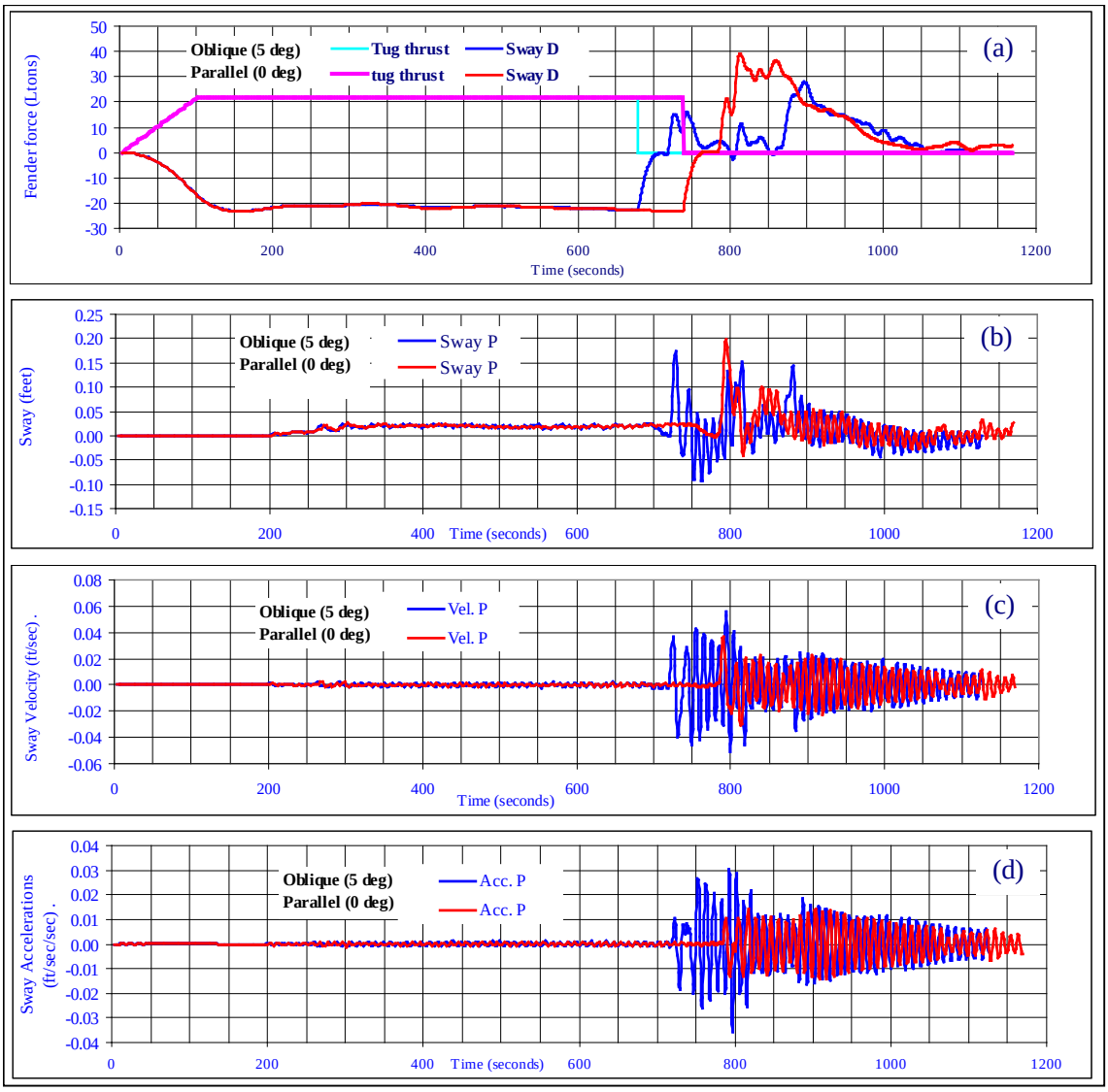

Figure 42. Effect of approach angles on the motion responses of MHP

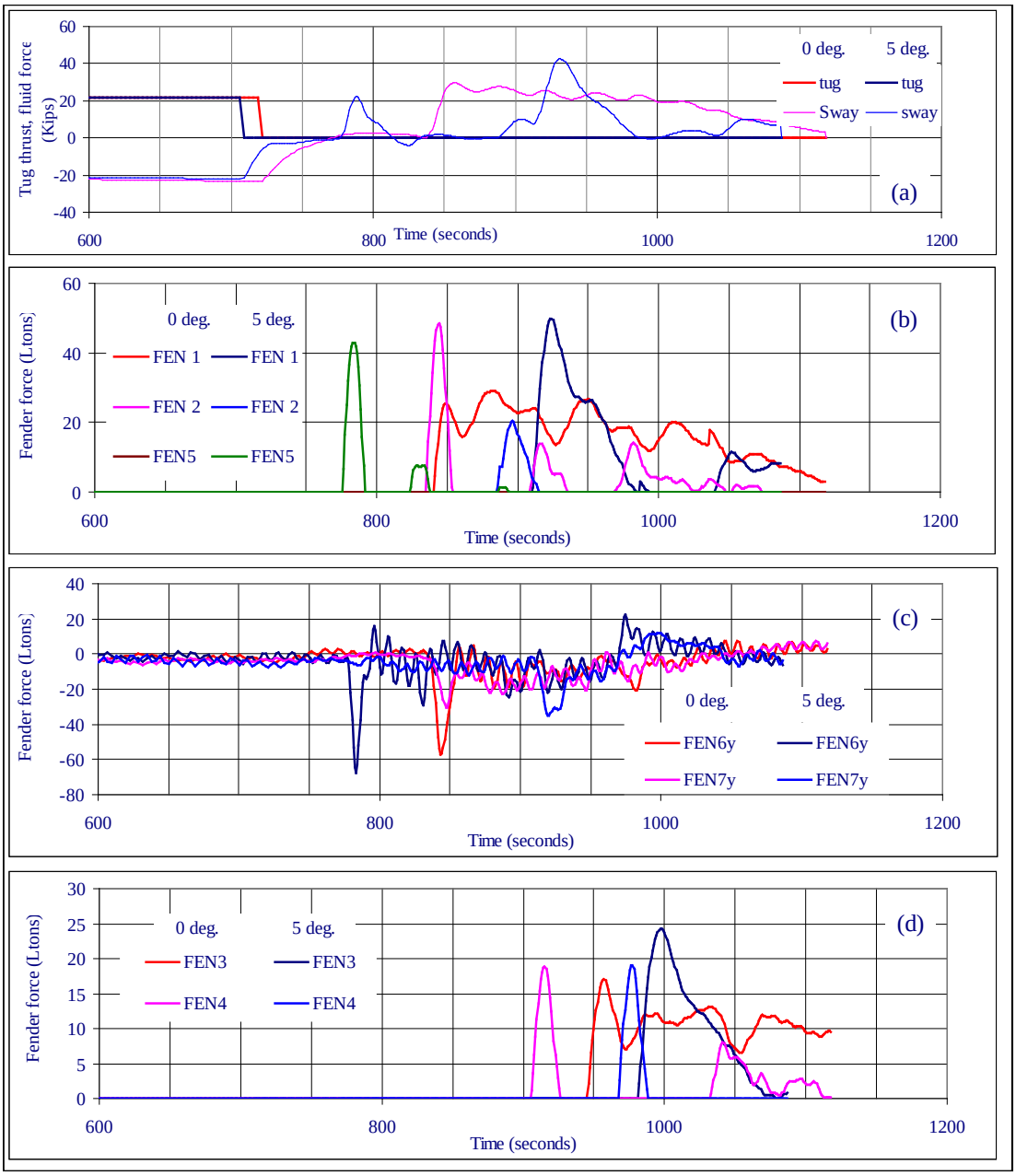

Figure 43. Performance of exterior foam fenders

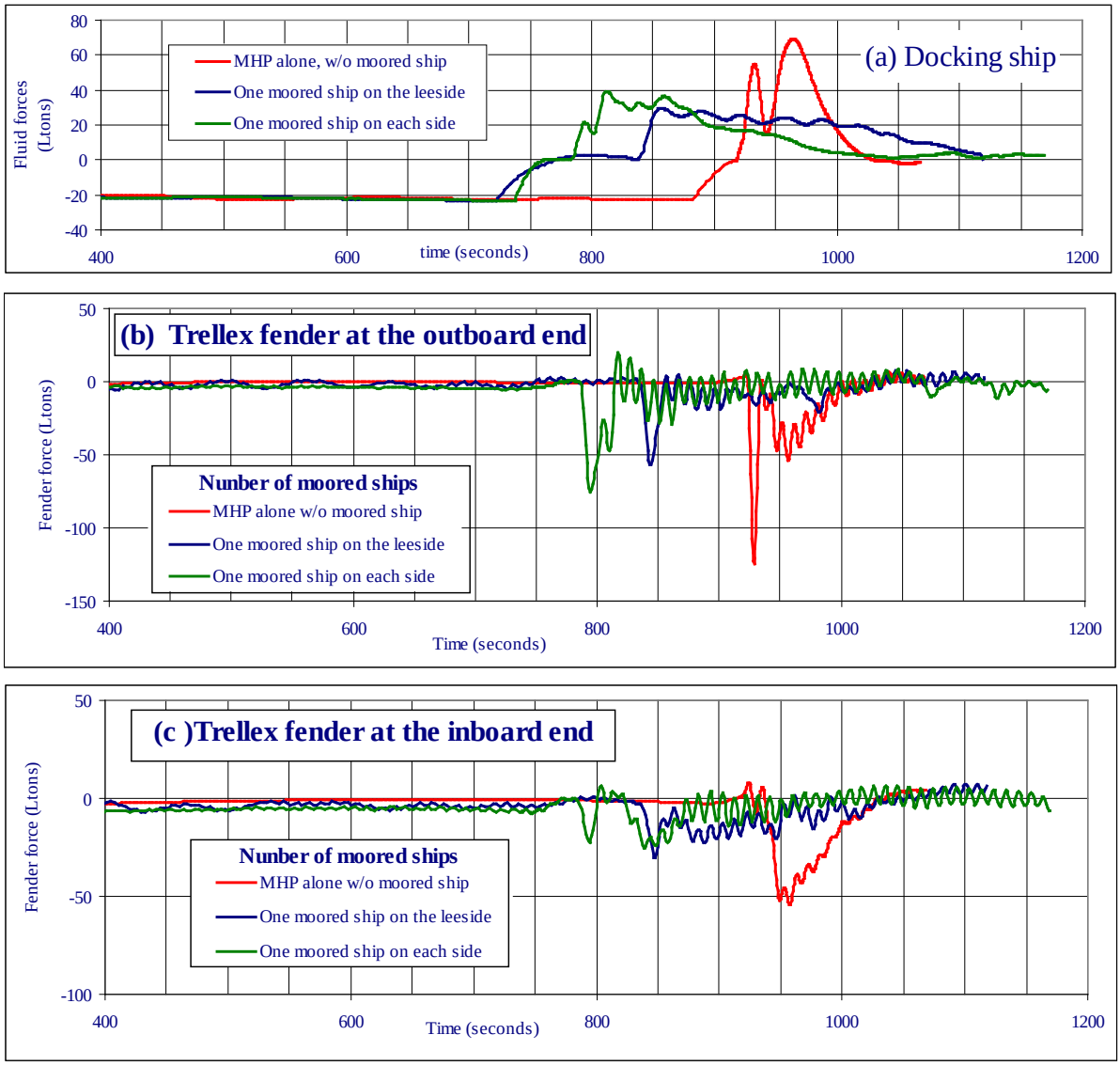

Figure 44. Effects of client ship configuration at the MHP

6.4 Summary

This exercise demonstrated the effectiveness of a RANS-based computation fluid dynamic code as a design aid. The present model successfully reconstructed a complex ship-structure event at a congested pier site in greater details than a physical model can accomplish. This code captured many important features of the transient flow around the pier and ships including the underkeel flow acceleration, separation in the wake trailing the docking ship, unique flow patterns between the ships and pier, and their impact on the participating ships. All simulation results are consistent within the scope of present study. The influence of moored ships at the pier on the ultimate berthing loads at the founding shafts is highly complicated but fully traceable. Ship responses and performance of coupling members are fully traceable to the driving fluid activities.

Even though, the present exercise did not go through the full length to quantify the exact influence of moored ships at the MHP, it clearly confirmed that a bare MHP is likely to see higher berthing loads than does the same pier with client ship moored alongside. Figure 44(a) indicates the pier tends to vibrate at its natural frequency (red) after docking ship impact about the instant position determined by the client ship actions. The client ships alongside shovels and shuffles the pier under the influence of the residual ambient currents. They modulate the pier behaviors but are unlikely to enhance the impact loads on the fenders. It further indicated that a parallel docking ship fairly represent ship docking events within small approach angles. Consequently, a standard model consisting of a bare MHP and a parallel docking ship is chosen for the rest of this investigation.

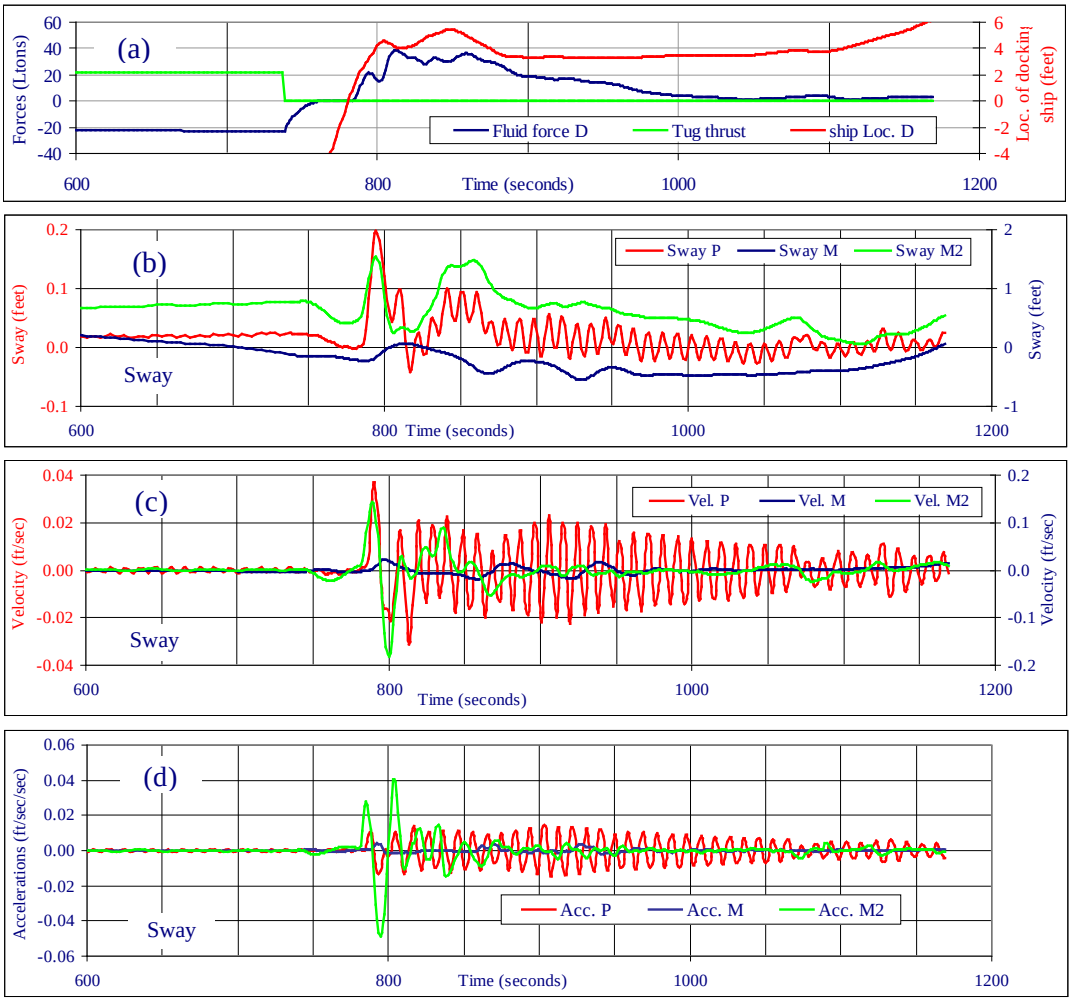

Figure 44(a). Effects of client ships

7.0 MHP PERFORMANCE DURING SHIP DOCKING ROUTINE

Floating piers are susceptible to shock impact of docking ships. Excessive motion induced by large docking ships may impair the operation safety of heavy equipment aboard the pier. A parametric study was conducted to explore the MHP performance and quantify the dynamic loads the founding shafts shall withstand during ship docking process. Prevailing parameters considered include berthing speed, fender properties, docking ship locations, and configuration of founding shafts. Findings are summaries in this chapter.

7.1 Berthing Speed

Berthing loads are primarily caused by the kinetic energy of the docking ship and enhanced by the water mass drawn by the docking ship in its wake. Both driving factors are correlated to the approach speed of the docking ship. A floating pier also bears direct current and wind forces. In the present exercise, the docking ship was brought to its berth under the power of tug boats. A constant tug thrust was applied to accelerate the docking ship to the desired approach speed before releasing the ship to free drifting toward the ship berth at MHP. The docking ship was accelerated to its terminal speed the select tug thrust can sustain from more than one half ship length away from the pier. This will provoke a fully developed wake behind the docking ship to provoke the worse case berthing loads in support of conceptual design. At the beginning of this test sequence, various tug thrusts were applied to observe the performance of docking ship and the nature of the ship wake it generates on its way. Selected cases are presented in Figure 45 to show the general trend of ship performance and the level of berthing loads experienced by the founding shafts.

Figure 45(a) illustrates the velocity a history of the docking ship subject to tug thrusts of 50, 75, and 100 kips, respectively. The docking ship, in each case, accelerate to a nearly constant speed when fluid resistance offsets the tug thrust and oscillates since under the influence of a pressure waves bouncing back and forth between the docking ship and the pier. The higher tug thrust accelerated the docking ship reached a higher speed as expected. As soon as the tug boat turned off its thrust, the docking ship decelerates rapidly by the fluid resistance as indicated by the sharp velocity decreases in Figure 45(a). The docking ship continued to drift on its momentum plus moderate push by the trailing water and landed on the foam fenders shortly after. Note that the pressure field in the gap between the docking ship and the pier continued to oscillate the docking ship but at an increasing frequency as the gap decreased. Foam fenders bounced the docking ship back (indicated by negative velocity) briefly before the trailing water pushed it back into the fender for the second impact.

It is interesting to note that the docking ship traveling faster in the open water also decelerated faster and eventually hit the foam fender at slightly higher approach speed than the one traveling at the lowest speed. However, the docking ship subject to 50-kip tug thrust loaded the founding shafts more than did the other two cases as shown in Figures 45(b) and (c). This reversed trend is attributed to the fluid forces associated to the docking ship induced flow presented in Figures 45(d) and (e). Note that the second peak of the berthing loads on the outboard founding shaft (FEN7y) clearly reflects the shapes and intensities of the associated fluid force histories, Figure 45(d). The docking ships subject to tug thrusts of 100 and 75 kips vibrated the MHP more

pronouncedly perhaps due to the higher direct fluid force on the MHP hull as shown in Figure 45(e).

The observation that a ship hit the pier at 0.31 fps (the case at 50-kip tug thrust) imposed higher berthing loads on founding shafts than did a ship hit at 0.35 fps (the case of 100-kip tug thrust) cannot be explained by the ship inertia alone. The additional berthing loads are fully traceable to the fluid forces generated by the docking ship induced flows via two paths. At the moment of the initial fender contact, the difference in the berthing load on the outboard founding shaft is about 23 Ltons in favor of the case of slower ship. At the same instance, the trailing wake exerted 28 Ltons more fluid force on the slower docking ship while the negative pressure gradient around MHP hull (see Chapter 6) imposed one tone more force on the pier in the opposite direction. These two forces combined apply a net of 27 Ltons more forces on the slower ship in the same direction of ship inertia. This extra force very well accounts for the difference in the total berthing load of 23 Ltons, considering the slight difference in the approach speed. Table 4 details the aforementioned force balance for the three cases in consideration. The last column shows the berthing loads attributable to docking ship inertia after deducting the fluid forces. The results are more in line with the approach speeds. The net fluid force contributions to the berthing loads on the outboard shaft are presented in Ltons (on the left column) and percentages of ship inertia contributions (in the right column). Note that the fluid force adds roughly from one to thirty percent of the ship inertia contributions. The trend seems in line with our position of ranking fluid contributions by the level of wake maturity.

Table 4. Force balance at the moment docking ship contact foam fenders

Tug thrust (kips)	Contact speed (fps)	FEN7y (Ltons)	Fluid forces (Ltons)				ship inertia contribution (Ltons)
			Ship	MHP	Net		
					Ltons	(%)	
100	0.35	101	14	-12.7	1.3	1.3	98.7
75	0.38	113	18	-8.5	9.5	9.1	103.5
50	0.32	124	42	-13.7	28.3	29.6	95.7

This set of numerical tests reveals an important message that it is hard to push a docking ship to a high approach speed unless the tug boat maintains its thrust up to the moment of fender contact. Once the tug turns off its power, the docking ship decelerates rapidly. This observation seems in line with the fact that large ships are normally docking at approach speeds around 0.2 fps. Consequently, a tug thrust of 50 kips may be used for the rest of this study without losing any generality unless otherwise specified.

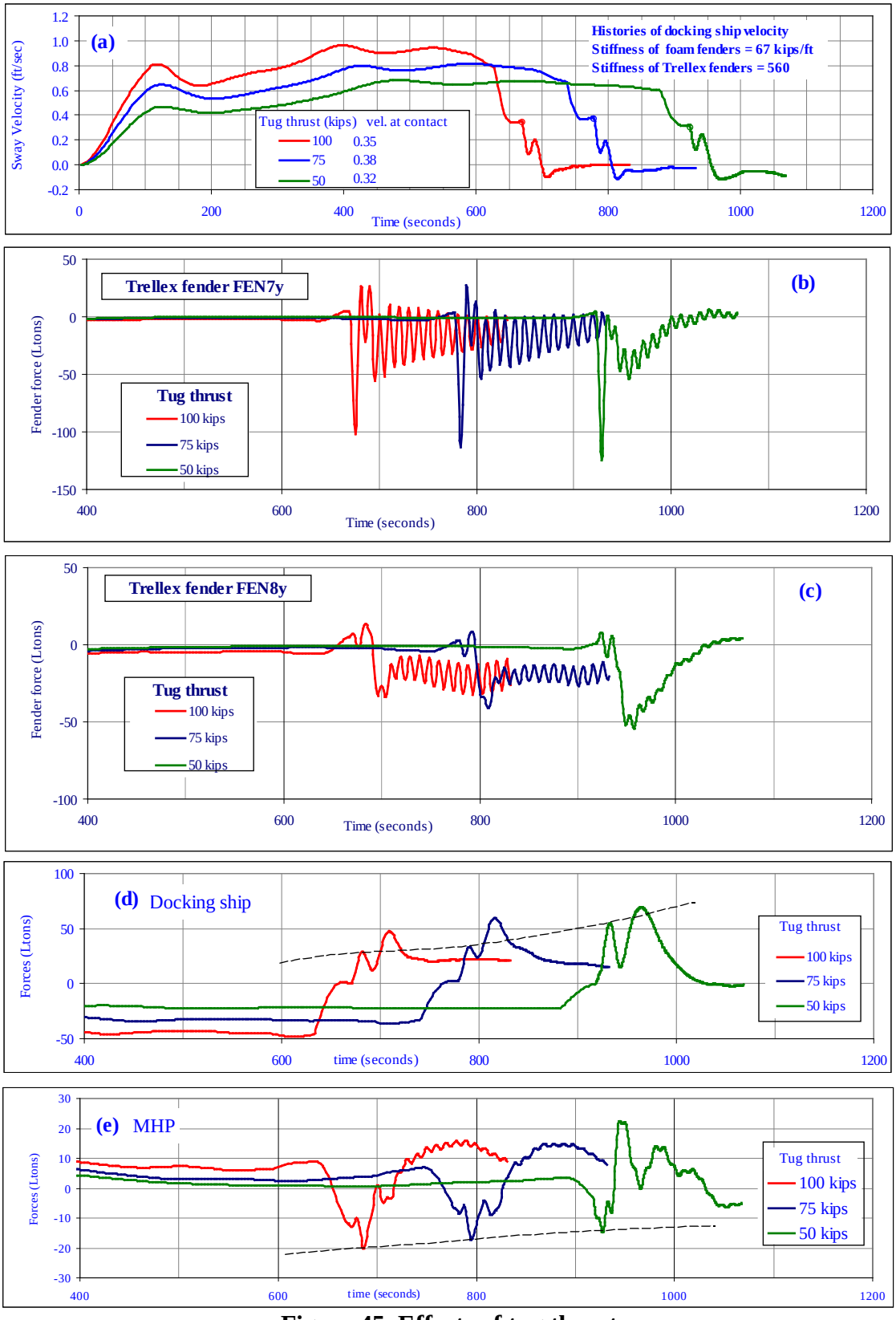

Figure 45. Effects of tug thrust

7.2 Effects of Fender Stiffness

Foam fenders are hung outside the MHP hull near the water surface to ease its interface with the client ships. During ship dockings, these foam fenders absorb the berthing energy and thereby protect the pier and ships. In general, softer fenders distort more over a longer duration to slow the pace of energy transfer and thus alleviate the berthing loads. However, their larger sizes to accommodate larger distortions, implying a longer standoff distance once ship docking is completed, hamper cargo transfer and logistic operations. The MHP design further introduces interior fenders to facilitate load transfer from the floating hull to the founding shafts. This component further complicates engineering tradeoffs for the proper fender selections. A sequence of tests was conducted to test the sensitivity of both types of fenders. Results are presented as follows for the purpose of identifying the worse case berthing loads on the founding shafts. Please refer to excel file "cmpr t2 cases No of client ships.xls" for supporting data.

Figure 46 summarizes the sensitivity of foam fenders to the berthing loads on founding shafts. This set of tests maintained the stiffness of interior fenders at 560 kips per foot and varied the stiffness of foam fenders from 34 to 134 kips per foot. Docking conditions were identical for all cases. Figure 46(a) depicts the histories of docking ship velocities at the midship after fender contact. The histories of ship performance are identical prior to fender contact and split due to fender actions thereafter. The docking ship under the influence of the trailing wake compressed foam fenders rather irregularly. Stiff foam fenders bounce the docking ship off while the wake drawn by the ship continues to force it into fenders. As a result, the foam fenders passed a highly transient berthing load to the MHP, which in turns caused the pier to vibrate as reflected by the loads on the interior fenders, Figure 46 (b) and (c). Obviously, the most stiff foam fender passed the highest berthing loads to the interior fenders and shook the MHP the most. The softest fender at 34 kips per foot, on the other hand, distorted steadily to the greatest extent, resulting in the least berthing loads on the interior fenders. The histories of fluid induced forces on the docking ship and MHP in general held similar shapes, but did not show a clear trend as a function of foam fender stiffness. This might have to do with the complicate near field flow pattern around the MHP. Nevertheless, this exercise delivers a clear message that a stiffer foam fender transfers higher berthing loads to the founding shafts.

Figure 47 shows the sensitivity of interior fenders to the berthing loads on founding shafts. This set maintained the stiffness of exterior fenders at 67 kips per foot and varied the stiffness of interior fenders from 280 to 1,120 kips per foot. Docking conditions remained identical for all cases. Results indicate that the berthing loads on the founding shafts are less sensitive to the interior fenders.

Consequently, the interior fender at 560 kips per foot and a moderate foam fender at 67 kips per foot as recommended by the conceptual design to date were chosen for the subsequent simulation efforts unless otherwise mentioned.

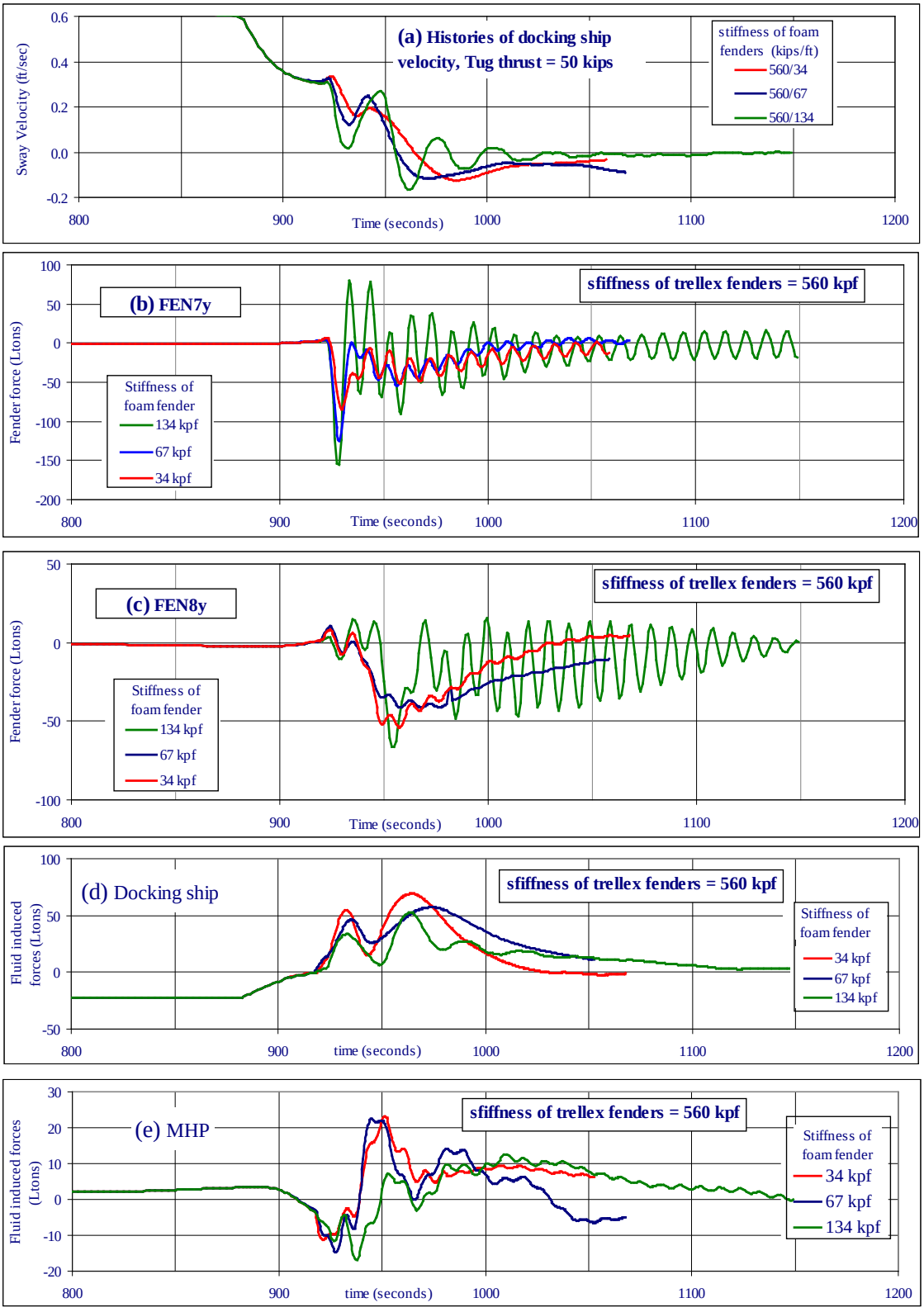

Figure 46. Effects of foam (outer) fenders

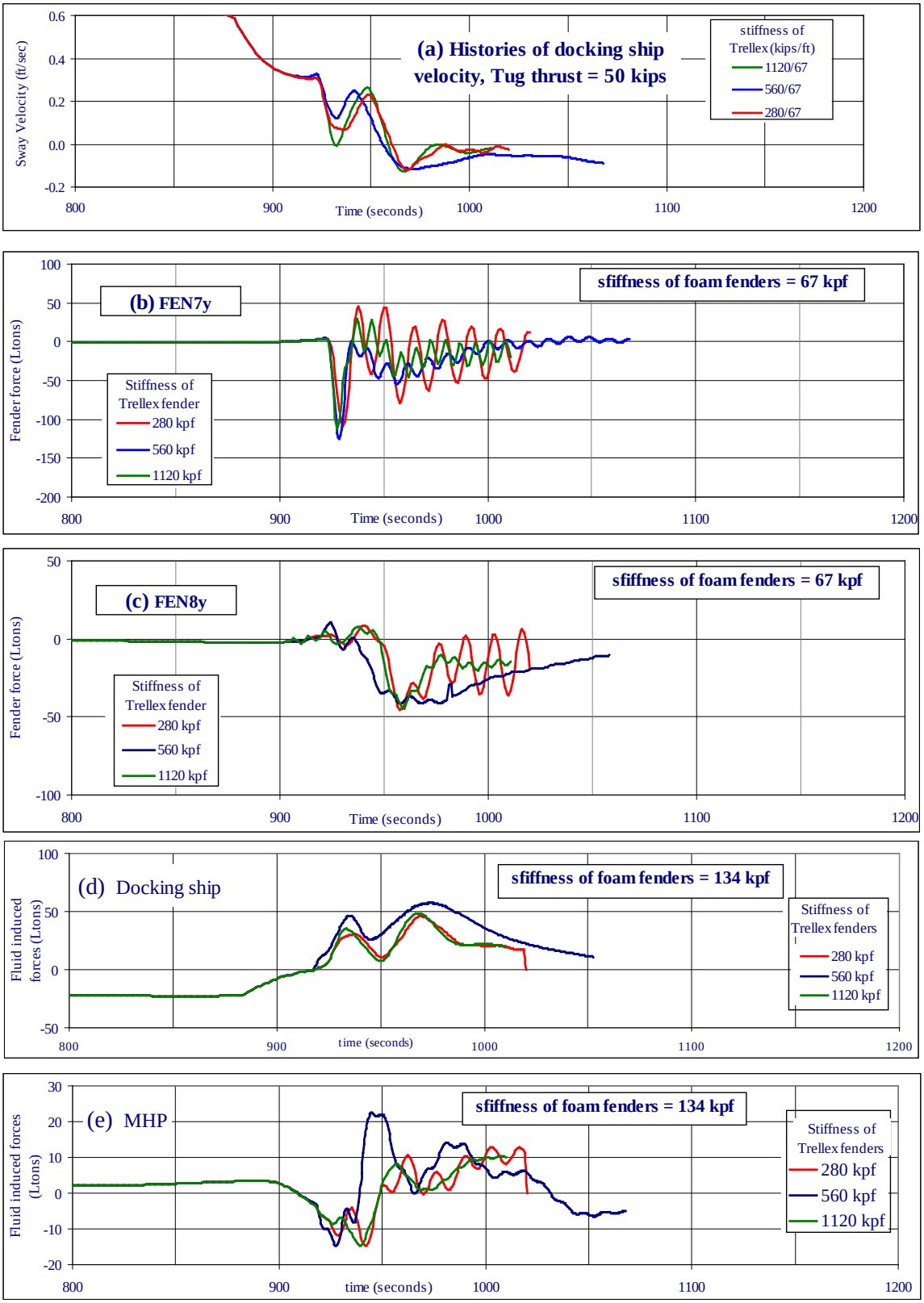

Figure 47. Effects of Trellex (inner) fenders

7.3 Effects of the Docking Ship Position along MHP

The MHP is freely afloat and only secured by a few discrete founding shafts. The pier responds to docking impact depending on where the ship lands. The following sequence was designed to observe the sensitivity of pier performance to contact location. In this sequence, a parallel docking ship was brought in via three different lanes relative to the pier as illustrated in Figure 48. They are designated as (a) the outboard lane with the stern of docking ship aligned with the outboard end of the pier, (b) the center lane with the midship of docking ship aligned with that of pier, and (c) the inboard lane with the bow of docking ship aligned with the inboard end of the pier. The docking scenarios are identical otherwise. Keep in mind that the fluid domain is bound by a solid wall near the inboard end.

The docking ship was pushed by tug thrust of 50 kips in all cases. All docking ships behaved similarly on their way except the one in the inboard lane moved noticeably slower than the others as depicted in Figure 49(a). A close-up view of the ship motion histories indicates the ship in the inboard lane pressed the foam fender slightly deeper and then oscillated more pronouncedly. This is anticipated as the solid wall confines the ship drawn wake in the inboard lane and forces the trailing water to more actively interact with the docking ship. The same water in the other two lanes is free to route around the ship. The fluid induced forces on the MHP look very much alike (Figure 49(c)), however, tend to rotate the pier in different ways according to their points of application (Figure 49(d)). In general, the fluid forces on MHP act to counter the forces imparted through docking ships.

Although the forces resulting from the ship inertia and fluid forces on docking ship and MHP are comparable, the resulting berthing forces on founding shafts are distinct (Figures 49(e) and (f)). The differences are obviously attributable to the docking ship location relative to the pier. The highest berthing load was seen at the outboard shaft with the docking ship approaches from the outboard lane. This berthing load is the highest ever observed up to this stage partly due to the docking ship location and partly due to the high approach speed of 0.45 fps. The docking ship was released much closer to the foam fenders than previous test cases.

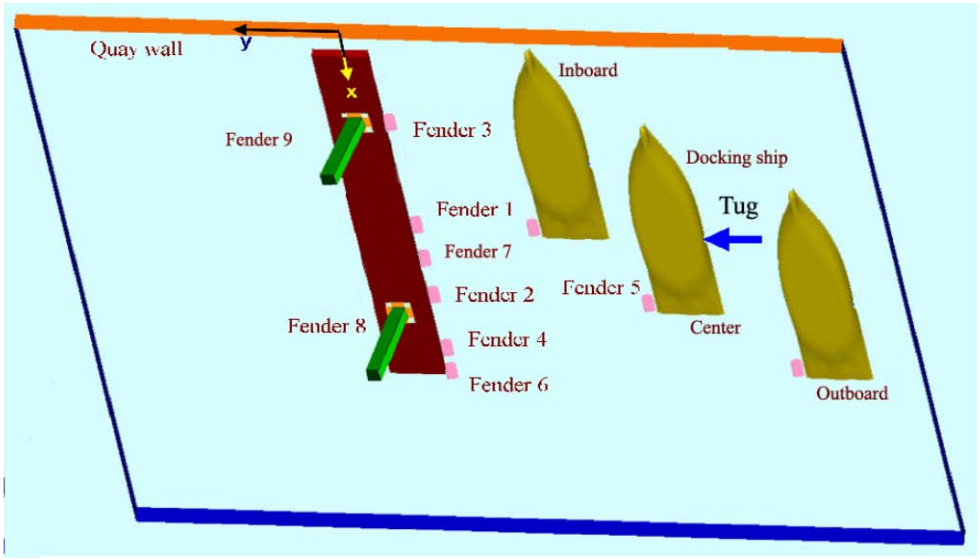

Figure 48. Layouts of ship lanes

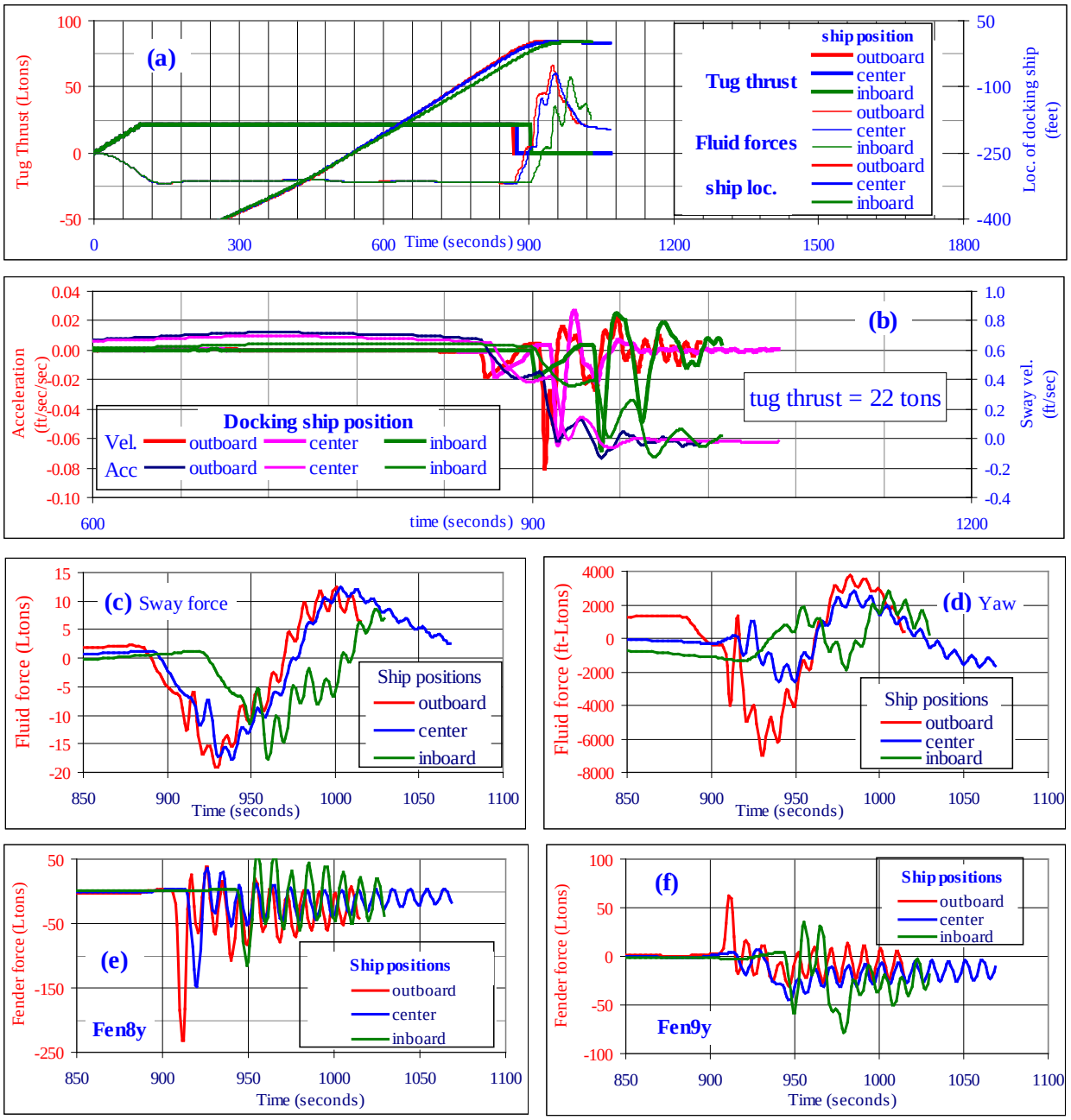

Figure 49. Sensitivity of docking ship locations along the pier

7.4 Summary

This chapter explored the behaviors of docking ships in the operational environment of MHP and their couplings with the pier. Prevailing structural and operational parameters were fully tested to gauge their sensitivities to the resulting loads on the founding shafts. The results established a fair scene at which the founding shafts and their fenders are likely to suffer the worst-case scenario impact by the docking ships.

Docking loads are transferred in full to the founding shafts through the outer foam fenders and then the inner Trellex fenders. The load paths are fully traceable. The load distribution varies with how and where the docking ship contacts the pier. The simulation concludes a pier secured by two founding shafts survives the worse-case scenario docking loads imposed by the largest admissible client ship. The resulting docking loads are well within the design capacity of the inner fenders around the founding shafts. The docking ship shakes the MHP slightly and hardly affects the service efficiency of the pier. Figures 50 and 51 present the fender loads and MHP responses to the worse-case scenario ship docking process in daily routines. Their magnitudes are summarized in Table 5 for design references.

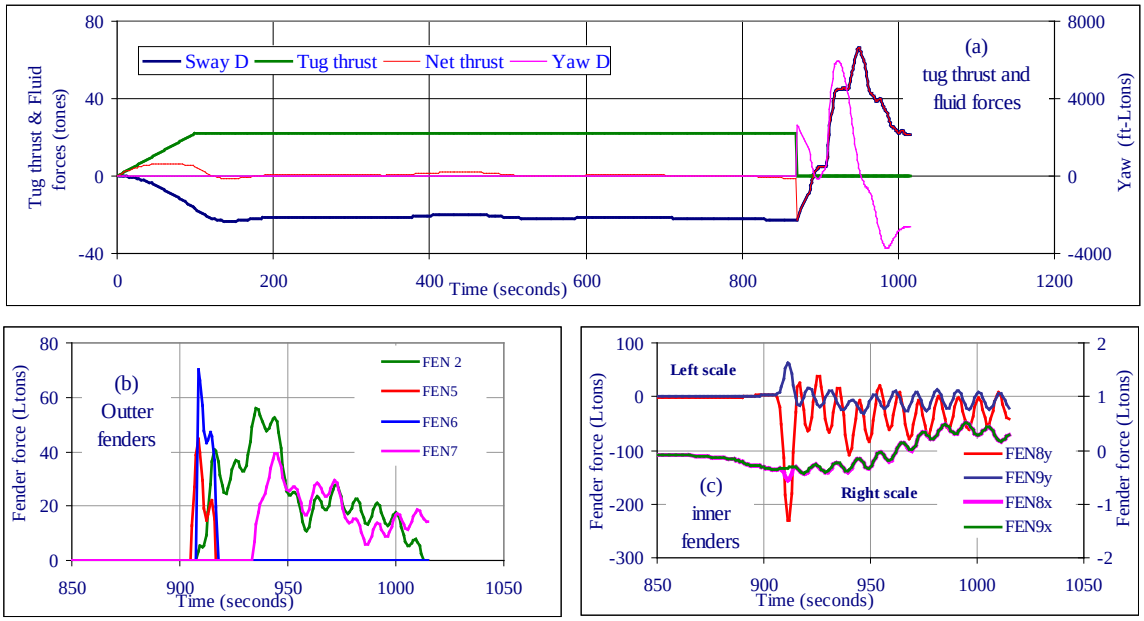

Figure 50. Typical berthing loads on founding shafts

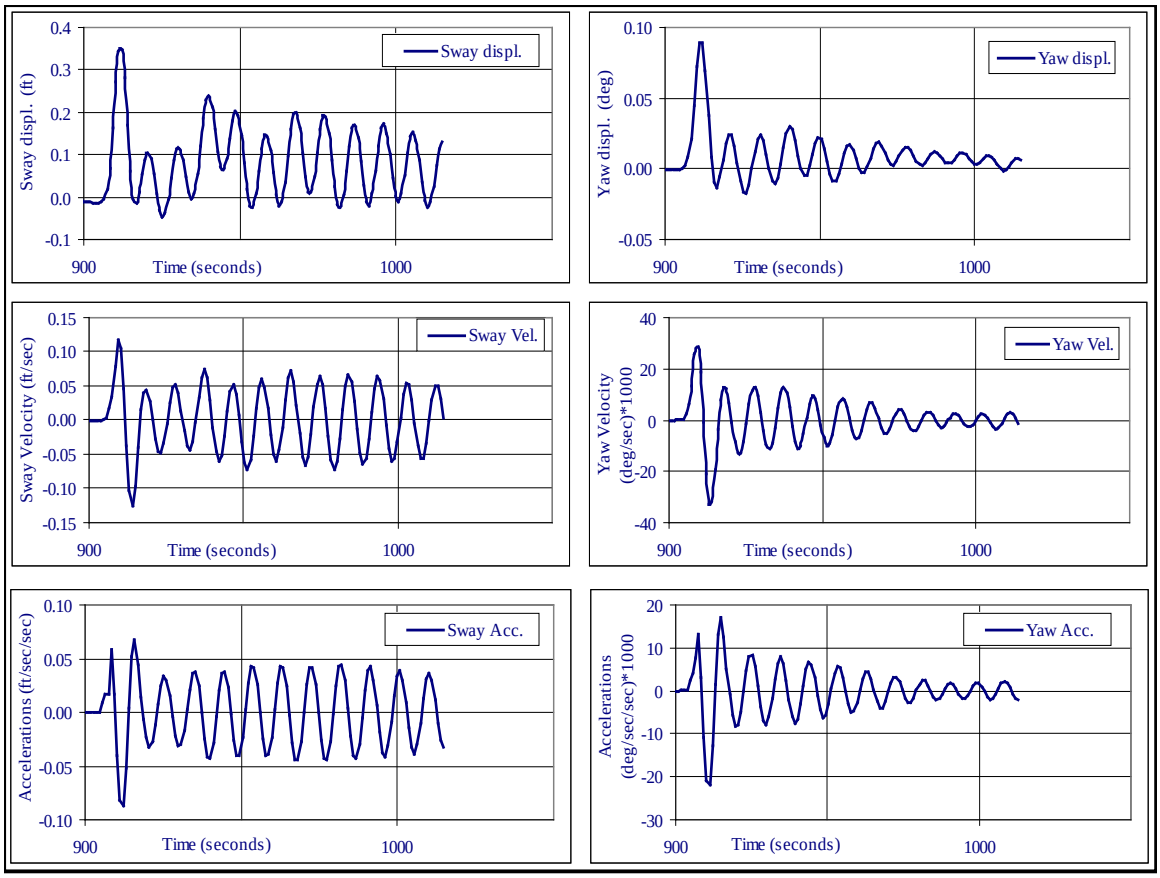

Figure 51. Motion kinematics of MHP

Table 5. Summary of MHP responses to docking ships

Magnitudes of MHP responses			
Sway		**Yaw**	
Displacements (ft)	**0.35**	Displacements (deg.)	**0.09**
Velocities (ft/sec)	0.13	Velocities (deg/sec)	0.03
Accelerations (ft/sec/sec)	0.09	Accelerations (deg/sec/sec)	0.02
Magnitudes of Fender reactions			
Inner fenders		**Outer fenders**	
Reactions (Ltons)	**231**	Reactions (Ltons)	**70**
tDeflections (ft)	0.9	Deflections (ft)	**2.3**

8.0 IMPACT LOADS INDUCED BY DRIFTING SHIPS

The simulation results so far conclude that normal ship docking in calm water is unlikely to damage a properly cushioned MHP or degrade the operation efficiency of this pier facility. A more severe challenge to the fender designs, however, may arise from a rare event with a large ship drifting in currents. Similar challenge may occur while docking ships in adverse currents and winds. The flowing sequence was designed to testify the survivability of the interior fenders subject to impact by drift ships.

The simulation code established its credibility for the present scenario through a vigilant pilot study to ensure a proper representation of the relevant hydrodynamics in scene. Details of the pilot study are not shown in this report. However, abundant evidence can be seen in the core analysis of this chapter. Results indicated that this code had captured all major hydrodynamic features in agreement with the basic physics of ship-current couplings.

8.1 Simulation Approach

This sequence assumed a scenario as depicted in Figure 52, which involves an upstream ship breaking away from its mooring and subsequently drifting with its length parallel to the MHP under the influence of currents and winds. The ship is originally at about one half of the ship length away form the pier. It is obvious that a ship hitting the pier head-on is the most destructive. However, a ship at such heading tends to shatter the pier hull beyond the concern of fender design and is thus excluded from the present study. The study considered four prevailing site parameters: (a) current speeds, (b) water depths, (c) impact locations, and (d) wind effects.

Throughout the sequence, the simulation began by establishing the background current from an otherwise calm water domain with the ship and pier held fast in their initial locations. A steady current entered from the left hand edge of the fluid domain and exited from the right hand edge. The impinging current gradually evolved to conform the presence of structures in scene over time. Once the current reached a steady state, the pier and ship were slowly released to avoid injecting undue disturbances to the ambient currents. The ship continued to drift at the speed sustainable by the current until landed on the pier through foam fenders. Unlike the tugboats, which actively maneuver the docking ship prior to fender contacts, the ambient currents push a drifting ship at all time. As a result, a drifting ship is expected to hit the MHP at substantial high speeds than does a ship in normal docking process.

This sequence completed six core series of numerical tests. The first three series measured the influence of the prevailing site parameters on drifting ship induced berthing loads. Series 4 testifies the significance of mechanical damping of the fenders to the simulation results. Series 5 tracks how additional founding shafts share the berthing loads. The final series summarizes the worse-case scenario impact loads the interior fenders are likely to experience in the adverse environmental conditions. Major findings are summaries in this chapter.

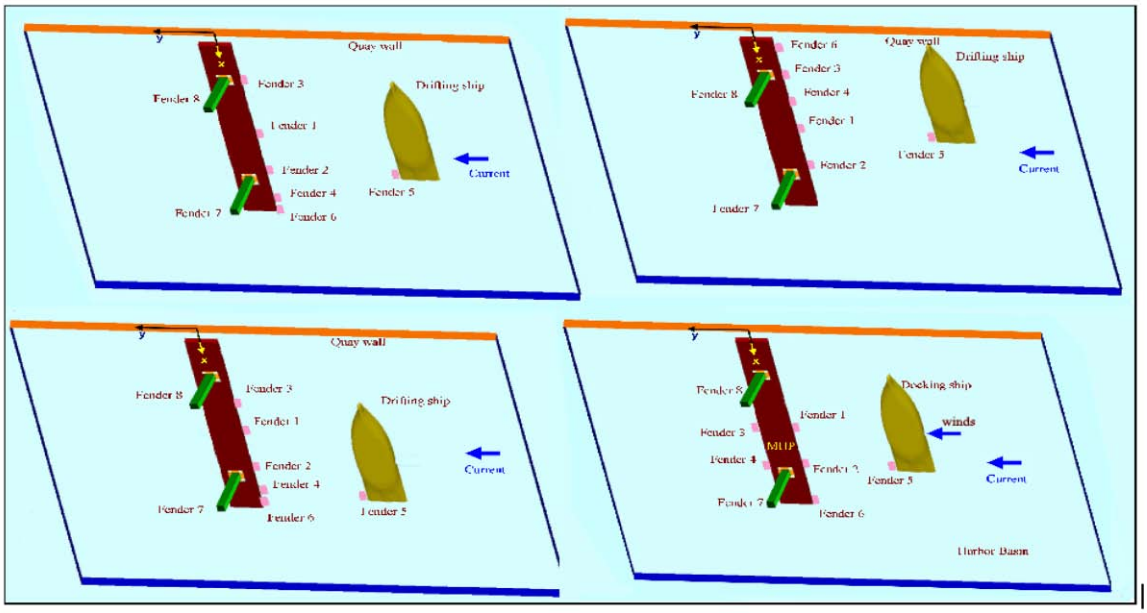

Figure 52. Ship docking in currents and winds

8.2 General features of Ships Drifting In Currents

Approach speed dictates the impact loads by drifting ship in currents. The ship speed is primarily driven by the current strength, but can change substantially in different water depth or under the influence of winds. A pilot study was devoted to observe the behavior of a drift ship in currents, its sensitivity to prevailing parameters, and in the mean time to inspect pier responses to drift ship impact. Findings will be used to compose the worse-case scenario environment to test the survivability of the pier design.

Figure 53 shows the evolution of velocity (arrows) and pressure (colors) fields during the first 300 time steps after the ship was released. The time increment is two seconds. The ship continues to accelerate until reaches a terminal speed sustainable by the current when the fluid resistance offset by the current thrust. Note the pressure on the upstream side of the drifting ship decreased as the ship picking up speed. Meanwhile, the pressure on the MHP redistributed in time as the ship drew near and increasingly sheltered the pier from currents. The uneven pressure force caused the pier to vibrate noticeably before ship impact. Figure 54 illustrates the hydrodynamic coupling between the ship and pier by the pressure evolution at the final stage as the drift ship approaches and impacts the pier. These nine images use different scales to show the details of the pressure gradients. The scale ranges from -1 to 0.2 for first two images, -1 to 0.5 for the third image, and -1 to 2 for the rest. The ship increasingly shelters the pier from current actions as the ship approaches. While the ship cuts off part of the ambient currents, a pressure system by the drifting ship is developing between the ship and the pier. The pressure redistribution along the MHP over time is clearly noticeable. Once the ship stopped at the pier, a strong positive pressure system developed rapidly on the current side of the ship to push the ship into the pier. In the mean time, a negative pressure system, decaying away from the ship, developed on the lee side of the ship. This pressure deficit acts to push the MHP against the currents and partially relieved the impact loads on the founding shafts. This effect is difficult to capture with conventional simulation models.

Figure 55(a) summarizes the evolution of ship motion in currents. The water depth in this case is 50 ft. The two speeds of 1.5 and 2.3 fps as shown are the most likely currents at future MHP sites identified by the MHP IPT. These currents will be used throughout this simulation sequence. The results suggest the model ship will eventually accelerate to a terminal speed of roughly one half of the current speeds, if time and space permits. The ship in 1.5-fps current had more or less approached its terminal speed, while the one in 2.3-fps current ran out of space to reach the associated terminal speed before fender contact.

The drifting ship apparently impacted the pier harder than did a well-performed docking ship, primarily due to the increased speeds. Figure 55(b) indicates the ship in 2.3-fps current imposed more than 100 percent of impact load over the one in 1.5-fps did, even the ratio of their approach speeds is roughly two. This reflects the significance of the current force contributions to the impact loads. Note the MHP felt substantial current loads far before ship impact (Figure 55(c)). At the onset the fully exposed pier experienced direct fluid force of 25 kips in 1.5-fps current and 50 kips in 2.3-fps currents, respectively. These forces decreased as the drift ship drew near to partially shelter the pier and regained the strength when the ship came sufficiently close to cast a positive pressure system on the pier. Once the drift ship stopped by the pier, this direct fluid force reduced drastically and reversed the direction to counter the berthing load imposed by the drifting ship. The trend is consistent with the pressure evolution observed in Figure 56. The counter force is of fairly significant 16 percent of the force exerted on the drift ship by the trailing water in the case of 2.3-fps current.

The drifting ship performance was further inspected in various water depths. Figures 56 to 58 illustrate the variation of the flow pattern around the drifting ship and pier in water depths of 28, 37, and 50 ft. The respective under keel clearances of the ship are 1, 10, and 23 ft, recall that the draft of the ship is 27 ft (8.23 m). As a result, the flow pattern varies drastically due to the distinct levels of pass blockage. The top right chart of each figure presents the water velocity component inline with the direction of ship drifting. The ship cut off the ambient current and deflected most of the water around its ends in 28-ft water, as witnessed by the drastic increase in the velocities astern and abow the ship. The change in flow pattern as the water depth (or under keel clearance) decreases was further illustrated in terms of velocity field in Figures 59 and 60. The velocity vectors in 50-ft water remain more or less in the same direction of the far field currents, whereas those in 28-ft water primarily go around the ship hull. Effects of current speeds and water depths will be discussed in greater details in the following sections.

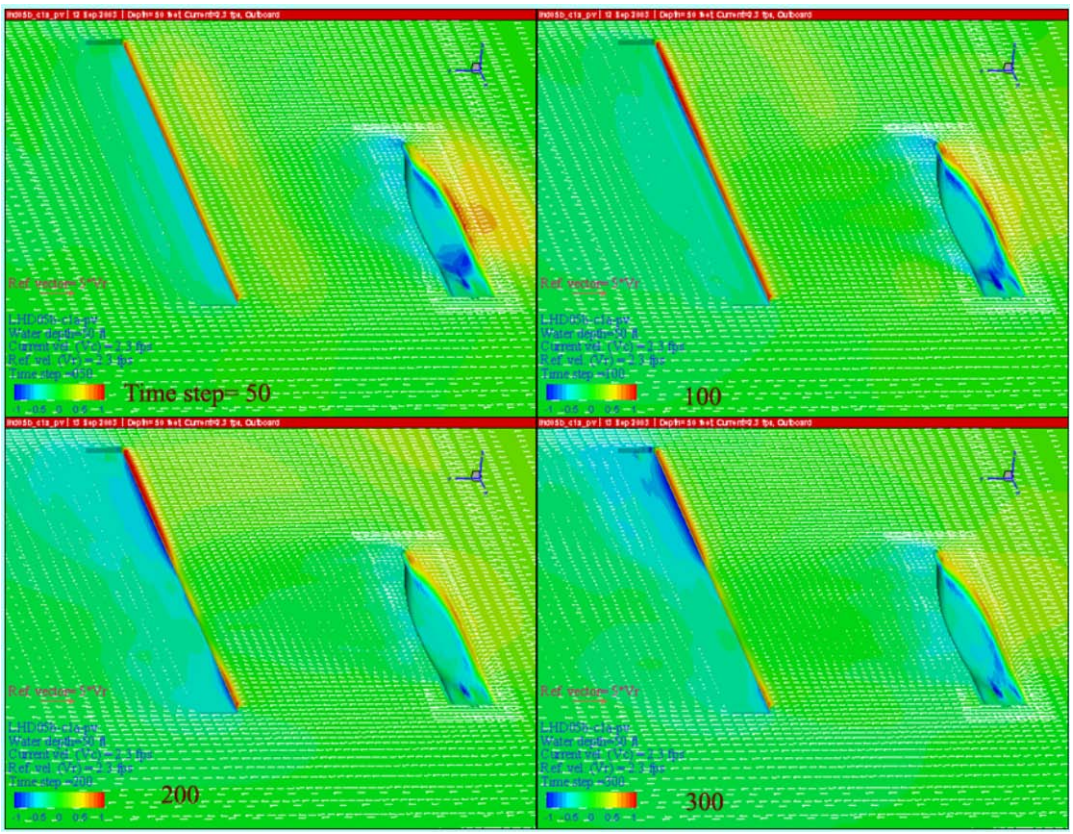

Figure 53. Evolution of pressure field upon ship.

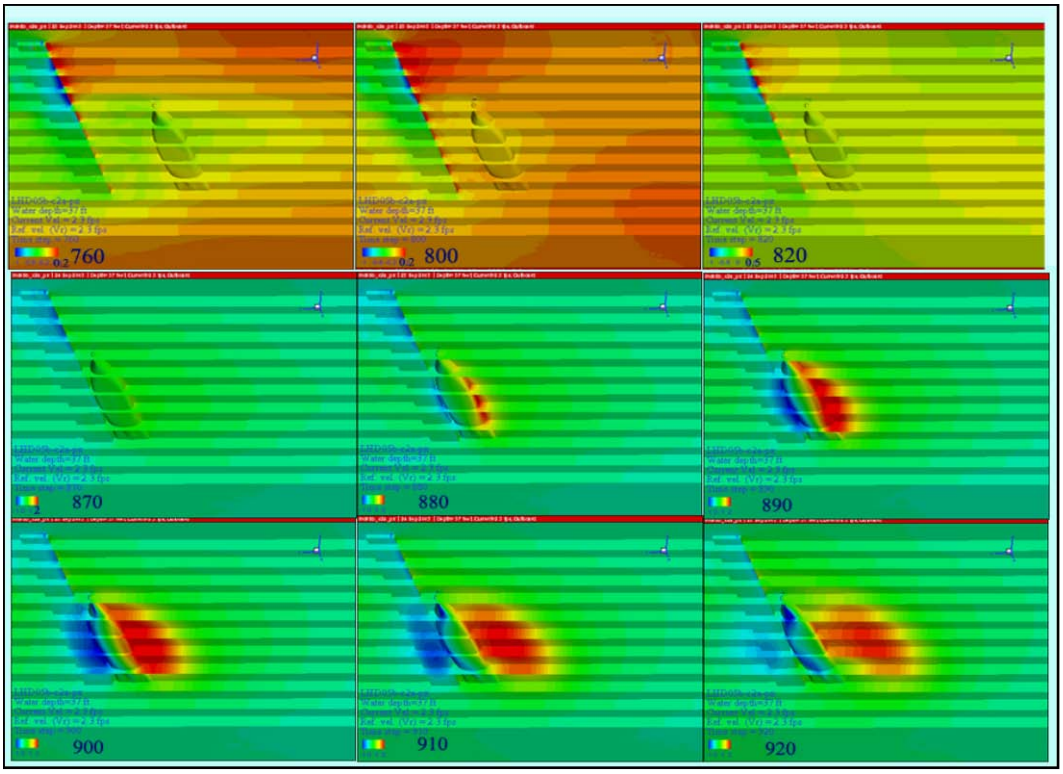

Figure 54. Evolution of pressure field at fender impact (time step~1 sec)

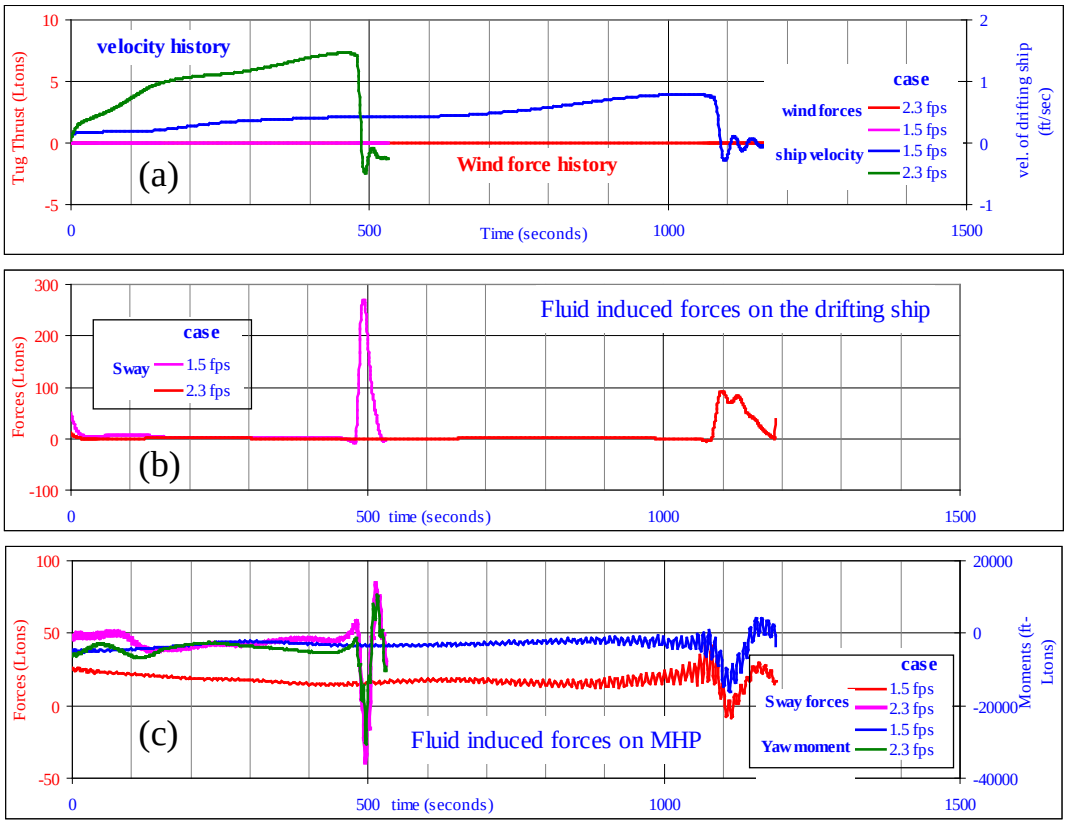

Figure 55. Ships drift in currents

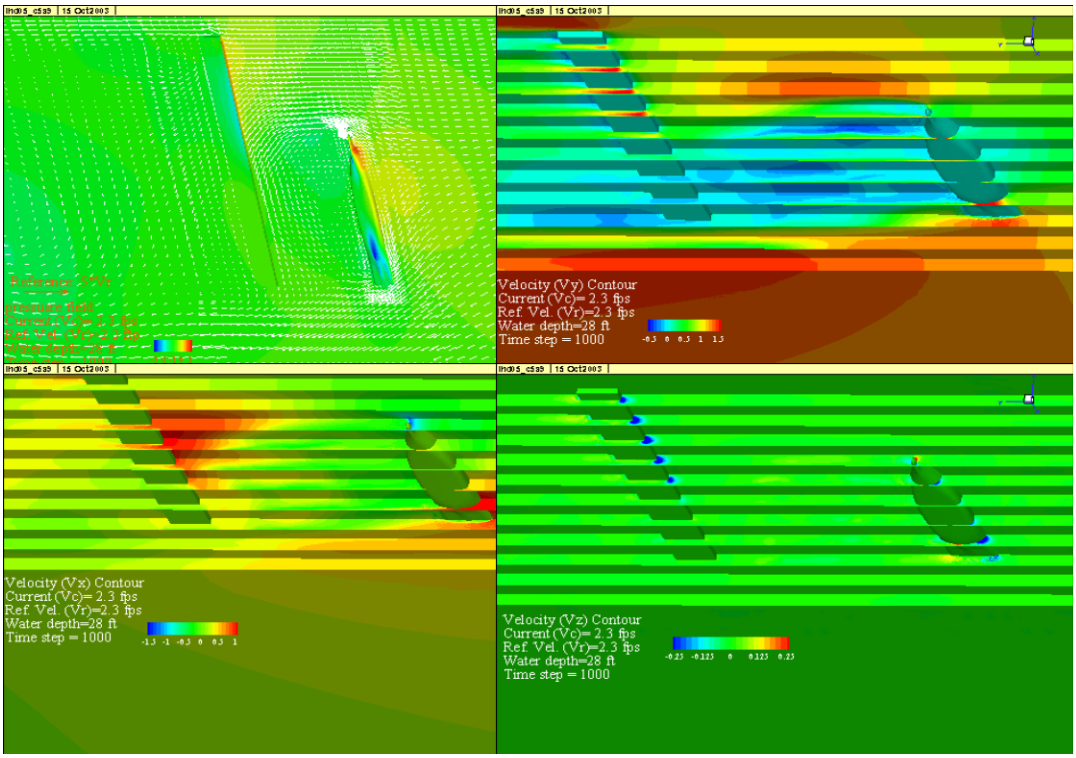

Figure 56. Typical flow fields for a drifting LHD in 28-ft water

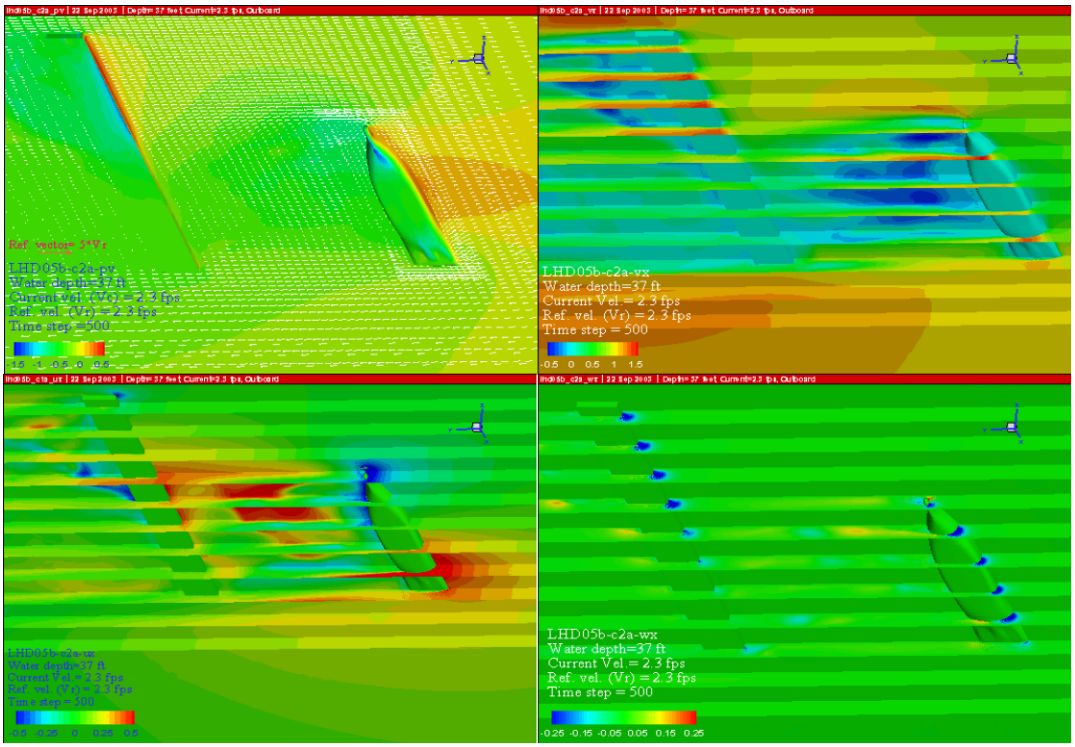

Figure 57. Typical flow fields for a drifting LHD in 37-ft water

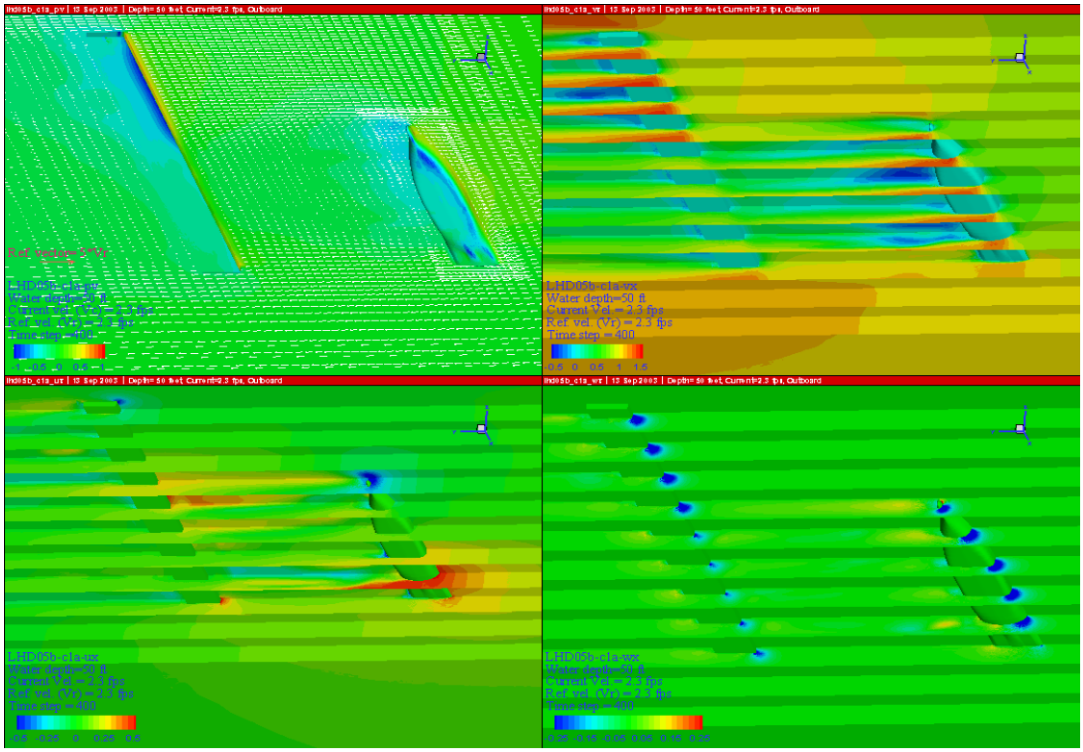

Figure 58. Typical flow fields for a drifting LHD in 50-ft water

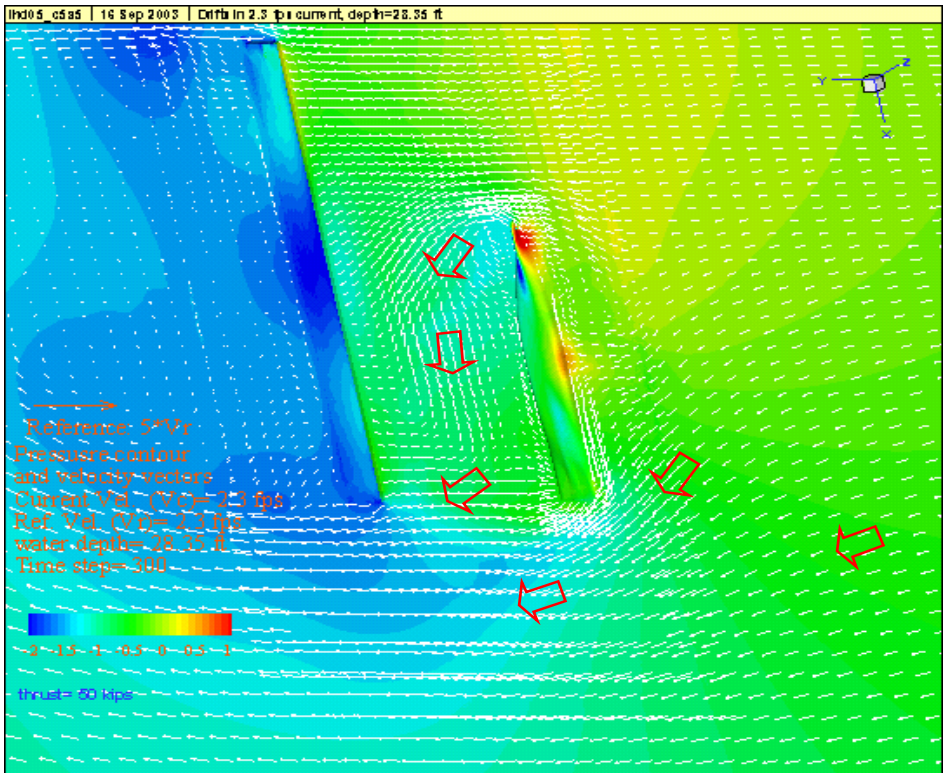

Figure 59. Typical flow pattern for a drifting LHD in 28-ft water

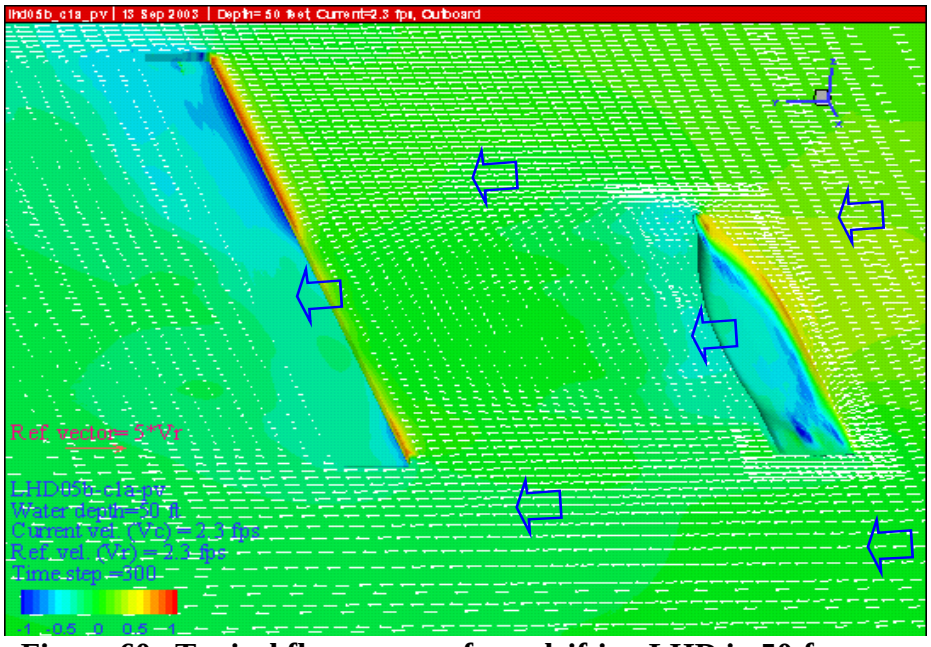

Figure 60. Typical flow pattern for a drifting LHD in 50-ft water

8.3 Effects of Mechanical Damping on Pier Dynamics

The MHP experiences low fluid damping in water plane due to its shallow draft and is thus susceptible to prolonged vibrations once initiated. For instance, a persistent oscillation was

noticed in the fluid induced forces as shown in Figure 55(c). In absence of this damping the unduly motion may grow extensively to impair the simulation in certain situations, such as the case with a ship drifting in the inboard lane illustrated by Figure 61. In this case, much of the trailing current in the ship lane was deflected by the ship through a narrow path next to the quay wall. This accelerated current imposes a much higher force at the inboard end of the pier and force the pier into substantial vibration, which continues to grow as the ship is approaching. Details are illustrated by the blue lines in Figure 62. These excessive vibrations are rarely seen in reality as they are supposedly constrained by the mechanical damping of the structure system.

A free decay test was therefore conducted to observe the sensitivity of the MHP motions to mechanical damping. Figure 63 summarizes the motion histories of a standalone MHP subject to an impulse velocity in each respective mode. A linear damping coefficient was added the inner fenders. This damping coefficient multiplied by the time rate of fender deformation gives the damping force. The results clearly illustrate the significance of mechanical damping to the MHP responses. Without mechanical damping, the pier vibrates persistently once motion starts as shown by the blue lines. These vibrations decay much faster by adding a minor mechanical damping to the system as indicated by the red and green lines.

The actual damping in the MHP system is not known. However, an arbitrary damping coefficient of 500 kip*sec/ft drastically reduced the unduly vibration observed in the example with a drifting ship in the inboard lane as shown by the red lines of Figure 62. The additional mechanical damping (100 kip*sec/ft) brought the berthing loads back to the more realistic range (Figure 64) inline with other cases with the ship drifting in central and outboard lanes. A damping coefficient of 100 kip*sec/ft will be used throughout the subsequent series of simulations to avoid over damping the legitimate motions.

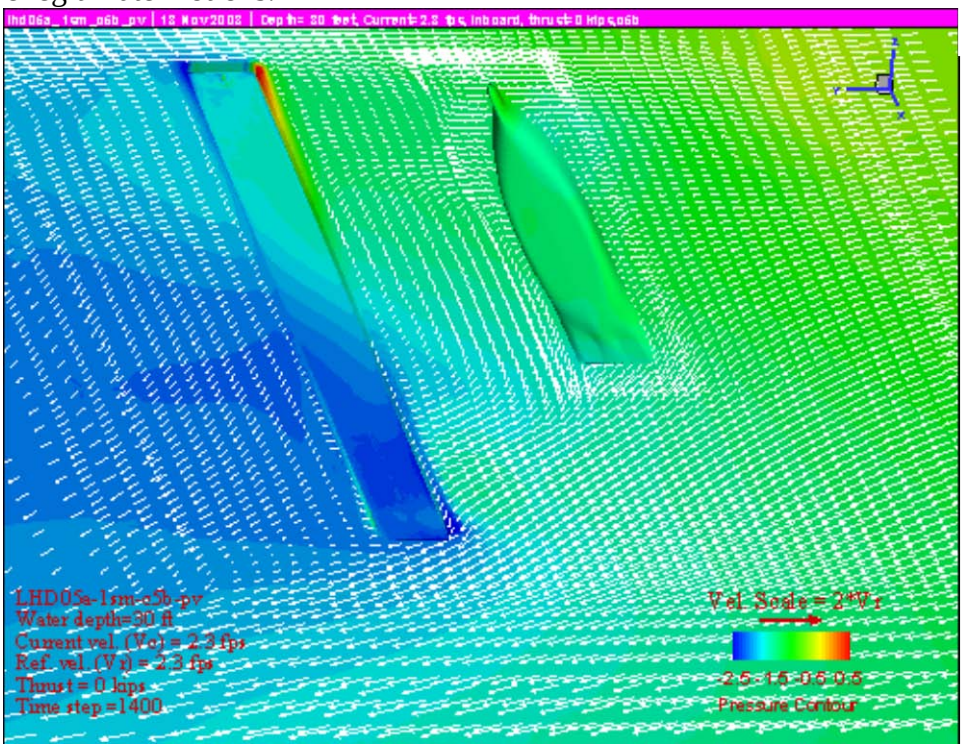

Figure 61. Case lhd05a_1sm_c5b at time step 1400: pressure and velocity fields.

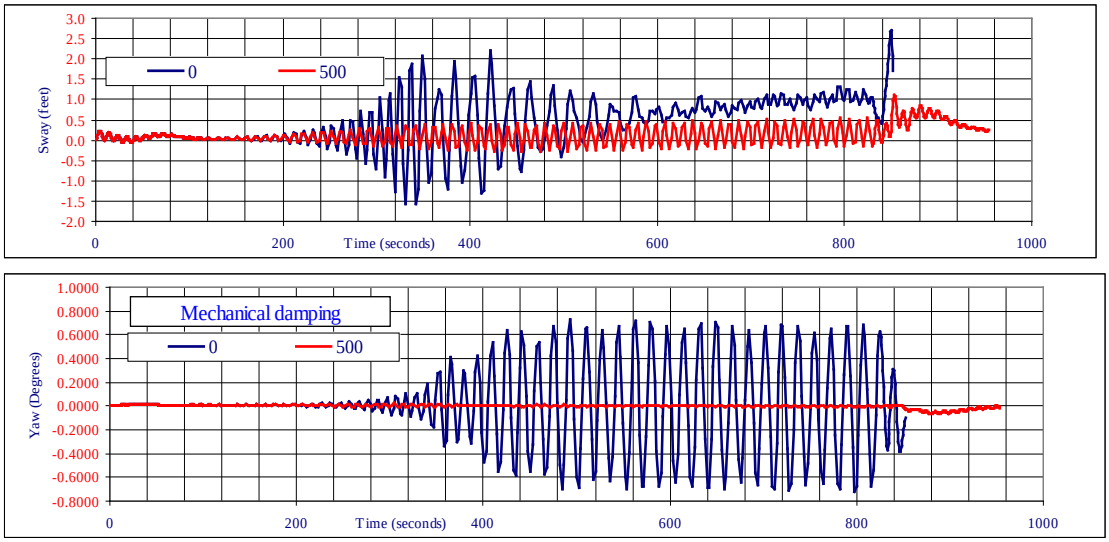

Figure 62. Case lhd05a_1sm_c5b at time step 1400: pressure and velocity fields.

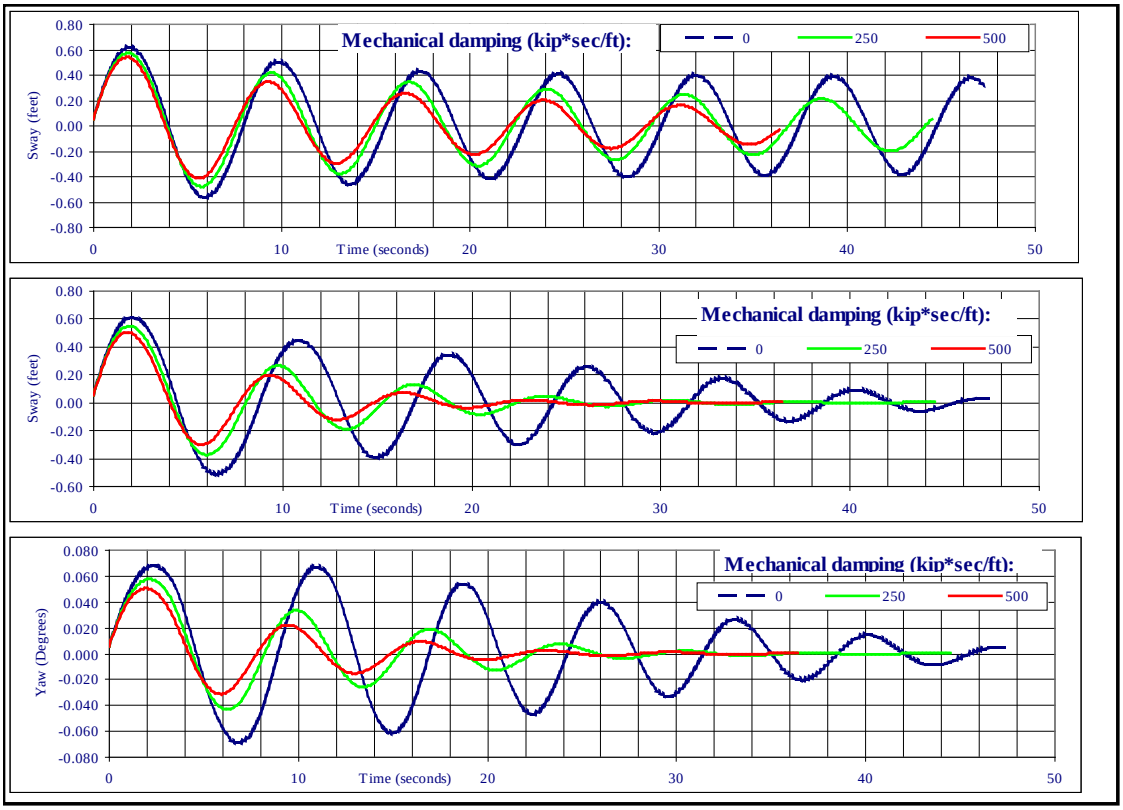

Figure 63. Sensitivity of mechanical damping of MHP

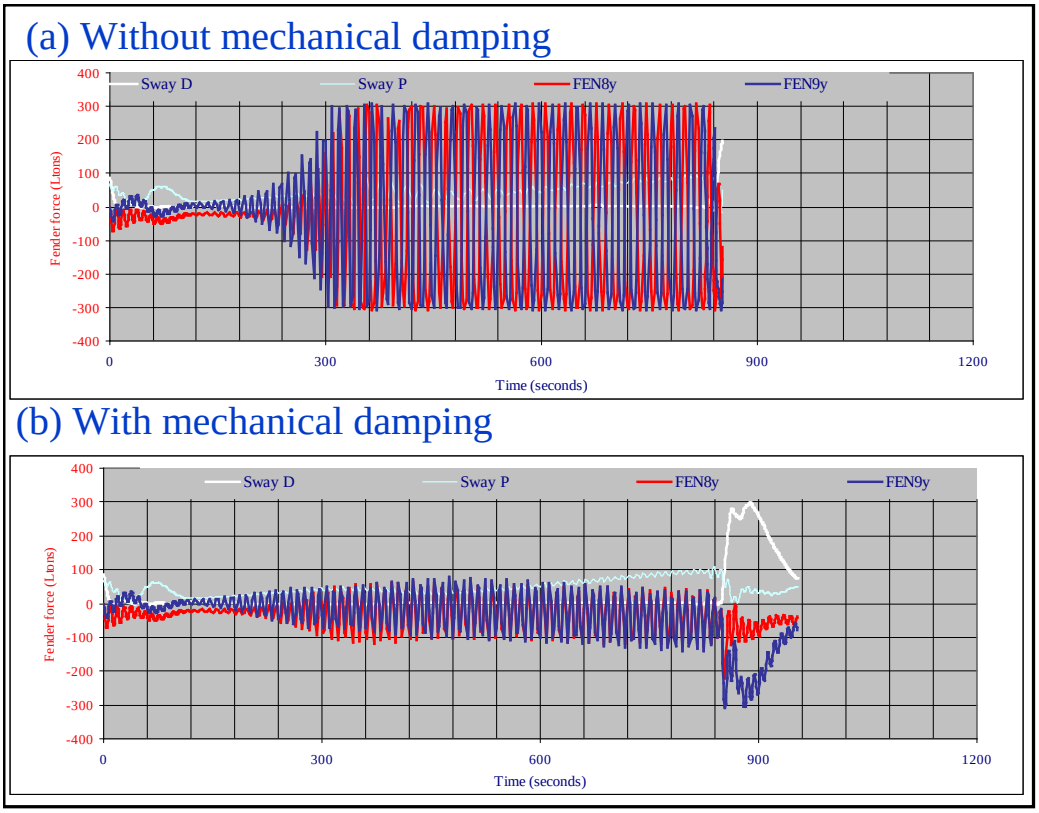

Figure 64. Effects of mechanical damping on Sway motion.

8.4 Effects of Water Depths

The efforts of Sections 8.1 and 8.2 established a reliable numerical basin capable of reproducing the process of ship-pier coupling in any known scenario within the scope of MHP operations. The simulation model had been cautiously fine-tuned in all numerical control parameters to achieve a consistent performance across the board. The simulation effort revisited the influence of water depth to the results of ship-pier coupling in a common scenario as described in Table 6. Results from four representative cases with respective water depths of 30, 33, 37, and 50 ft were presented to summarize the effects of water depth. This exercise traced the evolution of current induced forces on the drifting ship and its performance throughout the collision process and thereby quantified the impact forces on the pier as well its subsequent responses. The results drew a clear trend of water depth effects in the coupling process between the drifting ship and the MHP. (Case: LHD05b_1sm_c1a, c2a, c4a2 and c5a2).

Table 6. Model layout for the sensitivity study of water depth

Parameters	Descriptions	Parameters	Descriptions
Model ship	LHD; parallel to pier	Wind force	no
Ship lane	outboard	Tug assist	No
Initial ship location	600 ft from the pier	Foam fender, stiffness	67 kip/ft
Current speed	2.3 ft/sec	Interior fender, stiffness	650 kip/ft
Water depth	28.3, 30, 33, 37, 50 ft	Yielding load	700 kips
Founding shelves	2	Interior fender, damping	100 kip*sec/ft

Figure 65 summarizes the drift ship activities in various water depths since one minute before fender impact. The clock is synchronized to start at the instant ship contacts the fender to facilitate comparisons of ship, pier, and fluid activities of various cases. The drift ship reached a nearly constant speed on its way in all water depths but slowed down slightly before impacting the pier in response to the developing high pressure system between the ship and the pier. The ship apparently drifted faster in deeper water (Figure 65(a)), compressed the fender harder (Figure 65(c)), and thus transferred higher kinetic energy to fenders (Figure 65(b)). Figure 66(a) indicates that the water surrounding the ship, which flowed faster in deeper water before fender impact and decelerated faster during the impact, pushed the ship harder. More significant is that the fluid forces in deep water are closer inline with the forces induced by ship inertia (Figure 66(b)) and are thus more effective to escalate the overall impact loads. However, the fluid forces also subside faster in deeper water as the trailing water is allowed to pass the ship under the keel. On the contrast, the same water flow in shallower waters, which had to circulate around the ship ends, persisted much longer after fender impact. This effect was clearly demonstrated in Figure 67 by comparing the relevant force histories observed in 37 and 30 ft waters. Note that the fluid induced impact forces are twice as much as the ship inertia induced counterparts in the event of drifting ships. Although these two components do not peak at the same time, the fluid force (red) contributes more than does the inertia force (brown) in the 37-ft water at the moment foam Fender 2 experiences the maximum load (blue). In the 30-ft water, the contributions by the fluid force and ship inertia are about even. The same trend in the force magnitude and phase delay was also observed with the fluid induced forces on the MHP (Figure 66(b)). Again, this force acted to counter the impact loads imparted by the drift ship.

Figure 68 illustrates the process of impact load transfer through the foam fenders. Even though the ship drifted parallel to the pier, it did not contact all foam fenders at the same time due to its streamlined hull shape. Apparently, the first impact (Fender 2) transferred more impact load than did the second (Fender 7). These two impacts were closer aligned in deeper water, perhaps due to faster ship rotation, and resulted in much higher impact loads on the interior fenders as shown in Figure 69(a). Recall that the currents were identical for all four cases. The drift ship in 37-ft water almost topped out the capacity of the interior fender and severely buckled the fender in 50-ft water. Those in 30-ft and 33-ft waters landed on the pier much more softy.

Figures 70 through 72 provide an overview of the pier responses to drift ship impacts. The pier deflected and oscillated mildly under uneven fluid loads before ship impact, displaced markedly more on the impact for about 15 seconds, and then gradually returned to the oscillations prior to impact. In the scenarios under consideration, the pier may sway up to 0.9 ft at the maximum speed of 0.2 ft/sec (Figure 70) and yaw up to 0.12 degrees at the maximum speed of 0.025 deg/sec (Figure 71). The pier surges very mildly reflecting the geometry coupling through its yaw motion.

Throughout this series the load paths were clearly traceable. The impact forces experienced by the foam fenders (Figure 68) and interior fenders (Figure 69) are consistent with the histories of drifting ship dynamics and the ambient fluid activities in various water depths. The ship in deeper waters compressed the foam fenders harder but lasted a shorter duration. Figure 69(a) indicates that the interior fender around the outboard founding shaft (F8y) buckled in 50-ft water.

This is inline with a total impact load of more than 290 Ltons transferred through the foam fenders as shown in Figure 68. The yaw displacement of the pier enhances the fender reactions over its yielding capacity of 318 Ltons (700 kips). The loads transferred through foam fenders are 260 Ltons in 37-ft water, comfortably below the yielding capacity of interior fenders. Figure 73 summarizes the fender reactions. A major difference can be seen between the two cases in 37-ft and 50-ft waters. The interior fender in 50-ft water countered the ship impact at 700 kips like the one in 37-ft water, however, deflected six inches more.

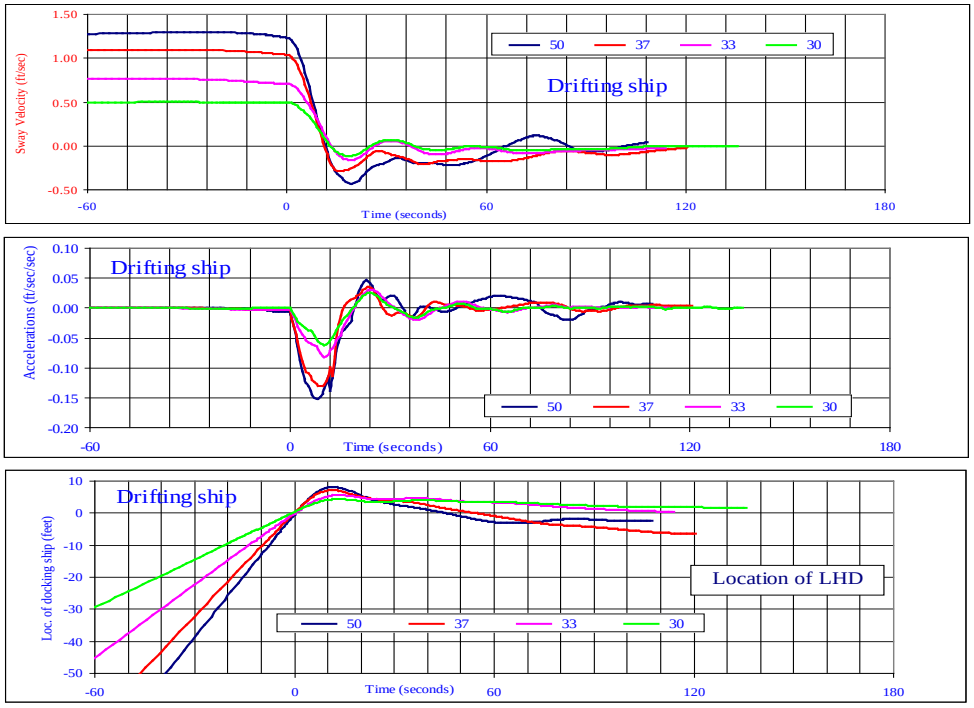

Figure 65. Sway motion of the drifting ship.

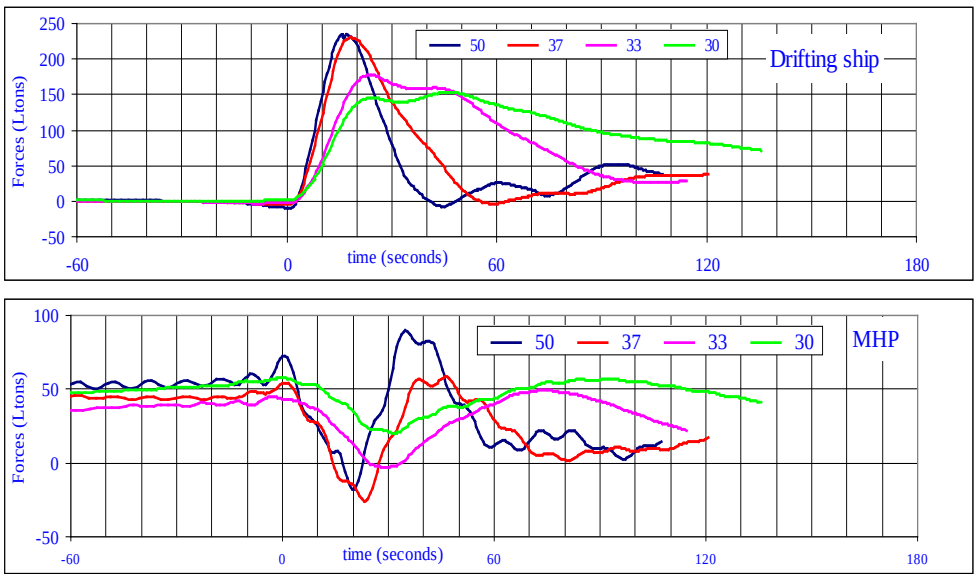

Figure 66. Fluid induced forces on drifting ship and MHP.

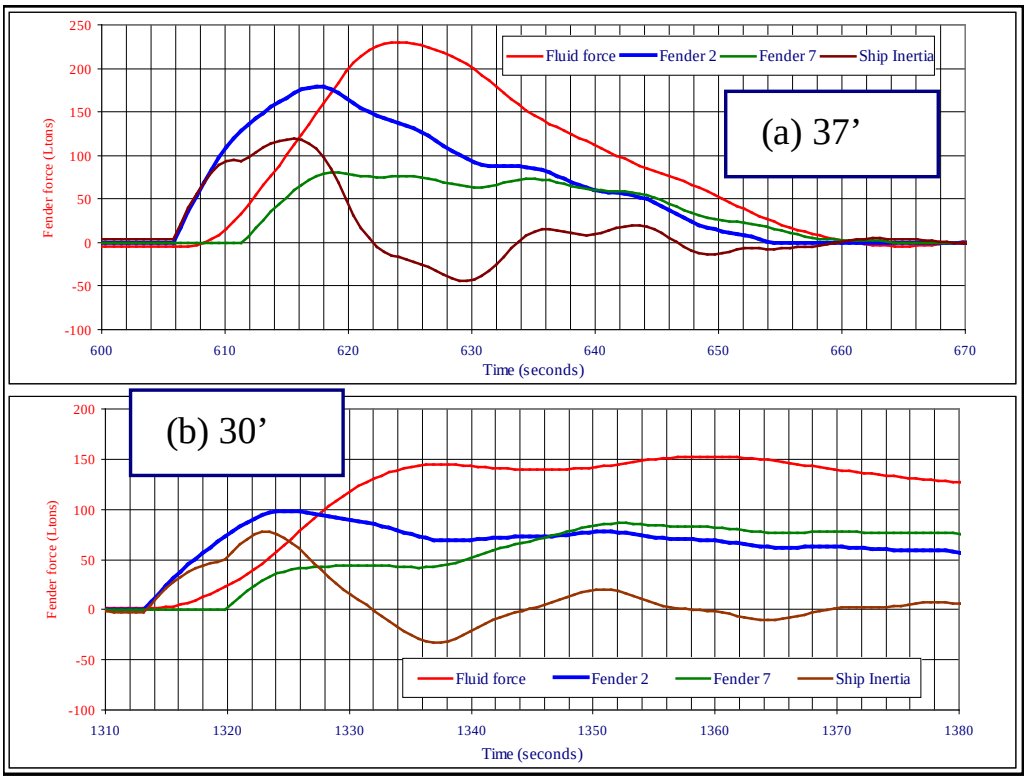

Figure 67. Evolution of fender forces versus fluid induced forces.

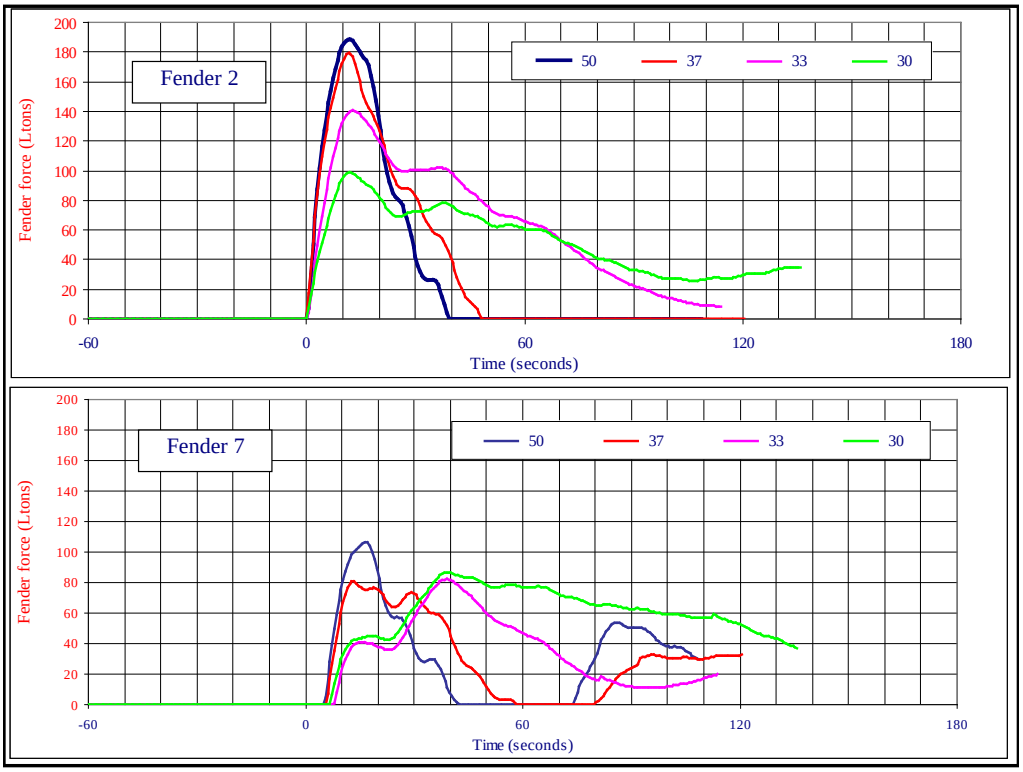

Figure 68. Force responses of foam fenders.

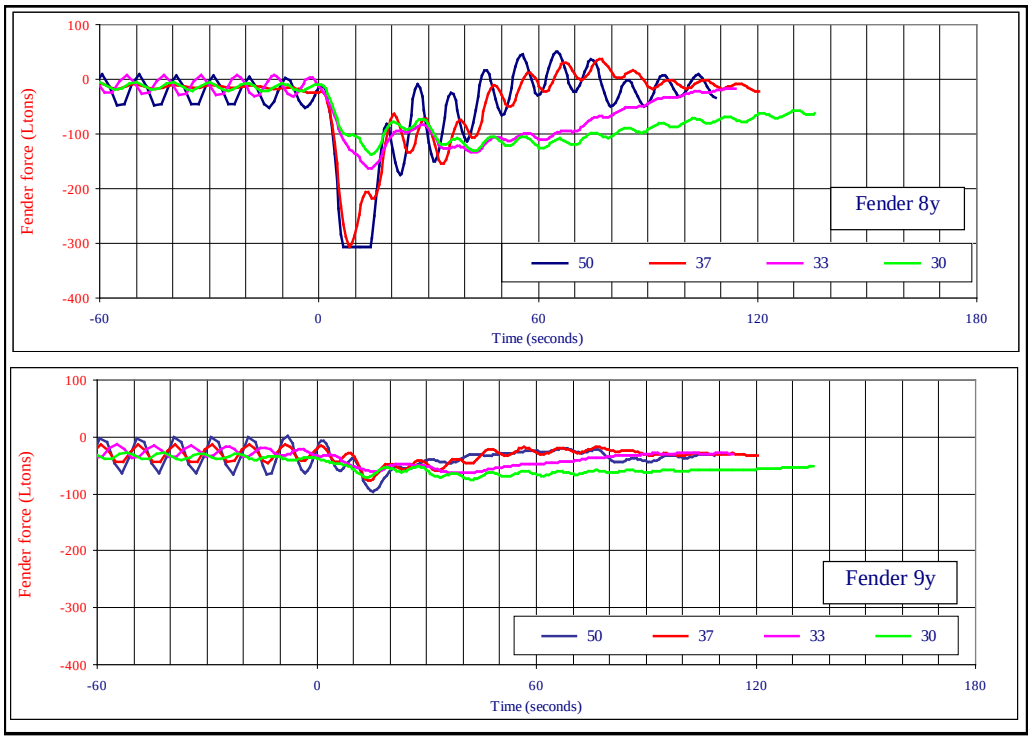

Figure 69. Force responses of Trellex fenders.

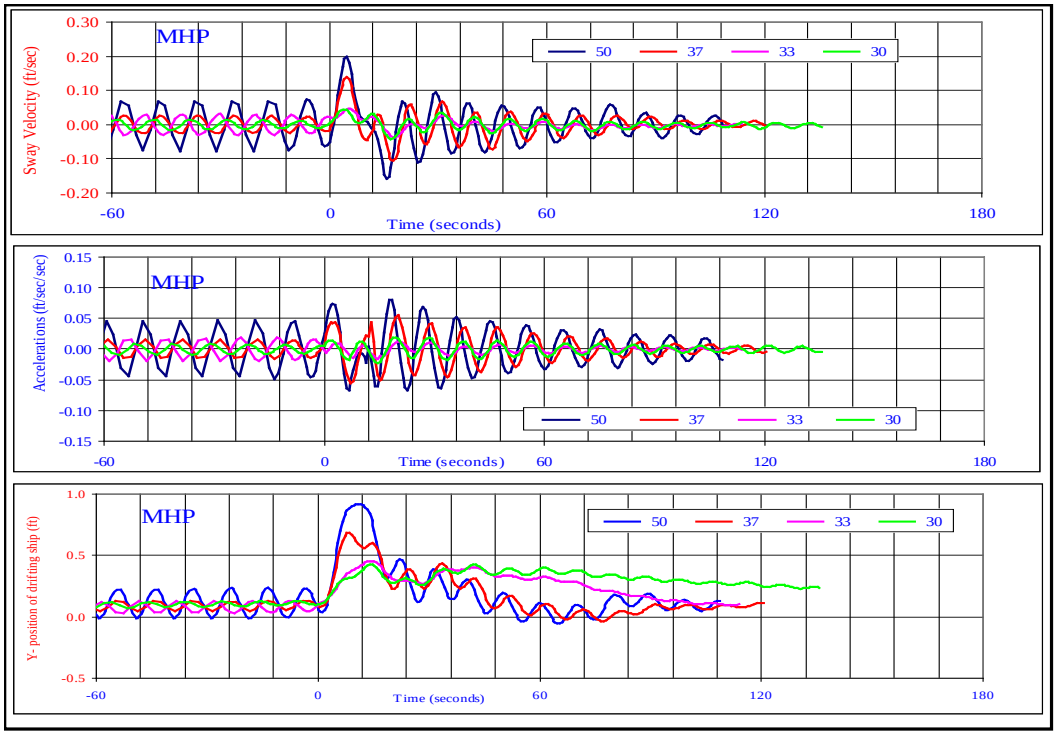

Figure 70. Sway motion of MHP.

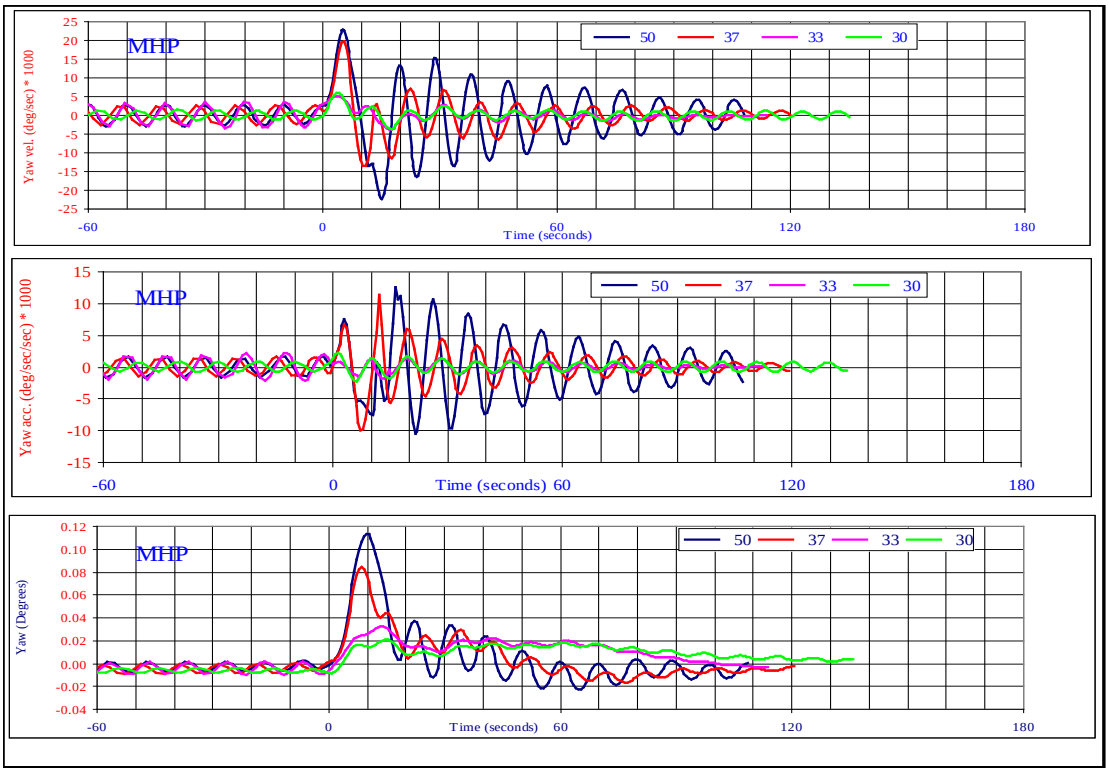

Figure 71. Yaw motion of MHP.

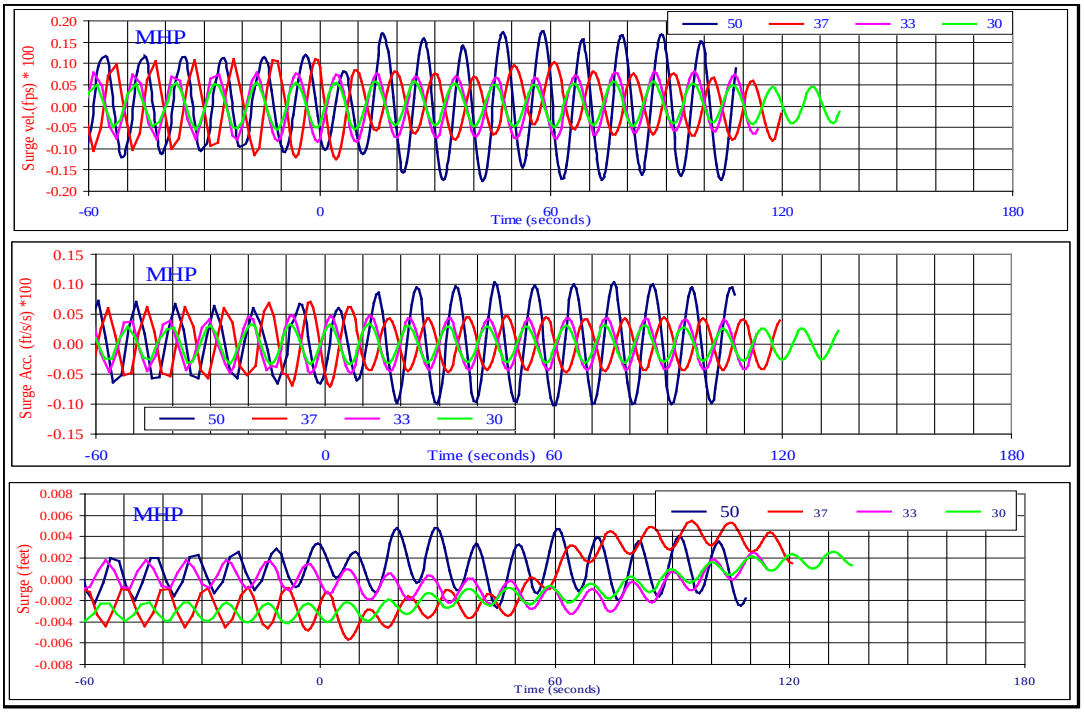

Figure 72. Surge motion of MHP.

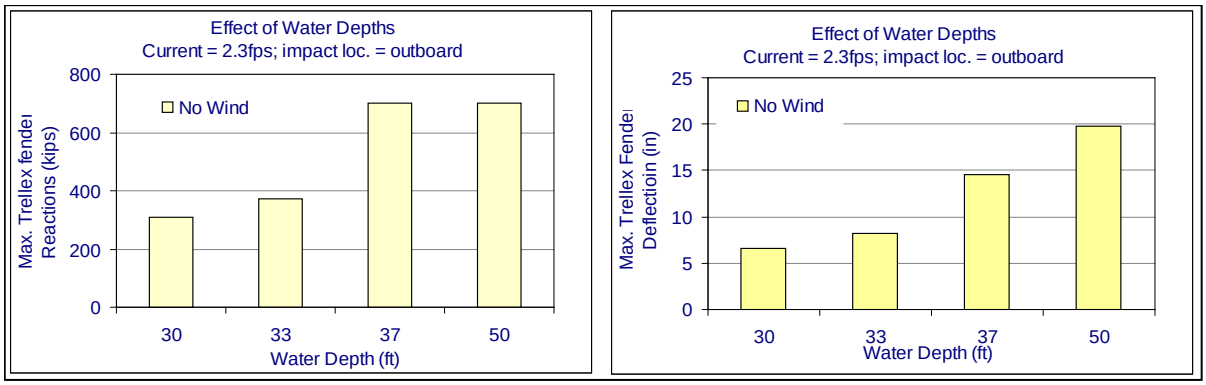

Figure 73. Fender reactions to drifting LHD in various water depths

8.5 Effects of Contact Locations

The previous series indicates that two founding shafts of single Trellex fenders withstand a ship drifting in the outboard lane with 1.5-fps current in 50-ft water and 2.3-fps current in 37-ft water, however buckled with 2.3-fps current in 50-ft water. Similar exercises were conducted for ship drifting in the center and inboard lanes in the same currents toward an MHP secured by two founding shafts. The results are in general similar to observations with the previous series and thus will not be reiterated in details. Only essential highlights are presented to show the influence of impact locations. As previously mentioned, the model ship drifting in the outboard lane in 50-ft water severely buckled the interior fenders. This ship in the central lane also buckled the interior fender in 2.3-fps current (Figure 74), or in 1.5 fps in the inboard lane (Figure 75). Figure 76 confirms that a ship drifting in the outboard lane impacts interior fenders the most severely in an identical environment and pier layout.

As a sanity check, fender deflections were reconstructed from the motion excursion of the pier. Figure 77 compares the reconstructed fender deflections with those predicted by the simulation model. The results from both methods are identical until the fender yields.

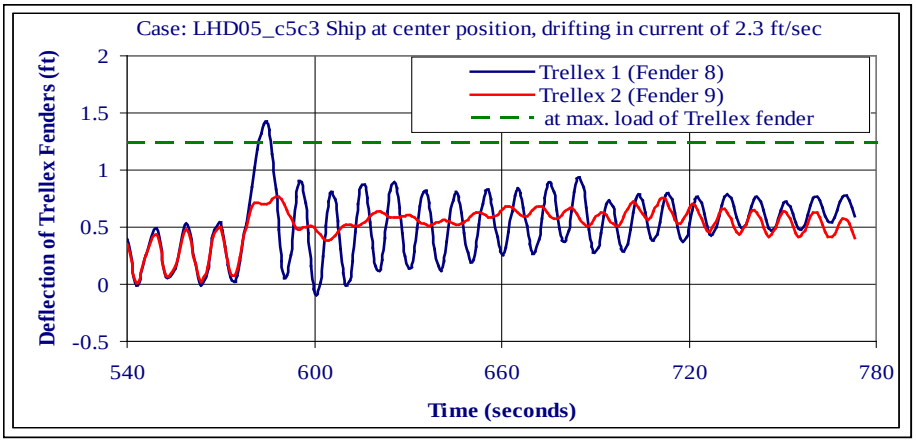

Figure 74. Docking ship in the center lane of 2.3-fps current buckled fenders

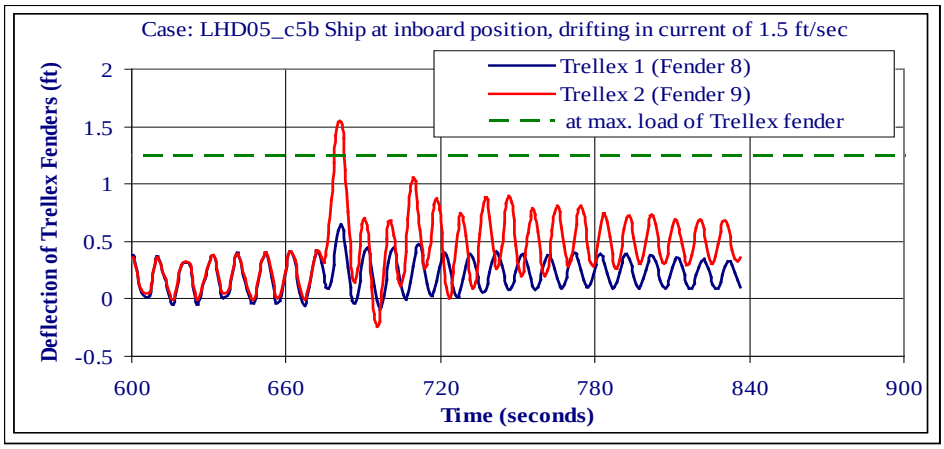

Figure 75. Docking ship in the inboard lane of 1.5-fps current buckled fenders

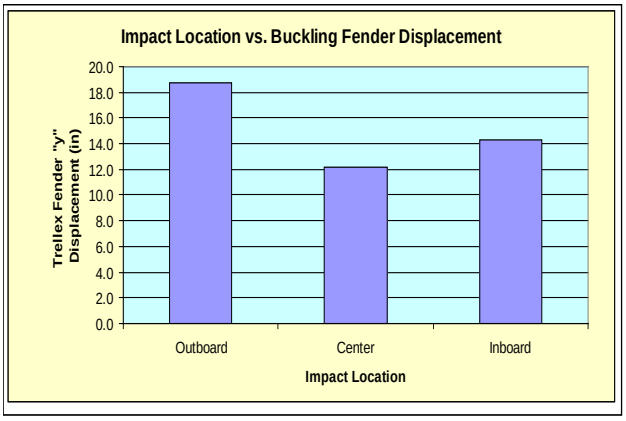

Figure 76. Effect of impact locations

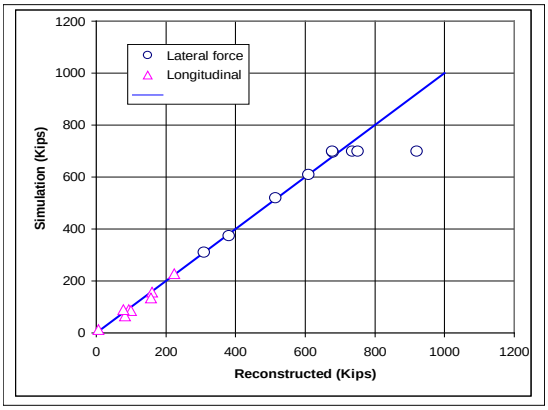

Figure 77. Verification of fender deflections

8.6 Wind Forces

Concurrent tail winds drive drifting ships to higher speeds and thus post more hazards to the pier. Wind loads will be included in the subsequent analysis to identify the worse-case scenario environment the present founding shaft design can withstand. A discrete force was applied to the drifting ship to represent the wind effects in the simulation model in the same manner as does the tugboat in the ship-docking scenario. Wind loads on ships are resulting primarily from form drag. These loads may be estimated, for the present purpose, by an empirical equation derived by Owens and Palo [Reference 17] from a collection of independent measurements as follows.

$$F_w = 0.5*\rho*V^2*C_d*A*f(\theta)$$

Where ρ=0.00237 lb-sec^2/ft^4, is the density of air

V is the wind velocity in ft/sec at the elevation of wind force application

A is the sail area, or projection area of the ship hull exposed to wind action

C_d is the drag coefficient

$f(\theta)$ is a normalized shape function dependent on incident wind angle θ.

Owens and Palo [Reference 17] suggested a mean value of 0.92 for the broadside drag coefficient C_d for large naval ships similar to the present model ship, LHD. The present simulation assigned a more conservative value of $f(\theta) = 1.0$ and a more generous sail area of 700-ft by 33-ft for the purpose of seeking the worst-case scenario wind loads. Wind velocity is the only parameter to be investigated. Figure 78 summarizes the wind force calculation for free stream wind speeds from 10 to 40 knots.

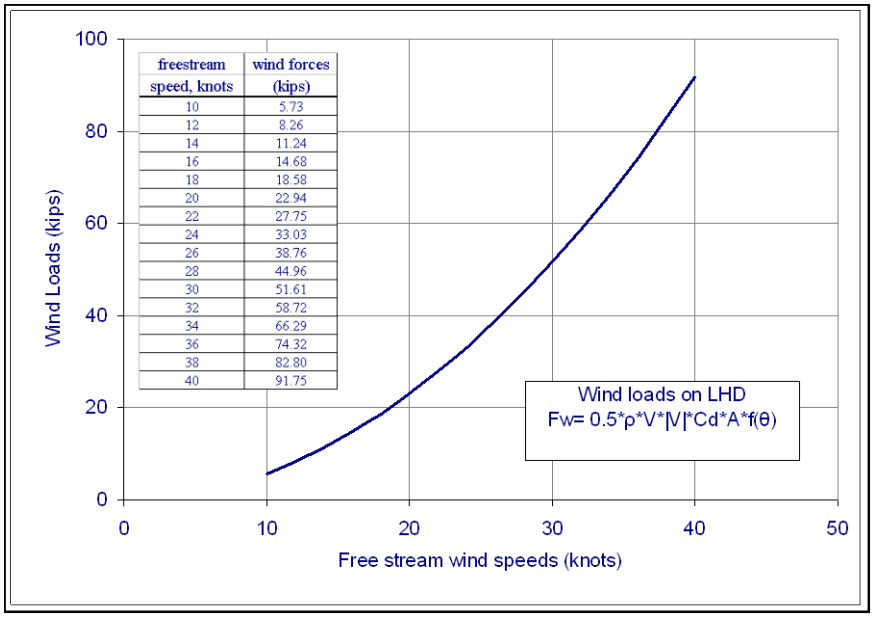

Figure 78. Wind forces

Wind forces drive the drifting ship in calm water in the same way tugboats thrust docking ships. This series considered wind force as a secondary force to the current driven ship drifting and thus focused on how winds accelerate a drifting ship and its subsequent impact load on fenders. The simulations added wind forces to the baseline scenario used for the assessment of current effects in Sections 8.3 and 8.4. Since the ship drifting in 2.3-fps currents is known to severely buckle the interior fenders of an MHP secured by two founding shafts, this series upgrades the mooring system to four shafts as illustrated in Figure 79. In order to emphasize the wind effect, the present series used two wind forces of 28 and 80 kips, which are associated with 22 and 38 knots wind, respectively. The overall layout of this series is summarized in Table 7.

Figure 80 indicates concurrent winds increase the ship drift speed. The increments in ship speeds, fluid forces, and pier responses to small wind force increments are noticeable. Figure 81 augments the wind effect by increasing the wind loads to 28 and 80 kips in 50-ft water. Winds kicked in after the ship had been drifting in the currents for 100 seconds. The results are compared with that of a ship drift in the same current without concurrent winds. The pier in the latter case was secured by two founding shafts. At the increased speed, the ship ran out of space to reach the terminal speed before impacting the foam fenders in all cases. However, the wind effects are visible. Figure 81(a) substantiates that winds are rather effective to escalate the ship speed in currents. While a 50-kip tug thrust only pushes the ship to 0.6 fps in calm water (Figure 45), a 28-kip wind force is capable of escalating the ship speed by 0.46 fps in 2.3-fps current. An 80-kip wind force drives the drift ship exceeding the ambient current speed. A faster drifting ship

also allows faster current around the ship. Consequently, concurrent winds may escalate the ultimate impact forces on the pier through direct force, higher ship approaching speed, and stronger trailing current in the wake. Their effects shall be properly accounted in the fender design. Figure 82(a) suggests that wind forces are more effective in accelerating the drift ship in deeper water as indicated by the changes in the slope of the velocity histories after winds kick in. Eventually, the wind force drove the ship in 50-ft water to a speed slightly higher than the ships in shallower depths. However, the small speed increment is sufficient to drive a noticeably higher fluid force on the drift ship after it contacts the fenders as shown in Figure 82(b).

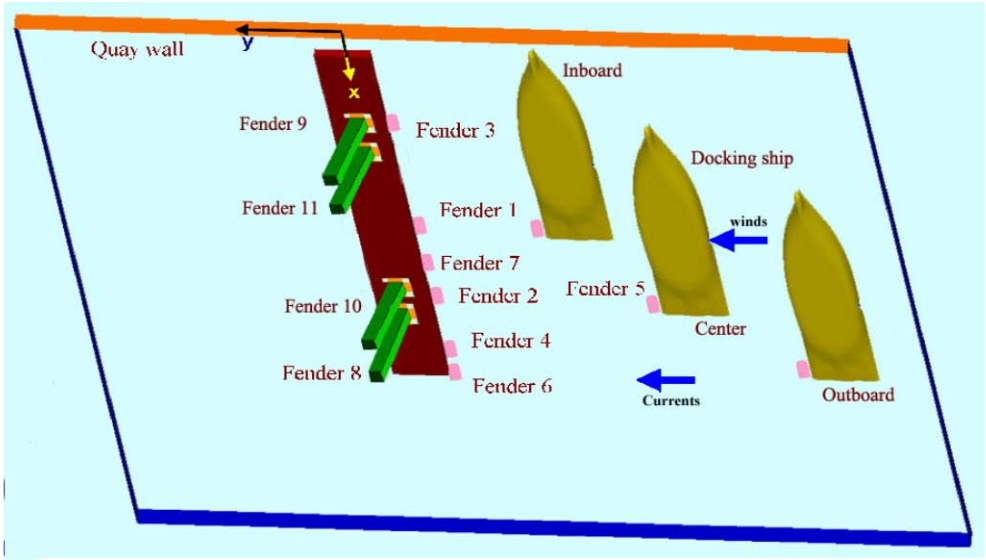

Figure 79. Layouts of MHP with four founding shafts and the locations of docking ships

Table 7. General layout for the sensitivity study of wind forces

Parameters	Descriptions	Parameters	Descriptions
Model ship	LHD; parallel to pier	Wind force	28 and 80 kips
Ship lane	outboard	Tug assist	no
Initial ship location	600 ft from the pier	Foam fender, stiffness	67 kip/ft
Current speed	1.5 and 2.3 ft/sec	Interior fender, stiffness	650 kip/ft
Water depth	30, 37, and 50 ft	Yielding load	700 kips
Founding shafts	4	Interior fender, damping	100 kip*sec/ft

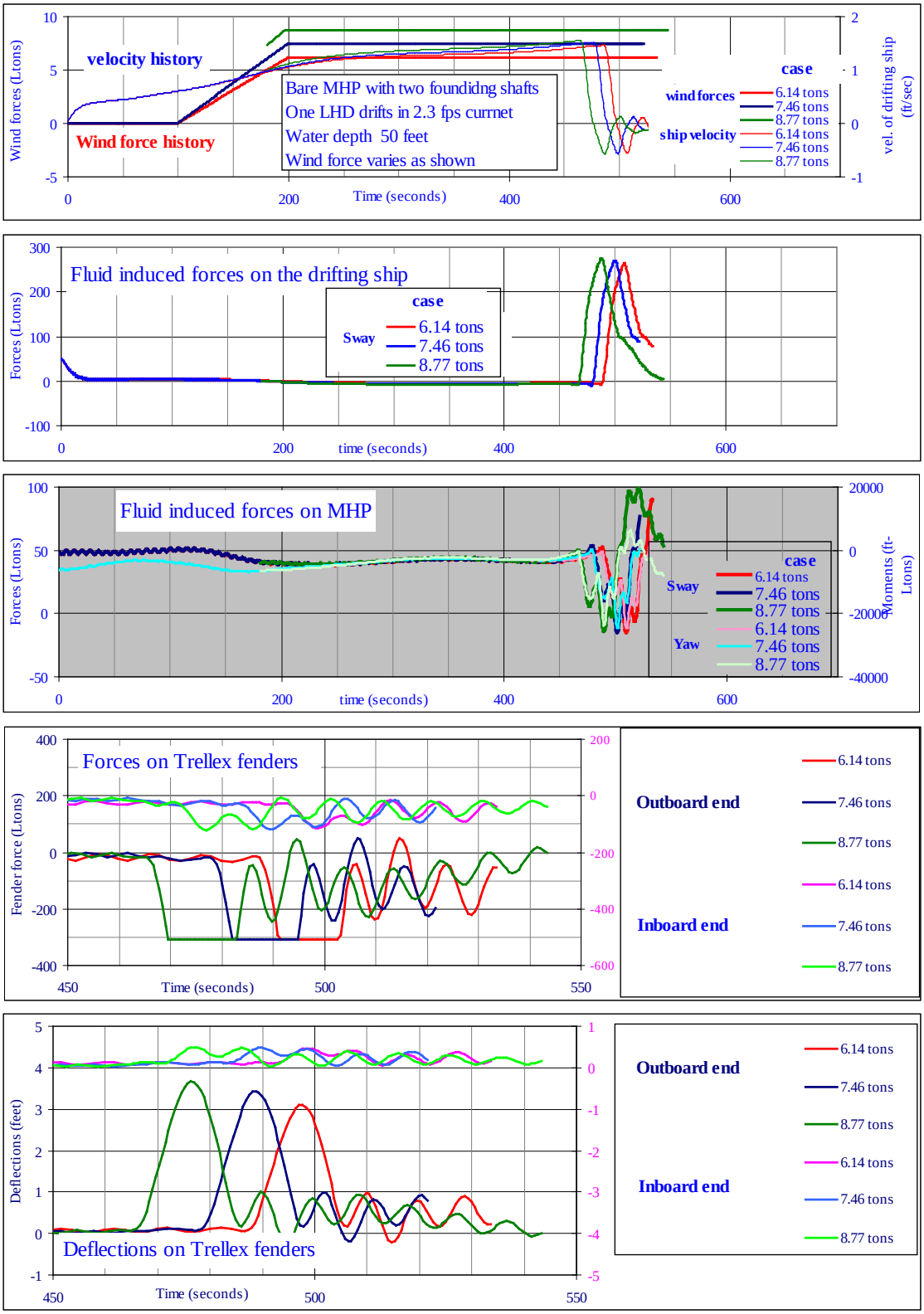

Figure 80. Effects of wind loads to ship drifting in current

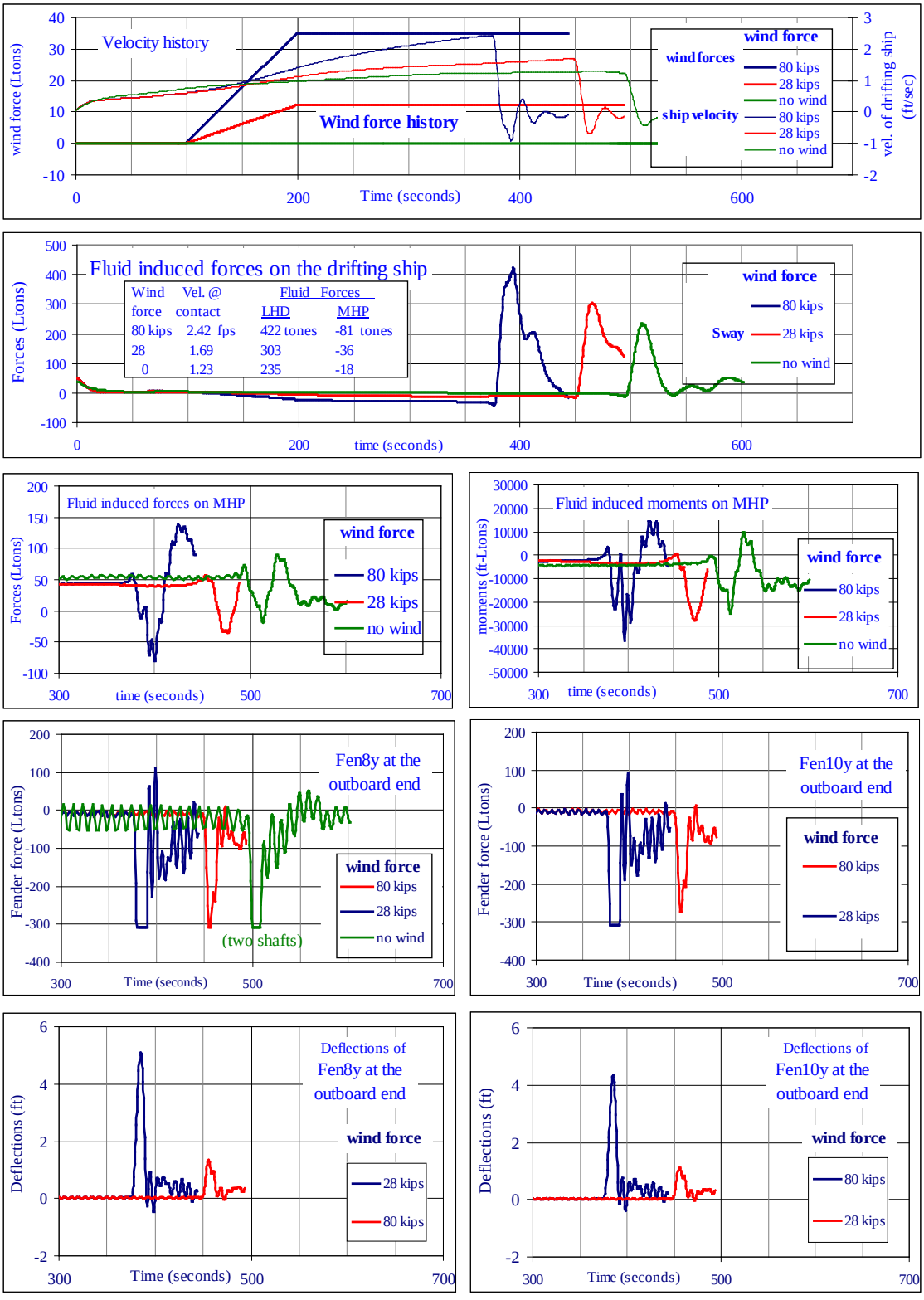

Figure 81. Effects of wind forces on MHP with four shafts

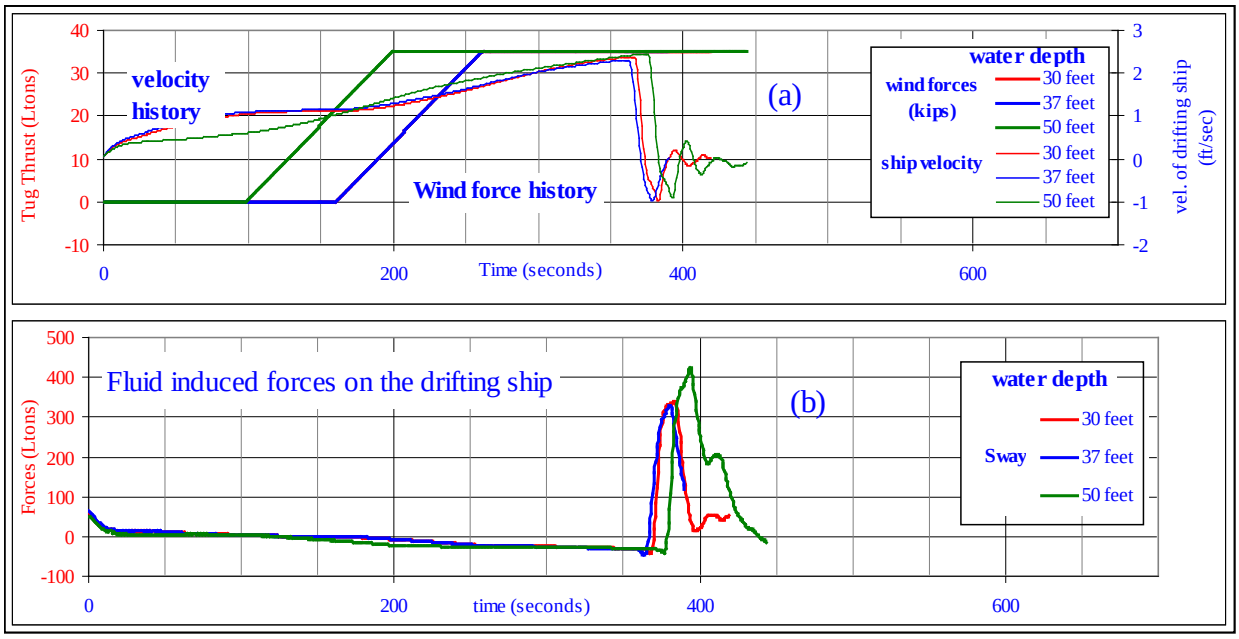

Figure 82. Wind effects in various water depths

8.7 Configurations of Founding Shafts

Each MHP module comprises a moon pool to engage a founding shaft. A four-module pier may engage two to four founding shafts depending on the site conditions. The exercises in Section 8.4 conclude that interior (Trellex) fenders of a MHP with two founding shafts did not survive the impacts by a drifting LHD in currents above1.5-fps in 50-ft water. Figure 75 suggests a ship hitting the pier near its ends buckled the fenders in 1.5-fps current while Figure 74 suggests a ship hitting the pier at the center buckled the fenders in 2.3-fps current. Figure 81 further indicates that a concurrent wind of 14 knots accelerated the ship in a 2.3-fps current and severely buckled the fenders.

Another series of simulation was conducted to quantify the holding capacity of a pier with four founding shafts. The pier was challenged in this series with a ship drifting in the outboard lane at 50-ft water with the worse-case scenario current of 2.3 ft/sec at the potential pier site. The results confirmed that a pier with four founding shafts survived the ship impact in the above mentioned environment. This pier was further challenged with concurrent winds of various intensities. Figures 83 to 85 compare the performance of interior fenders in both MHP layouts. The results indicate that the pier with four founding shafts is sufficient to withstand the worse-case scenario drift ship impacts with a small margin for 20-knot concurrent winds. Fenders began to buckle at concurrent winds of 22 knots. It can be seen the pair of founding shafts at the outboard end share the large impact loads and maintain within the yielding strength of the fenders. A ship in the same scenario will severely buckle the fenders in the design with two founding shafts.

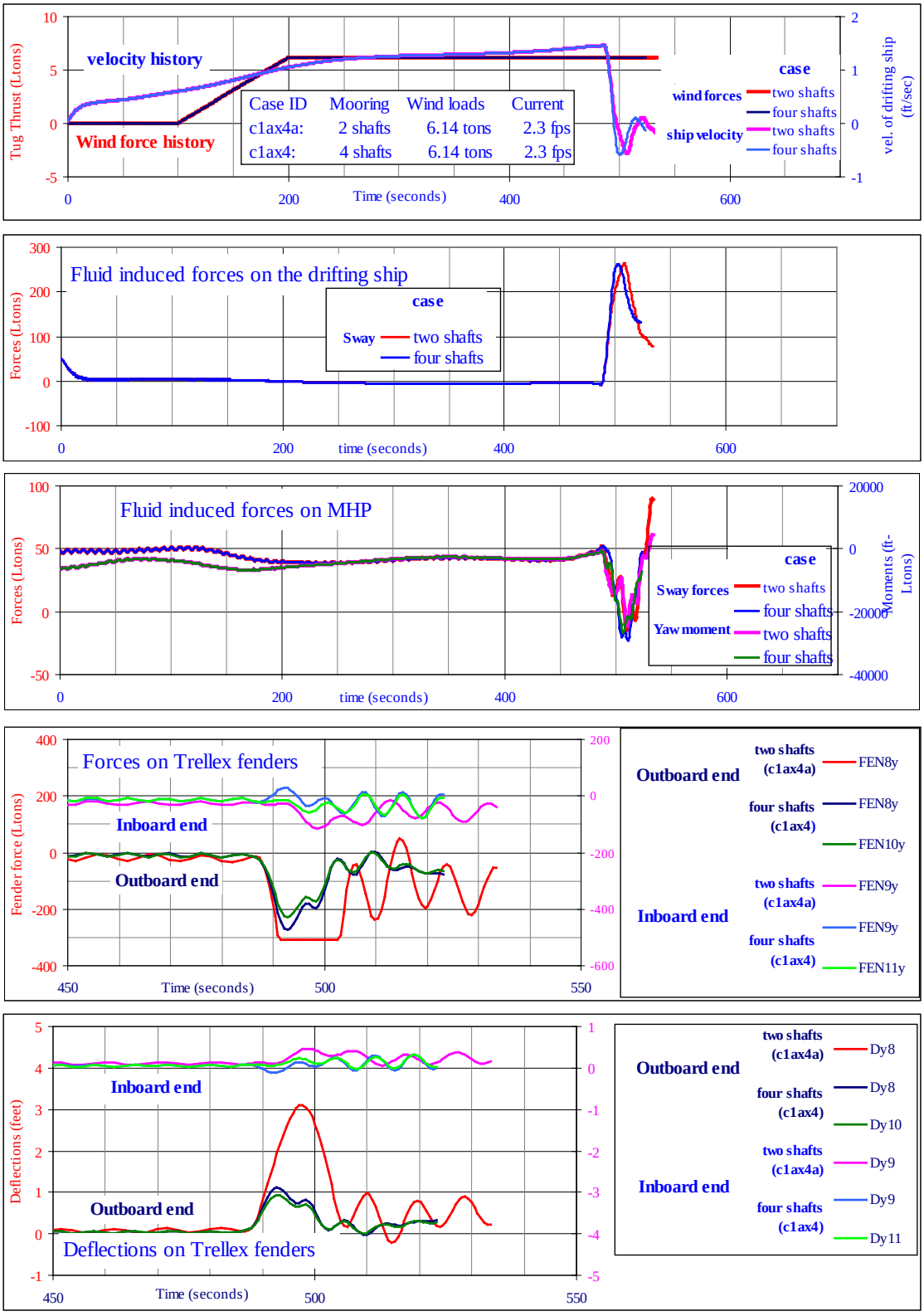

Figure 83. Effects of founding shaft configuration (Case LHD05b_1sm_c1ax4)

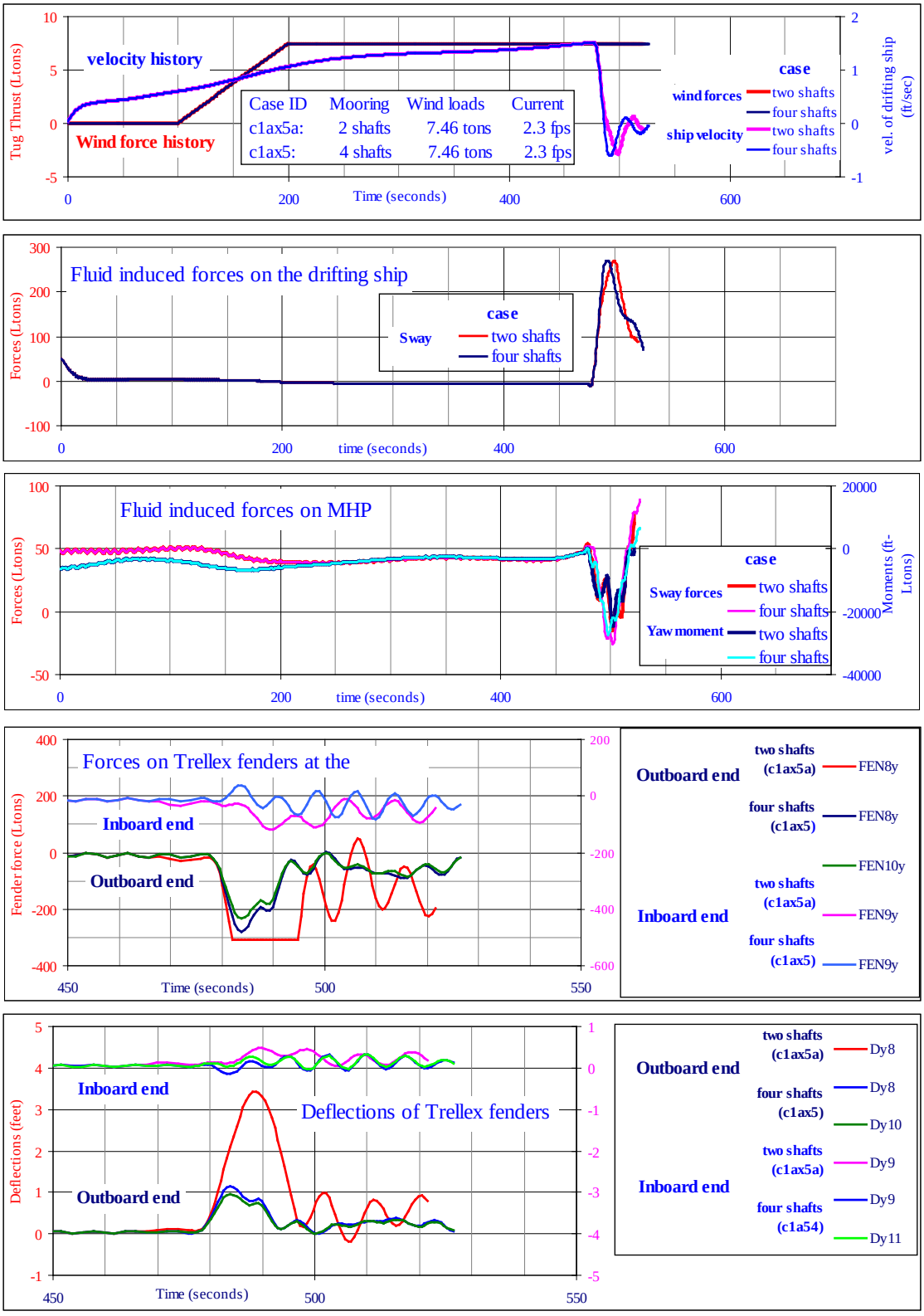

Figure 84. Effects of founding shaft configuration (Case LHD05b_1sm_c1ax5)

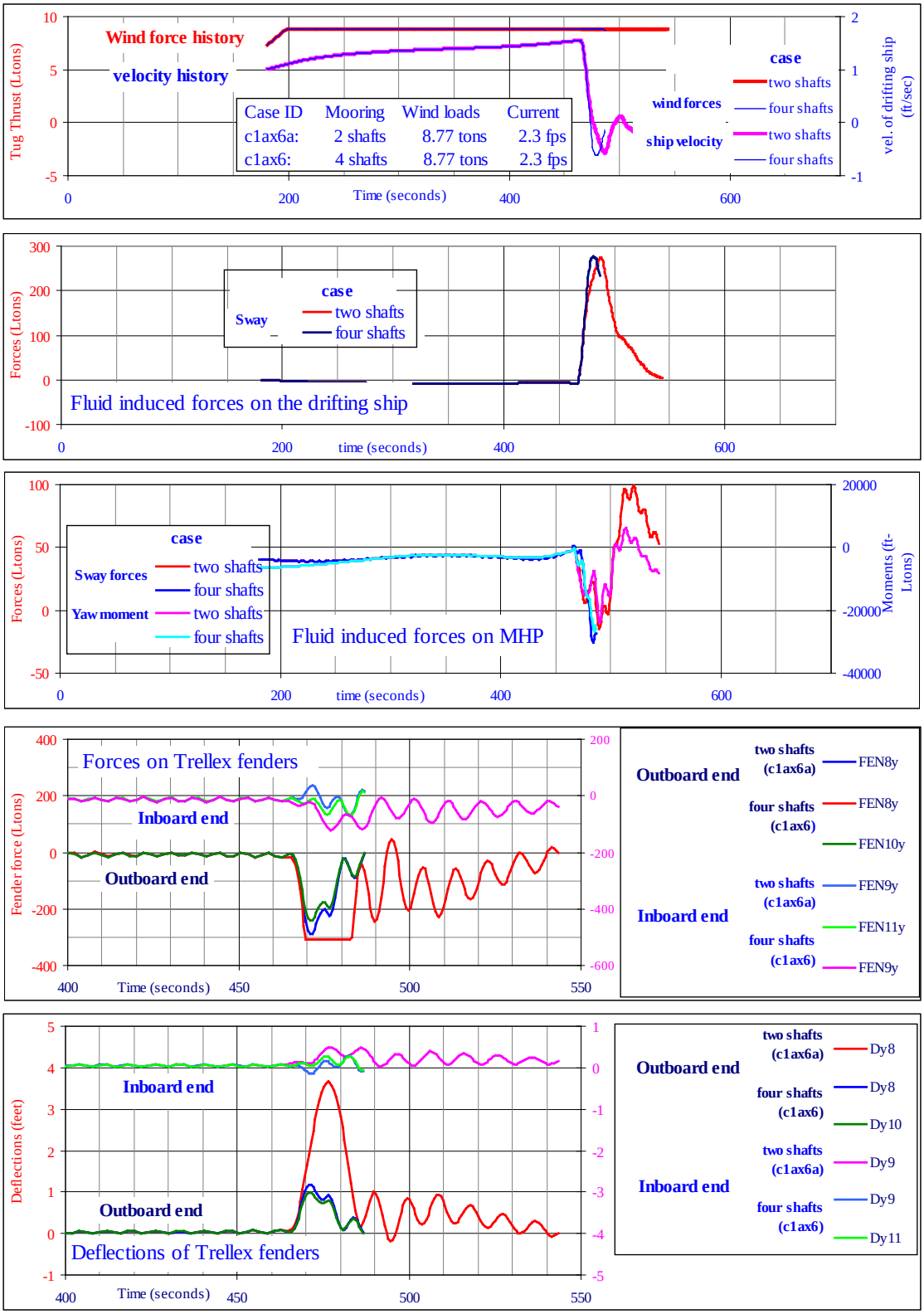

Figure 85. Effects of founding shaft configuration (Case LHD05b_1sm_c1ax6)Paths of Load Transfer

8.8 Paths of Load Transfer

The responses of the MHP secured by two and four founding shafts are further inspected for their consistency. Figure 86 addresses the load path during ship impact for the case with four founding shafts. The top chart summarizes the force balance among the fenders, while the bottom chart summarizes the impact forces attributable to the ship inertia force and currents. It can be seen that the impact forces were properly transmitted in full by the exterior foam fenders onto the interior Trellex fenders. The totals of these three sets of forces are essentially identical. The two founding shafts on the outboard end share the impact loads in according to their locations as anticipated. Ship inertia and fluid induced forces are comparable in this case. While ship inertia is responsible for the acute initial impact load, the fluid induced forces prolongs the impact duration. Fortunately, the fluid induced force evolved far behind the inertia force and did not substantially intensify the impact load by the ship inertia. The phase delay between the peaks depends on the stiffness of the exterior foam fenders. Soft foam fenders tend to delay the inertia force contribution to closer aligning with the fluid force contribution. This factor deserves closer attentions for fender designs.

Figure 87 depicts an essentially identical process for the pier with two founding shafts except the interior fenders buckled in this case. The load transferring was fully on track as did the previous case. Nevertheless, the loads on foam fenders flatted out as they retreated with the pier when the interior fenders buckled. The most noticeable difference exhibits in a more intensive oscillation of the pier after the ship inertia induced impact force subsided. The pier with two shafts displaced and oscillated three times as much as did the pier with four shafts as shown in Figures 88 and 89. This is attributable to the excessive deflections due to (interior) fender buckling. These excessive motions may degrade the efficiency of pier operations. However, bear in mind that the present analysis assumed unlimited fender deflections in the fenders. Real fenders will perhaps harden sooner and cause a severe shock impact on the founding shafts.

Similar behaviors were also observed with a pier with four founding shafts, if the interior fenders buckle under large environmental loads as illustrated by Figures 90 and 91. The ship was drifting in a 2.3-fps current subject to concurrent wind forces of 80 kips.

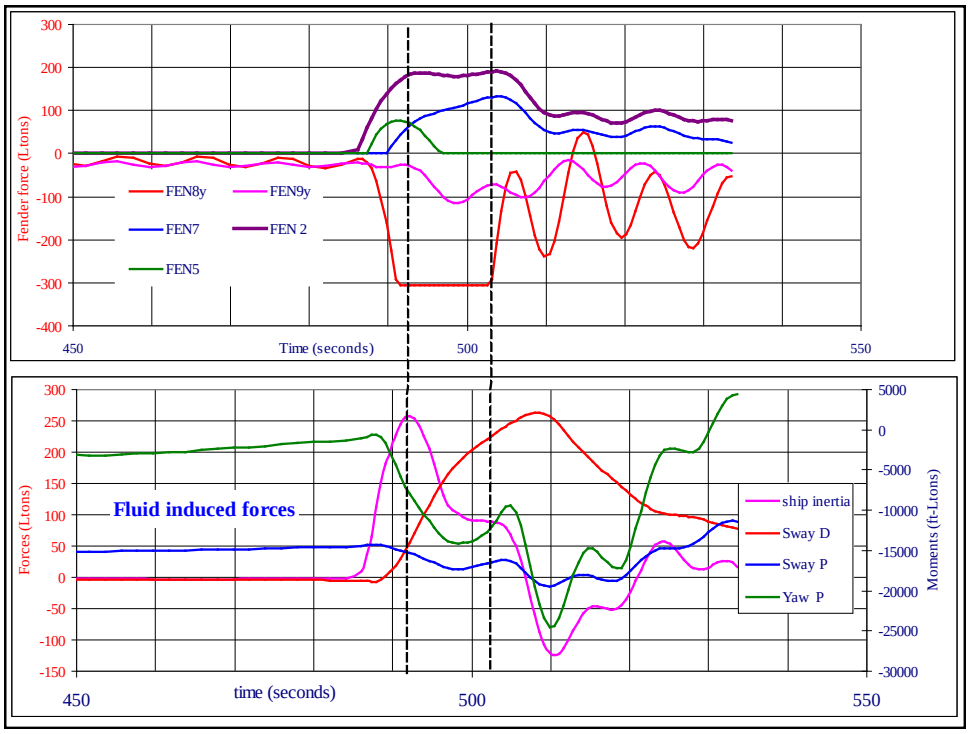

Figure 86. Comparison of load paths between buckled and unbuckled systems

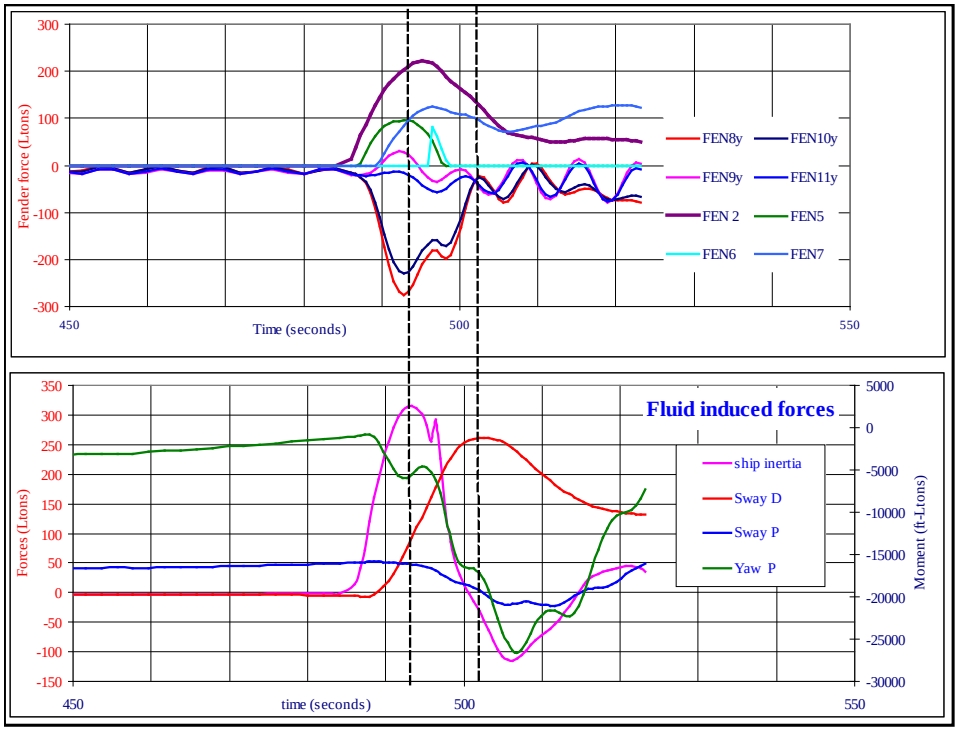

Figure 87. Comparison of load paths between buckled and unbuckled systems

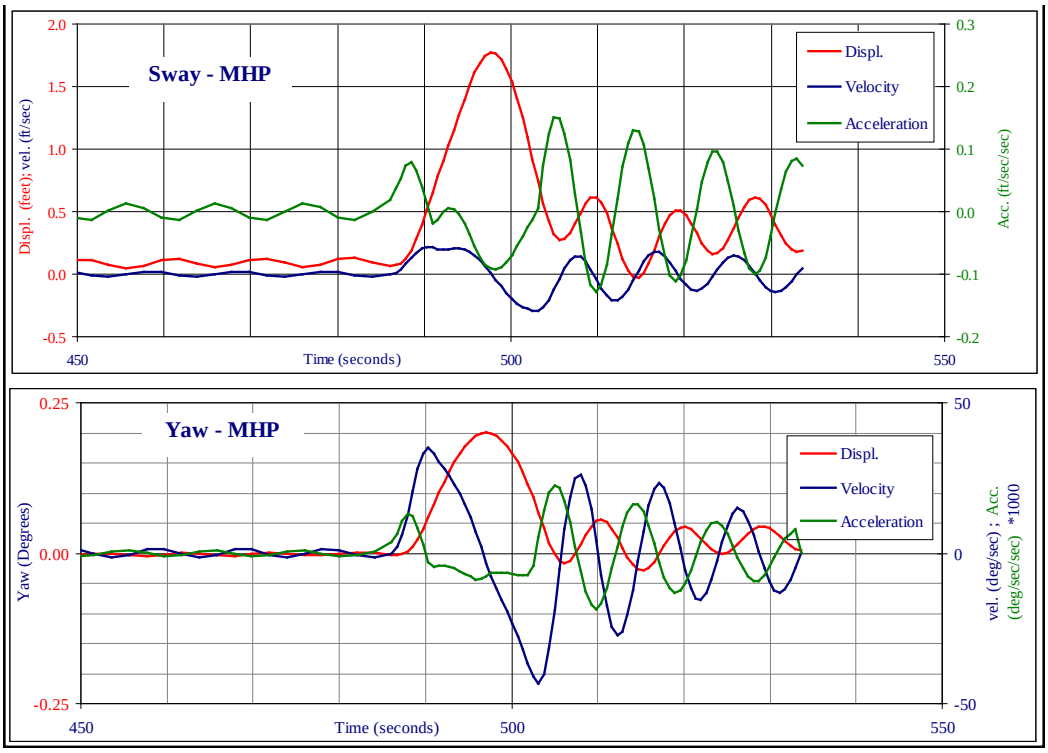

Figure 88. Motion kinematics of MHP (Case lhd05b_1sm_c1ax4a)

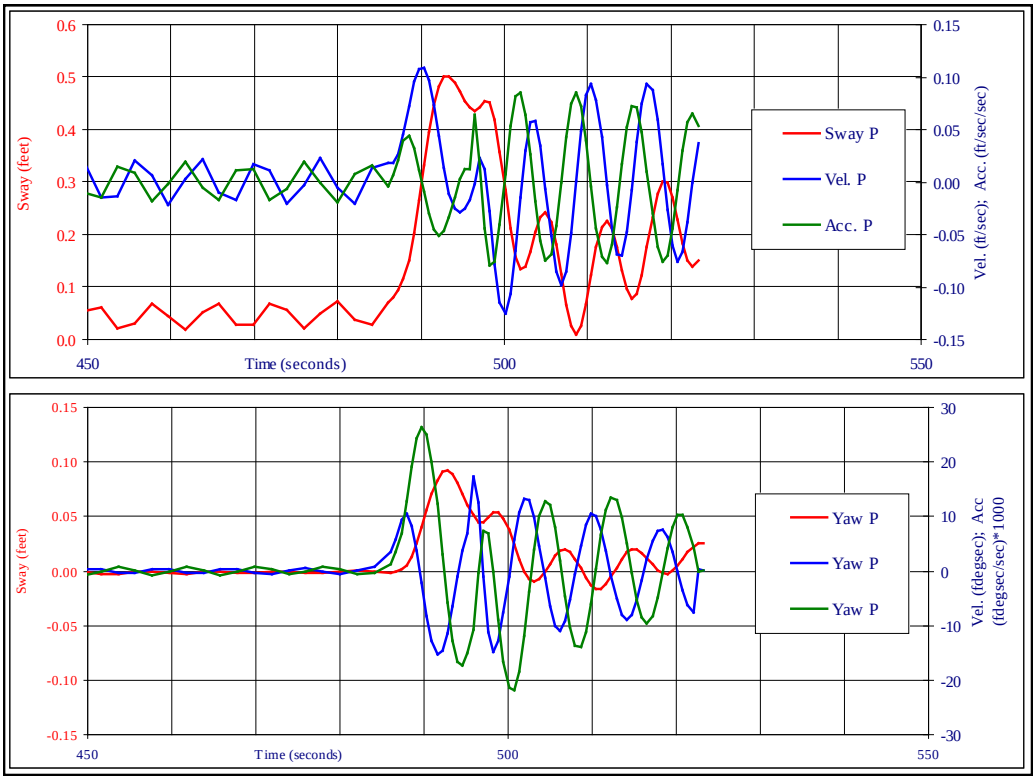

Figure 89. Motion kinematics of MHP (Case lhd05b_1sm_c1ax4)

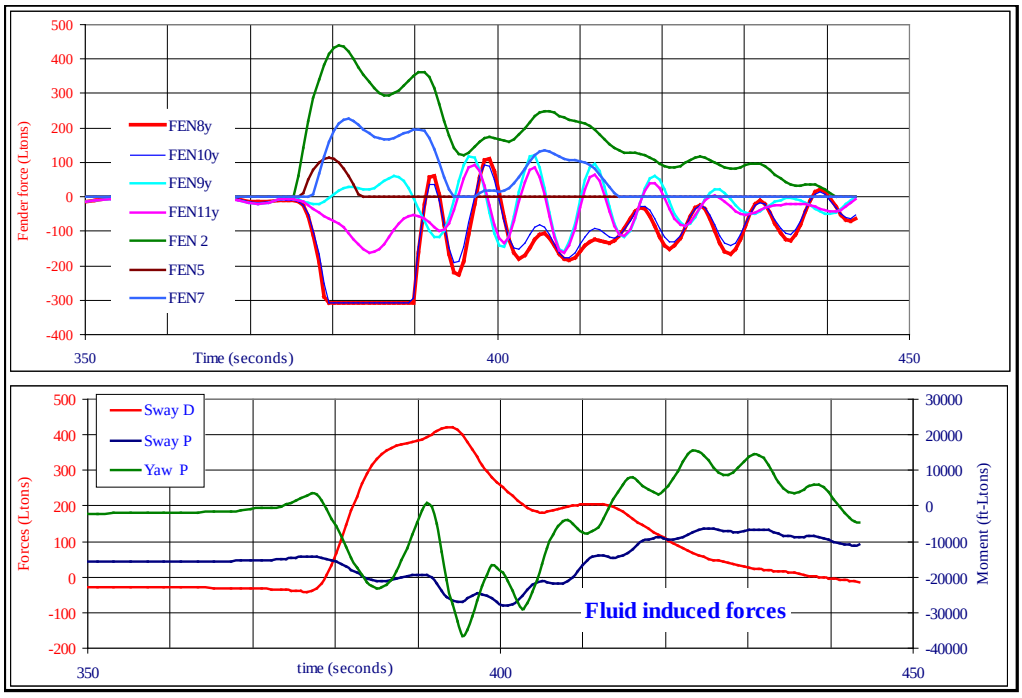

Figure 90. History of berthing load transferring (Case lhd05b_1sm_c1ax9)

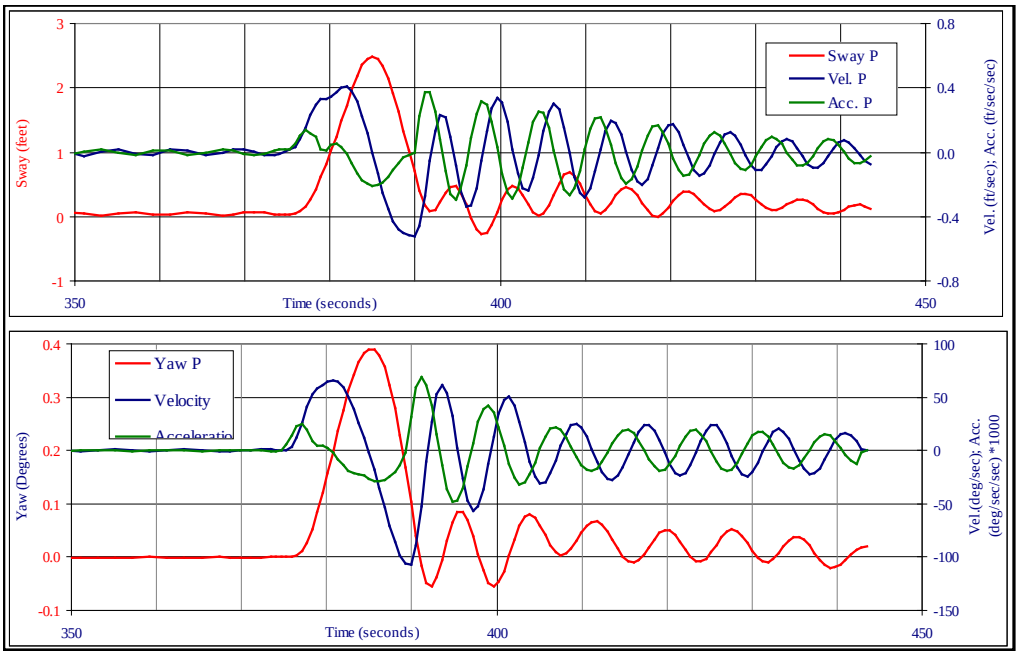

Figure 91. Motion kinematics of MHP (Case 1hd05b_1sm_clax9)

8.9 Drift Ship Induced Impact Loads and MHP Responses

This chapter analyzed the performance of a drifting ship in currents and its impacts on the MHP design and operations. The analysis further introduced concurrent winds to the scene to identify the worse-case scenario environment the conceptual MHP to date can survive.

A fully loaded LHD drifting in currents represents the most severe challenge to the MHP facility concerning the design capacities of founding shafts and fenders. This chapter recaptures the impact loads imposed by such ship drifting in the worst-case scenario currents identified for future MHP sites and the subsequent MHP responses for design references. Table 6 presents the range of environment conditions under consideration and the highlights of the simulation results.

Table 8. MHP responses to drifting ships (cmpr wind forces ser c5.xls)

water depth	feet	50	37	37	37	37	30	30	30	30
wind loads	kips	0	0	28	60	80	28	40	60	80
current speed (a)	fps	2.3	2.3	2.3	2.3	2.3	2.3	2.3	2.3	2.3
ship speed max (b)	fps	1.49	1.21	1.67	2.08	2.29	1.69	1.88	2.15	2.37
speed ratio=(b)/(a)*100	%	64.78	0.53	0.73	0.90	1.00	73.48	81.74	93.48	103.04
ship speed at contact	fps		1.12	1.65	2.08	2.29	1.694	1.88	2.15	2.37
max fluid force on LHD	tons		185	253	312	326	258	289	308	335
defl at Fen8y (c)	feet		0.77	1.19	1.99	2.97	1.2	1.5	2.2	4.7
defl at Fen10y (d)	feet		0.63	1.05	1.66	2.53	1.07	1.21	1.89	4
defl ratio=(d)/(c)*100	%		0.82	0.88	0.83	0.85	0.89	0.81	0.86	0.85

Figures 92 to 94 conclude the drift ship performance in currents, fluid induced forces on the ship and pier, impact loads on the interior fenders, and the resulting fender deflections in water depths of 50, 37, and 30 ft. Key results are listed in Table 8 to illustrate the influences of prevailing parameters, such as water depths and concurrent winds. Figure 95 provides a brief summary of the pier responses in 50-ft water.

Findings conclude:

- Ships drift faster in deeper water. A ship in deep water without concurrent wind may reach a terminal speed of roughly one half of the current velocity, provided space and time permit. Concurrent winds are very effective to accelerate the drift speed. An 80-kips wind was seen to drive the ship exceeding the current velocity. Trailing currents around the drift ship also flow faster with the ship.
- Ship speed dictates the impact loads more than linearly. Additional loads are attributed to the trailing currents. Currents impart comparable forces to the share due to ship inertia. Two components, however, peak at different times of ample phase lag. Ship inertia induced force accounts for the sharp initial impact load while the current induced force prolong the load duration.
- A ship drifting near the outboard end of the pier results in higher impact loads on the interior fenders than do the same ship drifting in other locations along the pier.
- For a pier with two founding shafts, the interior fenders buckle in 1.5-fps currents if the ship hits the pier at near its ends.
- For a pier with four founding shafts, the interior fenders survive 2.3-fps currents with a margin to withstand additional wind loads of 22 kips. The fenders buckle in the scene with 28-kip concurrent winds.
- The pier displaces extensively once the interior fenders buckle and vibrates noticeably after the impact loads subside.

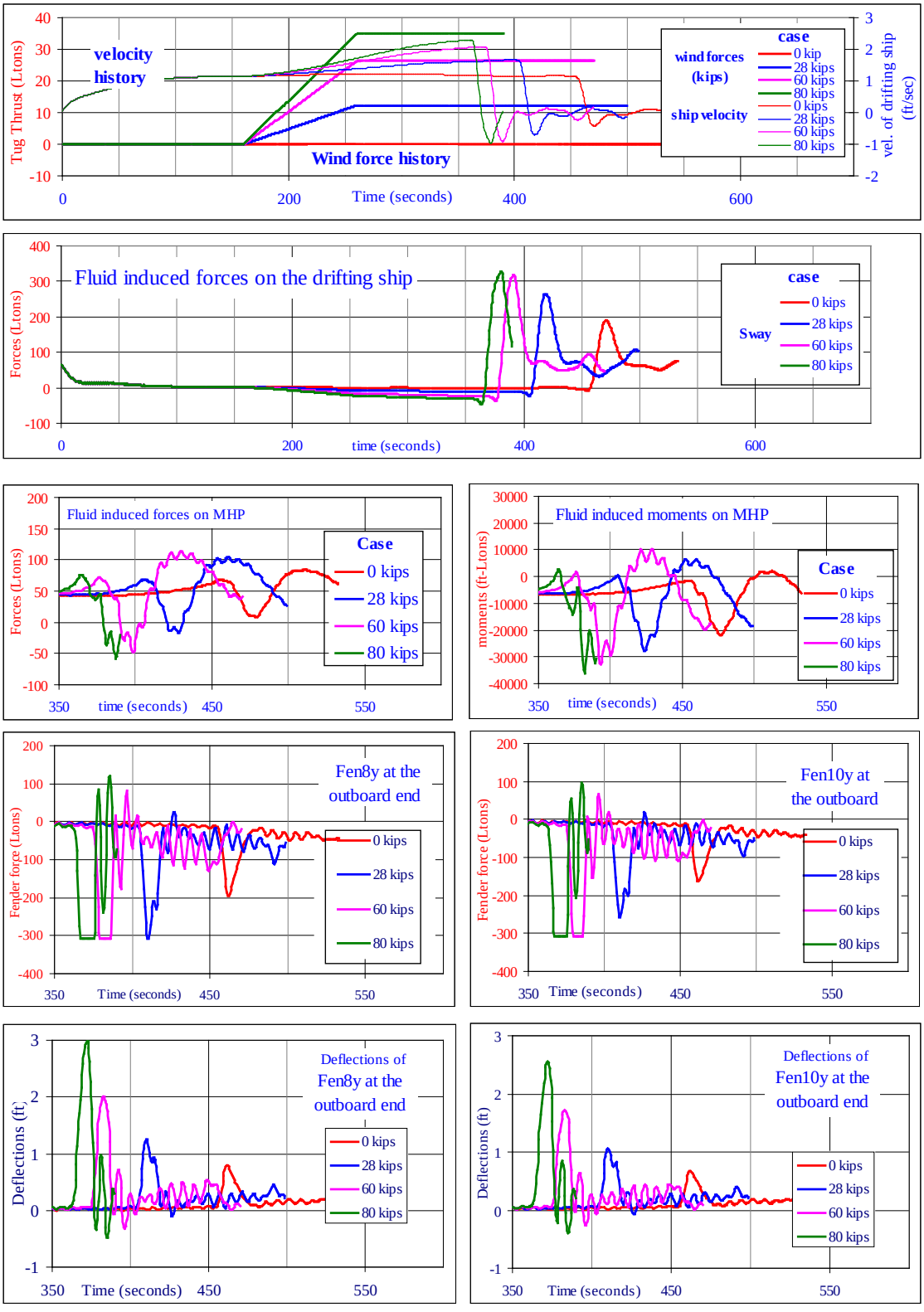

Figure 92. MHP responses to drifting ships in 37-ft water

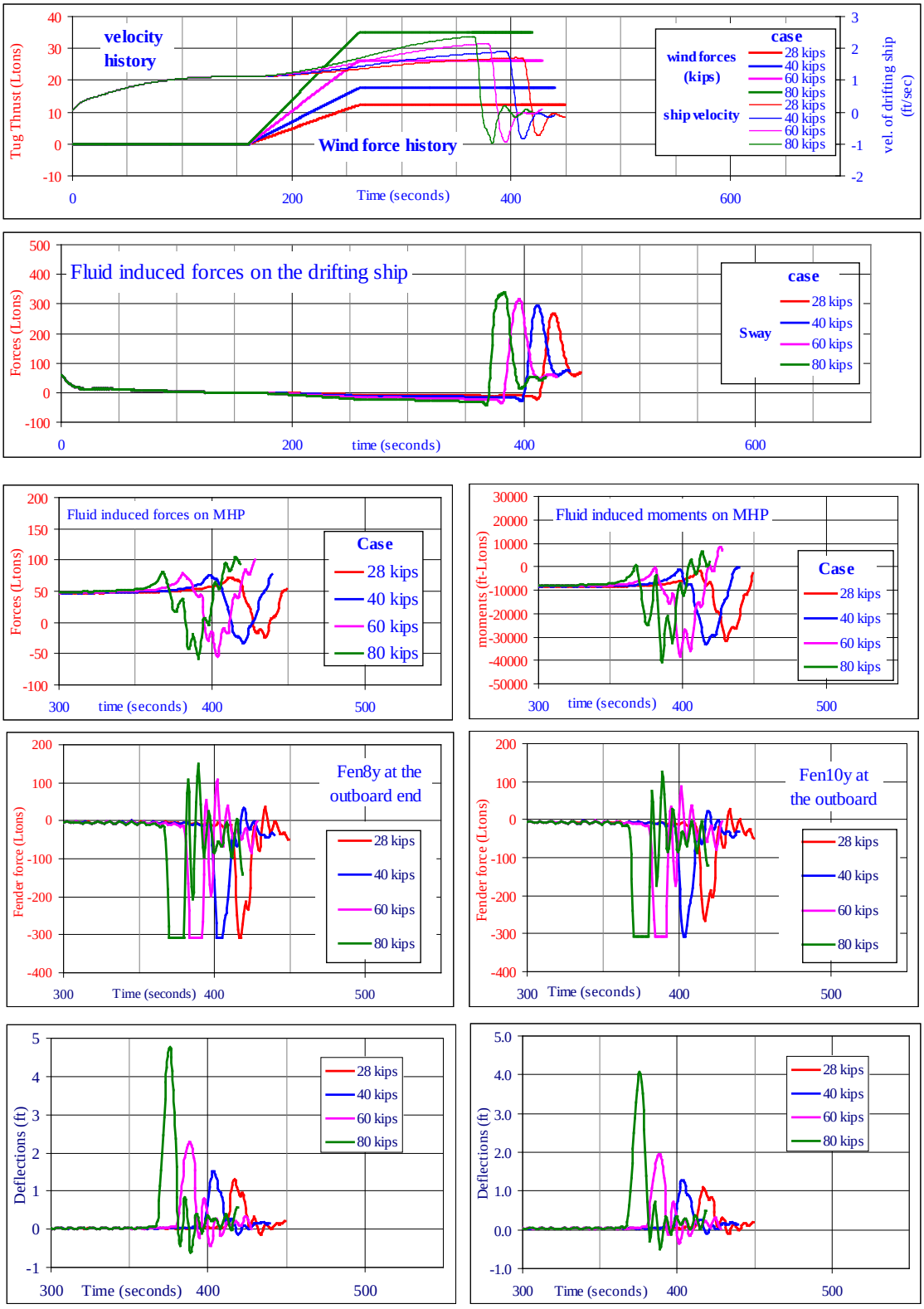

Figure 93. Berthing load on interior fenders in 30-ft water

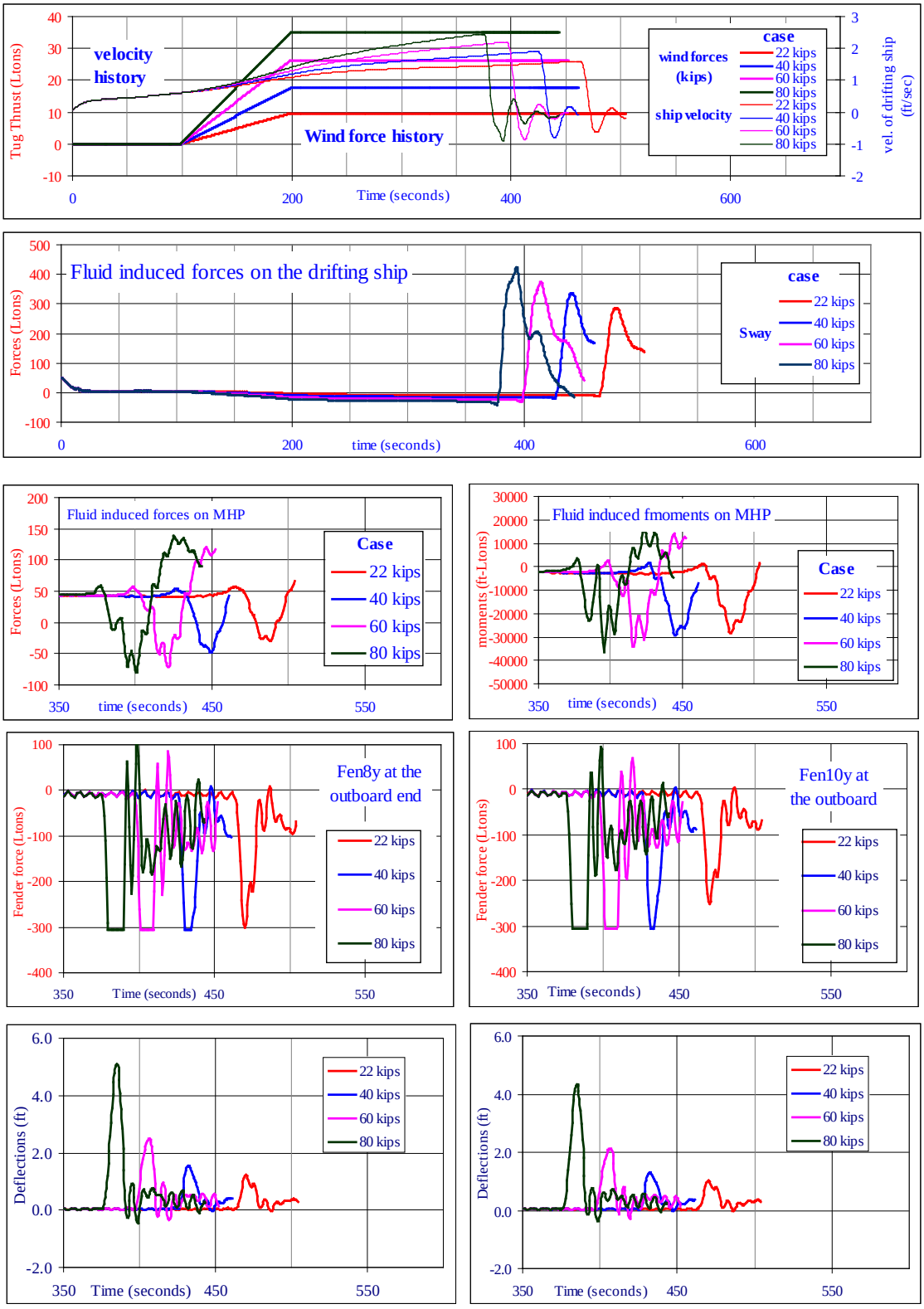

Figure 94. Berthing load on interior fenders in 50-ft water

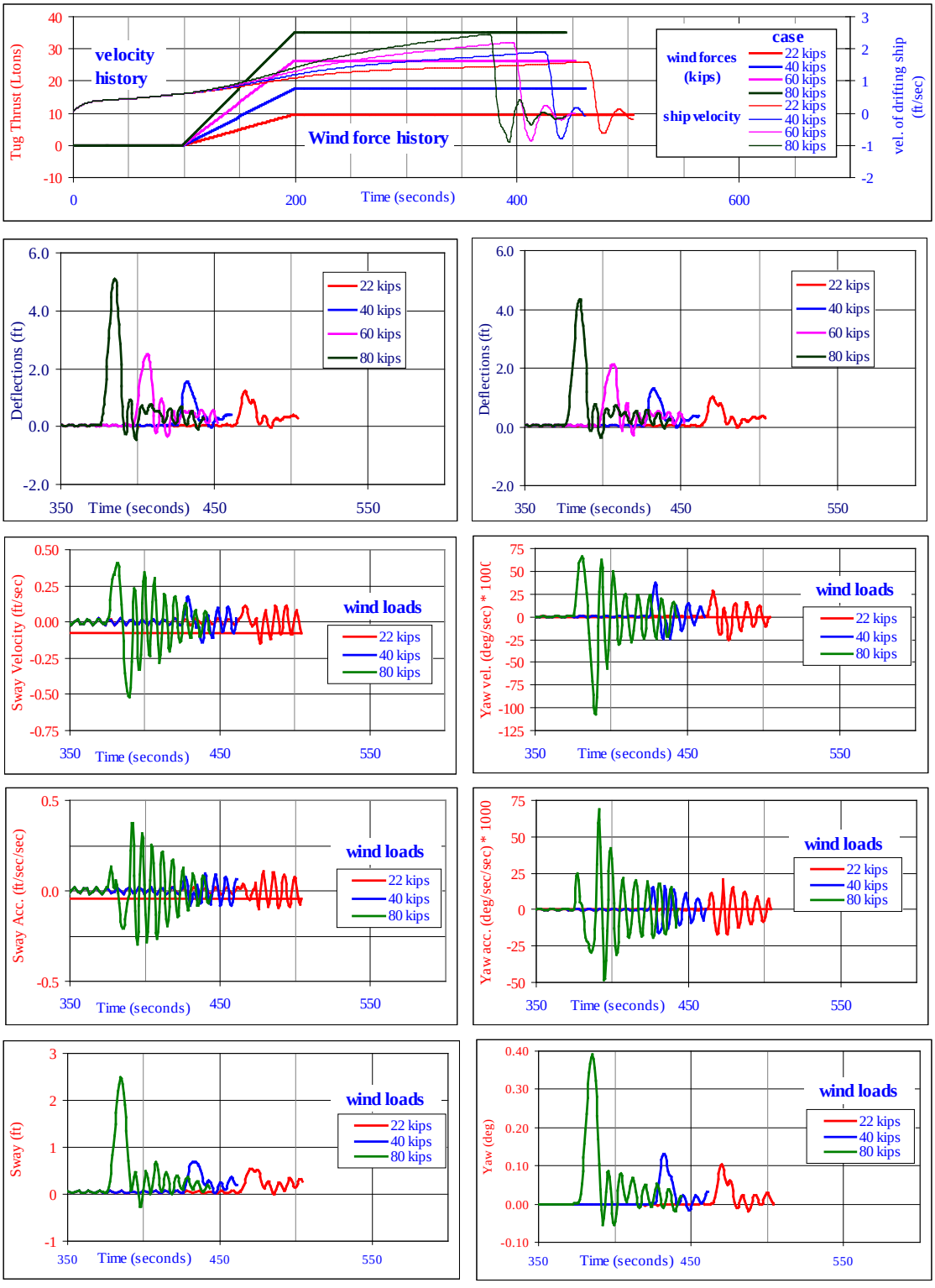

Figure 95. Summary of pier kinematics

9.0 CONCLUDING REMARKS

A floating pier permits lateral motion by nature and is hence more responsive to external loads than is a fixed pier. Its position keeping system dictates the stability and thereby influences the operation efficiency and survivability of the pier in adverse environments. The MHP is founded by multiple steel shafts, which engage the pier through moon pools in the pontoon modules. The founding pools are slightly larger and the founding shafts with fenders for the purpose to ease the installation and isolate the MHP hull from seismic ground motion. As MHP facility is intended for use in sheltered waters, where direct environmental loads are minor, the pier confronts major threats primarily from docking ships or drifting ships in currents. Like fixed piers, the MHP interfaces ships through fenders. In either case, the ship impacts the pier driven by the kinetic energies of the impinging ship and trailing currents. Only the MHP introduces another tier of fenders inside the founding pools to ease the load transfer from the pier to the founding shafts. The pier motions, nonlinear fender deflections, and gaps in the founding pools combined complicate the mechanism of load transferring. The load path is no longer predictable, as in the case of fixed piers, to justify the decoupled procedure for the impact load analysis. This study clearly demonstrated that the decoupled procedure misinterprets the mechanism currents engage a broadside ship and hence overly simplifies the compensation for the fluid induced loads.

This study traced the complex events of ship-pier coupling in at a congested MHP, comprising multiple ships moored alongside the pier, with a RANS-based computation fluid dynamic model. This model successfully captured all important features of the transient water flows in the scene, including the under keel flow, flow separations of the trailing wake in the ship path, unique flow activities in the gap confined by ships and pier, and their feedback to the participating ships. All simulation results are consistent with the anticipations by physic laws. Ship and pier responses as well as fender performances are fully traceable to the driving fluid activities. The effect of prevailing parameters pertinent to the ambient environment as well as ship and pier layouts on the impact loads and the subsequent load distributions is fully explored in the processes of ship docking and ship drifting in currents. The results conclude that a bare MHP without moored ship alongside in deep water is likely to experience the worst-case scenario impact loads in docking ship or drifting ship scenario regardless.

Ship speed dictates the fender loads. So does the location of impact along the pier but to a lesser degree. Water depth influences the approach speed of the impinging ship and thus indirectly affects the fender loads. Exterior foam fenders effectively buffer the ship impacts and smoothly relay the impact loads powered by the ship inertia and the trailing wake via interior fenders to the founding shafts. The ship inertia is responsible for the acute initial impacts while the thrust of trailing wake prolongs the intensity of the impact loads. These two components peak at different time separated by ample phase lag. The trailing wake accounts for 10 percent of the impact load in the case of docking ship, and 50 percent in the case of drifting ship in currents. Soft foam fenders tend to delay the maximum load induced by ship inertia to closer align with the maximum load induced by trailing wake. However, soft fenders also tend to transfer lower load induced by ship inertia.

A well performed docking ship is unlikely to damage the MHP or degrade its operational efficiency. The worse-case berthing loads imposed by the largest admissible client ship are well

within the design capacity of the interior fenders around the founding shafts. The docking ship only shakes the MHP slightly and hardly affects the service capacity of the pier. The design of interior fenders to date seems decent for the operational environment. Two founding shafts are sufficient to withstand the impacts by docking ships.

The interior fenders are capable of surviving the impact by the largest admissible ship drifting in 2.3-fps currents with a small margin to withstand 20-knot concurrent winds, if the pier is secured by four founding shafts. For a pier secured by two founding shafts, the interior fenders buckled if the same ship drifting in 1.5-fps current hits the pier at near its ends. The pier displaces extensively once the interior fenders buckle and vibrates noticeably after the impact loads subside.

REFERENCES

[1] Berger/Abam Engineers Inc. "Modular Hybrid Pier – Phase 2 Report," Sep 2002 .

[2] Huang, E. T. and Chen, H. C. "Long Wave Transformation in San Diego Bay" NFESC Technical Memorandum, TM-2420-SHR. 50 pages.

[3] Huang, E. T. and Chen, H. C. "Hydrodynamic Responses of Modular Hybrid Pier (MHP) to passing Ships," NFESC Technical Memorandum, TM-2411-AMP, Sep 2009. NFESC, Port Hueneme, CA 93043, 72 pages.

[4] Chen, H.C. and Chen, M."Chimera RANS Simulation of a Berthing DDG-51 Ship in Translational and Rotational Motions," International Journal of Offshore and Polar Engineering, Vol. 8, No. 3, pp. 182-191. 1998.

[5] Chen, H.C., Chen, M. and Davis, D.A, "Numerical Simulation of Transient Flows Induced by a Berthing Ship," International Journal of Offshore and Polar Engineering, Vol. 7, No. 4, pp. 277-284. 1997.

[6] Chen, H.C. and Huang, E.T., "Validation of a Chimera RANS Method for Transient Flows Induced by a Full-scale Berthing Ship," Proceedings, 22nd Symposium on Naval Hydrodynamics, Washington, D.C., August 9-14, 1998.

[7] Chen, H.C., Liu, T., Huang, E.T., and Davis, D.A, "Chimera RANS Simulation of Ship and Fender Coupling for Berth Operations," International Journal of Offshore and Polar Engineering, Vol. 10, No. 2, pp. 112-122. 2000.

[8] Chen, H.C., Patel, V.C. and Ju, S., "Solutions of Reynolds-Averaged Navier-Stokes Equations for Three-Dimensional Incompressible Flows," Journal of Computational Physics, Vol. 88, No. 2, pp. 305-336, 1990.

[9] Chen, H.C. and Patel, V.C., "The Flow Around Wing-Body Junctions," Proceedings, 4th Symposium on Numerical and Physical Aspects of Aerodynamic Flows, Long Beach, CA, 16-19 January, 1989.

[10] Chen, H.C. and Corpus, R., "A Multi-block Finite-Analytic Reynolds-Averaged Navier-Stokes Method for 3D Incompressible Flows," Individual Papers in Fluids Engineering, edited by F.M. White, ASME FED-Vol. 150, pp. 113-121, Proceedings, ASME Fluids Engineering Conference, Washington, DC, June 20-24, 1993.

[11] Chen, H.C. and Patel, V.C., "Near-Wall Turbulence Models for Complex Flows Including Separation," AIAA Journal, Vol. 26, No. 6, pp. 641-648. 1988

[12] Suhs, N.E. and Tramel, RW, "PEGSUS 4.0 Users Manual," Arnold Eng Dev Center Rep AEDC-TR-91-8, Arnold Air Force Station, TN, 1991.

[13] Huang, T.S., "Interaction of Ships with Berth at Floating Terminals," TM-65-90-03, Naval Civil Engineering Laboratory, Port Hueneme, California. 1990.
[14] Chen, H.C., Liu, T., Chang, K.A., and Huang, E.T., "Time-Domain Simulation of Barge Capsizing by a Chimera Domain Decomposition Approach," Proceedings of the 12th ISOPE Conference, Vol. III, pp. 314-320, KitaKyushu, Japan, May 26-31. 2002.
[15] Chen, H.C. and Huang, E.T., "Numerical Simulation of Dynamic Responses of a Floating Pier in Ship Berthing Operations" Paper No. EM-2003-136, Proceedings, 16th ASCE Engineering Mechanics Conference, University of Washington, Seattle, July 16-18, 2003.
[16] Huang, E.T. and Chen, H.C., "Ship Berthing at a Floating Pier," Proceedings, 13th International Offshore and Polar Engineering Conference, Vol. III, pp. 683-690, Honolulu, Hawaii, May 25-30. 2003.
[17] Owens, R. and Palo, P. "Wind-Induced Steady Loads on Ships," NCEL Technical Note TN No. N-1628, Naval Civil Engineering Laboratory, Port Hueneme, Ca 93043. April 1982.